

AD743548

**INTERACTIONS OF STRESS WAVES WITH
CRACKS IN ROCK MEDIA**

**Paul J. Blatz
Mark H. Wagner**

FINAL REPORT

May 1972

**Sponsored by
Advanced Research Projects Agency
ARPA Order No. 1597, Amend. 2
Program Code 1F10**

DISTRIBUTION STATEMENT A
Approved for public release;
Distribution Unlimited

The views and conclusions contained in this document are those of the authors and should not be interpreted as necessarily representing the official policies, either expressed or implied, of the Advanced Research Projects Agency or the U. S. Government.

Prepared by
SHOCK HYDRODYNAMICS
A Division of the Whittaker Corporation
15010 Ventura Boulevard
Sherman Oaks, California 91403

D D C
RECORDED
JUN 15 1972
REGISTERED

**INTERACTIONS OF STRESS WAVES WITH
CRACKS IN ROCK MEDIA**

**Paul J. Blatz
Mark H. Wagner**

FINAL REPORT

May 1972

Sponsored by

**Advanced Research Projects Agency
ARPA Order No. 1597, Amend. 2
Program Code 1F10**

**This research was supported by the Advanced
Research Projects Agency of the Department
of Defense and was monitored by the Bureau
of Mines under Contract No. H0210019.**

**Principal Investigators: P. J. Blatz/M. H. Wagner (213) 783-7210
Project Officer: T. E. Ricketts (612) 725-4608**

**Effective Date of Contract: 25 January 1971
Contract Expiration Date: 25 May 1972
Amount of Contract: \$61,387**

**The views and conclusions contained in this document are those
of the authors and should not be interpreted as necessarily repre-
senting the official policies, either expressed or implied, of the
Advanced Research Projects Agency or the U. S. Government.**

Prepared by

**SHOCK HYDRODYNAMICS
A Division of the Whittaker Corporation
15010 Ventura Boulevard
Sherman Oaks, California 91403**

DOCUMENT CONTROL DATA - R & D

(Security classification of title, body of abstract and indexing annotation must be entered when the overall report is classified)

1. ORIGINATING ACTIVITY (Corporate author) SHOCK HYDRODYNAMICS 15010 Ventura Boulevard Sherman Oaks, California 91403	2a. REPORT SECURITY CLASSIFICATION UNCLASSIFIED 2b. GROUP
---	--

3. REPORT TITLE
INTERACTIONS OF STRESS WAVES WITH CRACKS IN ROCK MEDIA

4. DESCRIPTIVE NOTES (Type of report and inclusive dates)
Final Report, January 1971 - May 1972

5. AUTHOR(S) (First name, middle initial, last name)
Paul J. Blatz
Mark H. Wagner

6. REPORT DATE May 1972	7a. TOTAL NO. OF PAGES 90	7b. NO. OF REFS 12
-----------------------------------	-------------------------------------	------------------------------

8a. CONTRACT OR GRANT NO. H0210019 b. PROJECT NO. ARPA Order No. 1597, Amend. 2 c. Program Code 1F10 d.	9a. ORIGINATOR'S REPORT NUMBER(S) 3160-13 9b. OTHER REPORT NO(S) (Any other numbers that may be assigned this report)
--	--

10. DISTRIBUTION STATEMENT
Distribution of this document is unlimited.

11. SUPPLEMENTARY NOTES This contract was monitored by the Bureau of Mines.	12. SPONSORING MILITARY ACTIVITY Advanced Research Projects Agency
---	--

13. ABSTRACT

Two-dimensional numerical techniques have been applied to obtain solutions of problems of stress wave interactions with cracks in rock media. The SHEP code, a finite-difference Lagrangian program that incorporates a comprehensive elastic-plastic-hydrodynamic behavioral model, was utilized as the basic numerical program in this study. Significant new capabilities of the code developed during this program were (a) the treatment of antiplane shear, or out-of-plane displacement (where the motion is dependent only on the in-plane coordinates) and (b) the incorporation of a dynamic brittle fracture criterion, (known as the Griffith criterion).

In-plane problems considered were the propagation of a stress wave through a semi-infinite space containing (a) a semi-infinite crack, (b) a finite stationary crack, and (c) a finite running crack. The crack was oriented at a 30° angle with the wave front in these problems. The computations demonstrated that it is possible to observe the diffraction of the shear wave fronts and to follow the flow of energy through the crack.

An ideal but relatively simple problem was chosen as a test vehicle for the out-of-plane program, namely the antiplane shear loading of a crack. In the case of a stationary crack, the code solution was shown to give excellent agreement in all respects with the analytical solution. Using the Griffith criterion, moderately good agreement was obtained for the case of the running crack.

14.

KEY WORDS

LINK A

LINK B

LINK C

ROLE

WT

ROLE

WT

ROLE

WT

Wave Propagation
Crack Propagation
Fracture
Rock Mechanics
Two-Dimensional Numerical Techniques

ABSTRACT

Two-dimensional numerical techniques have been applied to obtain solutions of problems of stress wave interactions with cracks in rock media. The SHEP code, a finite-difference Lagrangian program that incorporates a comprehensive elastic-plastic-hydrodynamic behavioral model, was utilized as the basic numerical program in this study. Significant new capabilities of the code developed during this program were (a) the treatment of antiplane shear, or out-of-plane displacement (where the motion is dependent only on the in-plane coordinates) and (b) the incorporation of a dynamic brittle fracture criterion (known as the Griffith criterion).

In-plane problems considered were the propagation of a stress wave through a semi-infinite space containing (a) a semi-infinite crack, (b) a finite stationary crack, and (c) a finite running crack. The crack was oriented at a 30° angle with the wave front in these problems. The computations demonstrated that it is possible to observe the diffraction of the shear wave fronts and to follow the flow of energy through the crack.

An ideal but relatively simple problem was chosen as a test vehicle for the out-of-plane program, namely the antiplane shear loading of a crack. In the case of a stationary crack, the code solution was shown to give excellent agreement in all respects with the analytical solution. Using the Griffith criterion, moderately good agreement was obtained for the case of the running crack.

In running the SHEP program, it is necessary to dampen oscillations at the wave front by the incorporation of a fictive viscosity. In the case of pressure, a quadratic viscosity component is added. In the case of shear, a linear term is normally added. A linear viscosity tends to increasingly spread the wave front, however. A study of the origins of this viscosity term has led to the development of an alternate formulation for the viscosity term which is cubic and applies both to pressure and shear. This alternate formulation will eventually replace the so-called anisotropic or Navier Stokes linear viscosity.

BLANK PAGE

TABLE OF CONTENTS

		Page
1.	INTRODUCTION	1
2.	SUMMARY	1
2.1	Problem Area	1
2.2	Plan of Research	2
2.2.1	Task 1 - Interaction of Stress Waves with Single, Semi-Infinite Cracks	2
2.2.2	Task 2 - Interaction of Stress Waves with Single, Finite Cracks	3
2.3	Major Accomplishments	3
2.3.1	In-Plane Numerical Solutions	4
2.3.2	Dynamic Griffith Criterion	13
2.3.3	Analytical Comparison Problems	14
3.	NUMERICAL SOLUTIONS OF IN-PLANE PROBLEMS	14
3.1	Computational Method	15
3.1.1	Physical Model	15
3.1.2	Surfaces of Discontinuity	15
3.2	Material Properties	18
3.3	Case 1 - Interaction of Stress Wave With Single, Semi-Infinite Crack	20
3.4	Case 2 - Interaction of Stress Wave With Single, Finite - Length Crack	30
3.5	Case 3 - Interaction of Stress Wave With Single, Finite-Length Crack, With Crack Growth	40
4.	ANTIPLANE SHEAR LOADING OF A STATIONARY CRACK	56
4.1	Formulation	56
4.2	Analysis	57

TABLE OF CONTENTS (Continued)

	Page
4.3 Numerical Solution	59
5. ANTI-PLANE SHEAR LOADING OF AN ACCELERATING CRACK	66
5.1 Analysis	66
5.2 The Griffith Criterion	68
5.3 The Fictive Viscosity	74
REFERENCES	81
APPENDIX - CORRECTION TO THE ROTATIONAL TERM IN THE STRESS CALCULATIONS	82

1. INTRODUCTION

The objective of this program was to apply two-dimensional numerical techniques to the solution of problems of stress wave interactions with individual, plane cracks in rock media. Computer codes suitable for solving a wide range of fluid and solid mechanics problems have been available or under development for several years and efforts to extend these techniques to the quantitative analysis of wave interactions with cracks and of crack motion are now feasible. Shock Hydrodynamics two-dimensional SHEP (Shock Hydrodynamic Elastic Plastic) code was utilized for this purpose in this program. Analytical studies were also conducted in conjunction with the numerical work.

2. SUMMARY

2.1 PROBLEM AREA

Excavation processes in rock media typically involve the action of strong dynamic stresses introduced either from explosive, mechanical, or other impulsive loading sources. The propagation of stress waves in homogeneous, isotropic media is reasonably well understood. In-situ rock media, however, typically contain large scale discontinuities in the form of cracks, joints, and faults. Interactions of stress waves with these discontinuities can cause slippage along the cracks, or extension (propagation) of the cracks, or separation. The interactions can also alter the characteristics of the stress wave transmitted across the discontinuity.

This study is concerned with an analysis of the detailed mechanisms involved when strong stress waves interact with the crack surfaces in jointed rock media. Of particular interest are cracks which are obliquely oriented relative to the wave front. The understanding thus obtained can contribute to the advancement of knowledge of excavation processes in various media, and how to control and/or improve such processes.

The technical approach used to study the details of stress wave-crack interactions was based on two-dimensional numerical analyses of the dynamic phenomena occurring under various conditions of stress wave loading and crack orientation relative to the wave front. The computer program used to obtain the numerical solutions was the SHEP code. SHEP is a finite-difference Lagrangian program employing a comprehensive hydrodynamic-elastic-plastic behavioral model. SHEP has been under intensive use and development for the past six years and has been applied to a broad spectrum of wave propagation problems.

A major difficulty in examining wave interactions with discontinuities such as cracks or fracture surfaces arises due to the constraint of the continuum model which is normally assumed in numerical analyses of wave propagation. Special routines in the SHEP code alleviate this difficulty by permitting crack surfaces to be explicitly defined in the computational grid. Thus the grid is not coupled across the crack, and slippage and/or separation can occur.

2.2 PLAN OF RESEARCH

The contract work was divided into the following two tasks, corresponding to analyses of stress wave interactions with

- a) single, semi-infinite cracks and
- b) single, finite-length cracks.

2.2.1 Task 1 - Interaction of Stress Waves with Single, Semi-Infinite Cracks

This task was concerned with the analysis pertaining to cracks which are semi-infinite in extent, or which intersect with the ground surface. The work initially consisted of the selection and determination of the problem specifications (such as media properties, loading wave characteristics, and crack orientation and condition). SHEP code solutions of the problems defined were then set up and run. These solutions provide

complete quantitative data for all the state and motion variables of interest throughout the computing field at regular intervals of time. In addition, spatial plots of the principal stress, particle velocity, and displacement fields were obtained at selected times during the event. Following completion of the solutions, analysis and interpretation of the results were performed to characterize the transmitted stress waves.

2.2.2 Task 2 - Interaction of Stress Waves with Single, Finite Cracks

This task was concerned with cracks of finite length, so that the interaction of a stress wave with a crack tip could be examined. The problems were selected so that comparisons between the cases of semi-infinite (Task 1) and finite (Task 2) cracks could be made.

Also included in this task was the development of a dynamic Griffith fracture criterion, to enable the study of crack propagation. In conjunction with this, the SHEP code was generalized to accommodate anti-plane shear, or out-of-plane displacement.

To verify the suitability and accuracy of the code, and modifications made thereto during the course of the program, for analyses of wave/crack interactions, analytic solutions of selected test problems were obtained and used to check out corresponding numerical solutions obtained with the code.

2.3 MAJOR ACCOMPLISHMENTS

Primary program accomplishments included

- a) The completion of SHEP code solutions of three in-plane stress wave/crack interaction problems.
- b) The codification of the equations of anti-plane shear (z-independent) to provide a new capability for SHEP code analyses.
- c) The formulation of a dynamic Griffith criterion for analyses of crack propagation with the SHEP code.

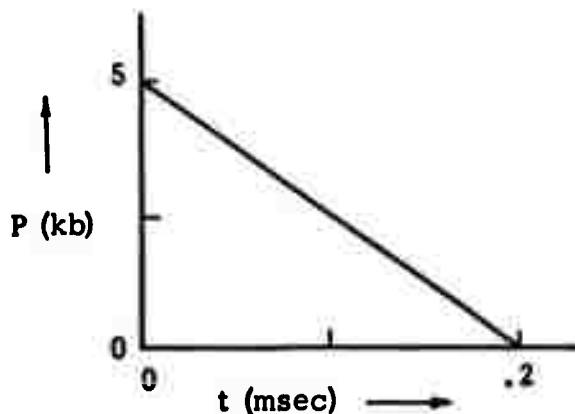
These items are summarized in the following sub-sections.

2.3.1 In-Plane Numerical Solutions

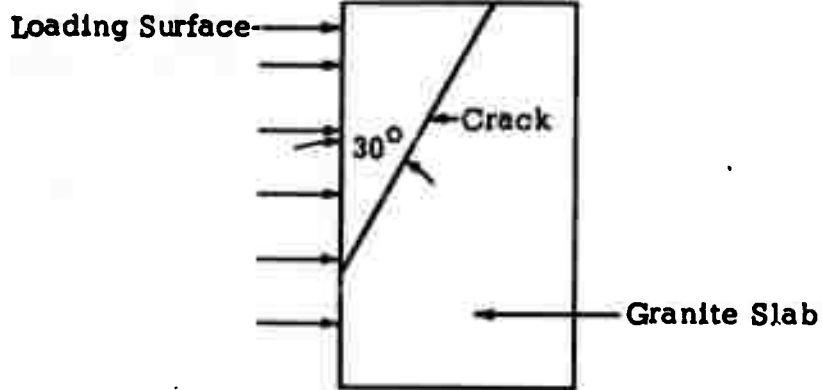
Three problems of wave interactions with cracks were selected for analysis by means of code solution, as depicted in Figure 1. These problems were chosen to demonstrate the utility of numerical techniques for obtaining detailed information on the response of cracked media subjected to impulsive loads, in general, and, in particular, for assessments of the wave interactions in the vicinity of a crack. It is noted that the explicit definition of a crack surface such as specified in these problems is not generally amenable to treatment through conventional code techniques, which normally assume a continuous material model.

The rock medium selected for these problems was granite. The material properties assumed for the granite are described in Section 3.2 of this report. The problems were run in plane geometry, assuming plane strain; the variables are thus independent of the z-coordinate (perpendicular to the cross-section shown).

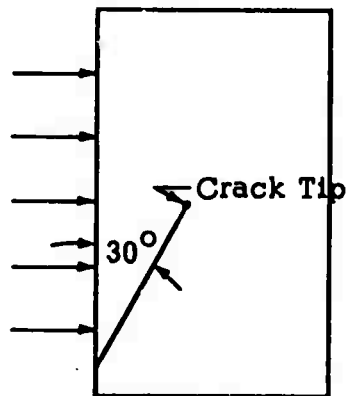
The first problem selected for analysis (Case 1) consisted of interactions of a stress wave with a crack oriented at a 30° angle with the wave front. The stress wave was generated by uniformly loading the left face of the granite block with a pressure pulse. A triangular pressure pulse of 5 kilobars peak magnitude and 0.2 millisecond duration was used for this problem, as sketched below:



CASE 1. INTERACTION OF STRESS WAVE WITH SINGLE, SEMI-INFINITE CRACK



CASE 2. INTERACTION OF STRESS WAVE WITH SINGLE, FINITE-LENGTH CRACK



CASE 3. INTERACTION OF STRESS WAVE WITH SINGLE, FINITE-LENGTH CRACK, WITH CRACK GROWTH

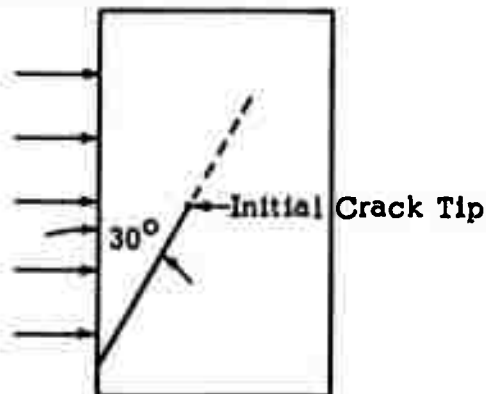


Figure 1. Specifications of Problems for SHEP Code Solutions.

The crack in this problem was characterized by a free slip condition and zero width. Opening of the crack was allowed to occur if stress components normal to the crack went into tension.

The second problem considered (Case 2) involved the interaction of a stress wave with a finite-length crack. The angle of orientation of the crack and the applied pressure loading were the same as in the first problem. The crack extended from the loading surface (lower left) to the crack tip, situated on the horizontal mid-plane of the block.

Case 3 was the same as the second problem, except that crack growth was permitted. This case demonstrates the provisions in the code which can be used to model crack propagation. In this case, dynamic decoupling of lattice points in the computing mesh occurs when a specified criterion is satisfied.

SHEP code solutions of these three problems were successfully completed. Plots depicting the particle velocity field and the principal stress field occurring in the test block were obtained for several times during the interactions. In addition, time histories of pertinent parameters at several stations in the field were recorded. These results are discussed in detail in Section 3 of the report. Some representative results of these code solutions are shown here, in Figures 2 to 7.

For Case 1, the principal stress field, for a time of .3 msec, and the particle velocity field, for a time of .5 msec, are shown in Figures 2 and 3. As the wave encounters the crack, the principal stress vectors may be seen (Figure 2) to rotate into a direction transverse to the crack surface, reflecting the fact that the crack surface can not bear shear stress. This interaction produces a dilatational wave and trailing shear wave which propagate across the block, as indicated in the velocity field plot (Figure 3). The peak stress in the transmitted wave was reduced by about 25% from that in the incident wave.

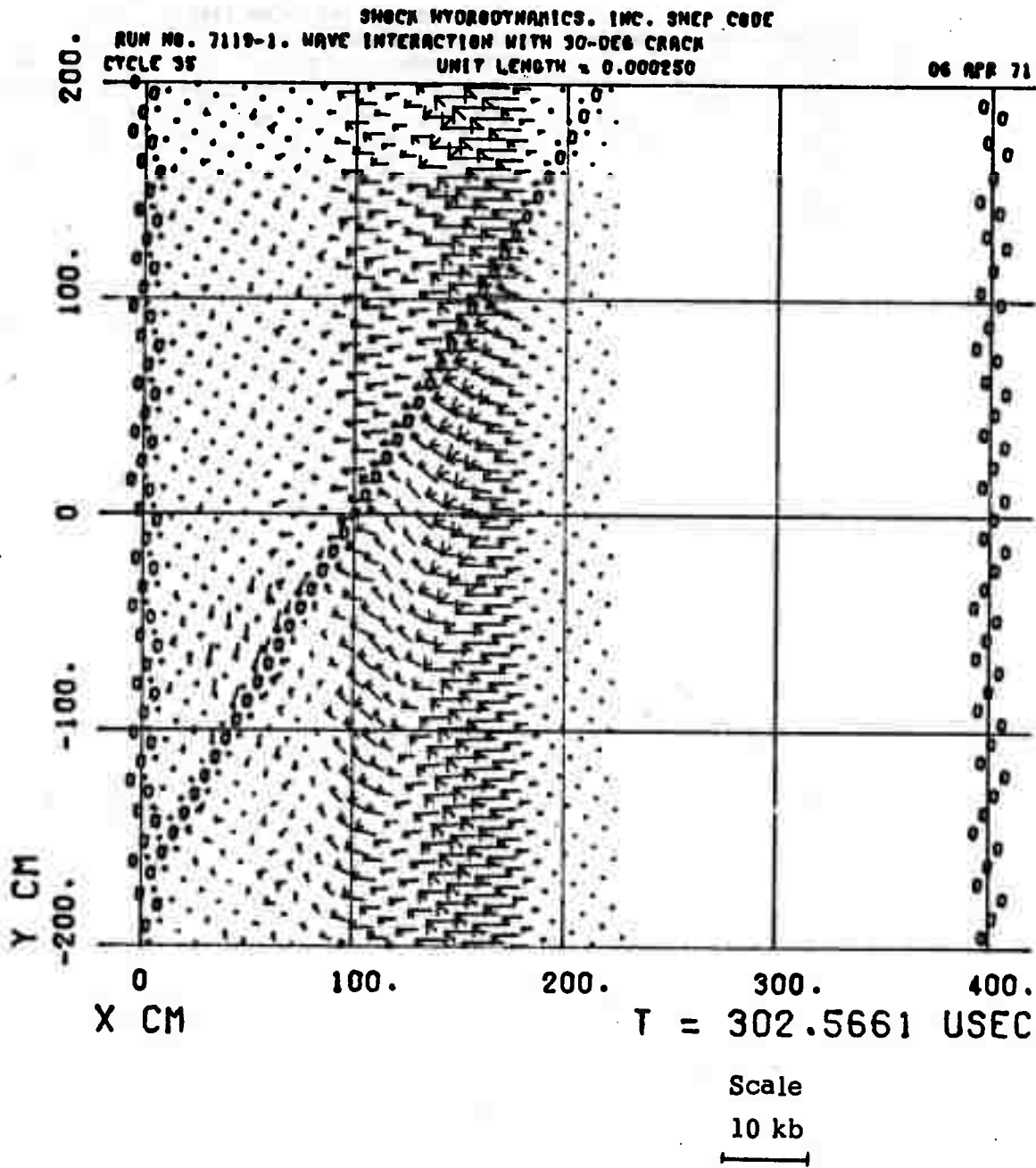


Figure 2. Principal Stress Field, Case 1

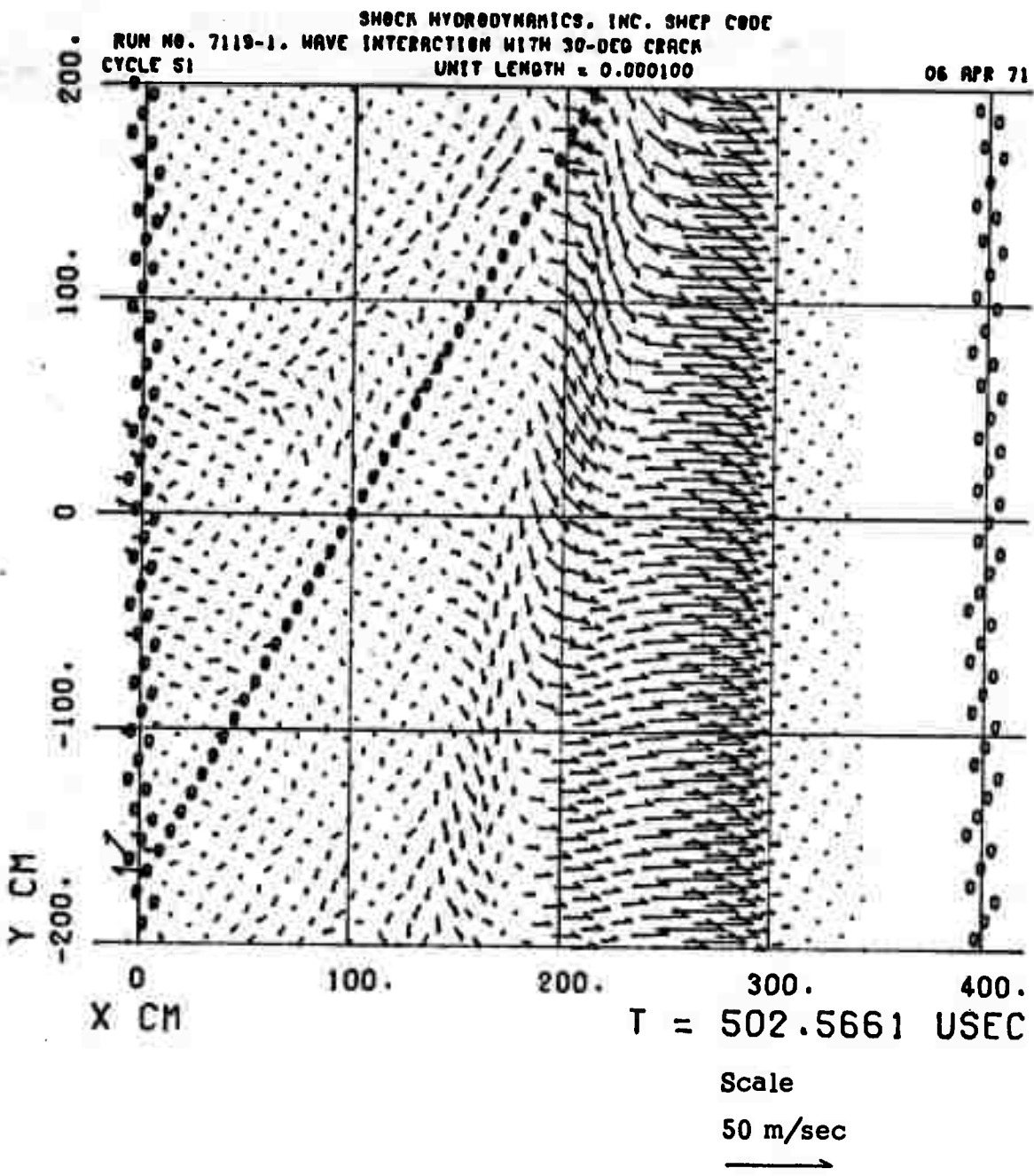


Figure 3. Particle Velocity Field, Case 1

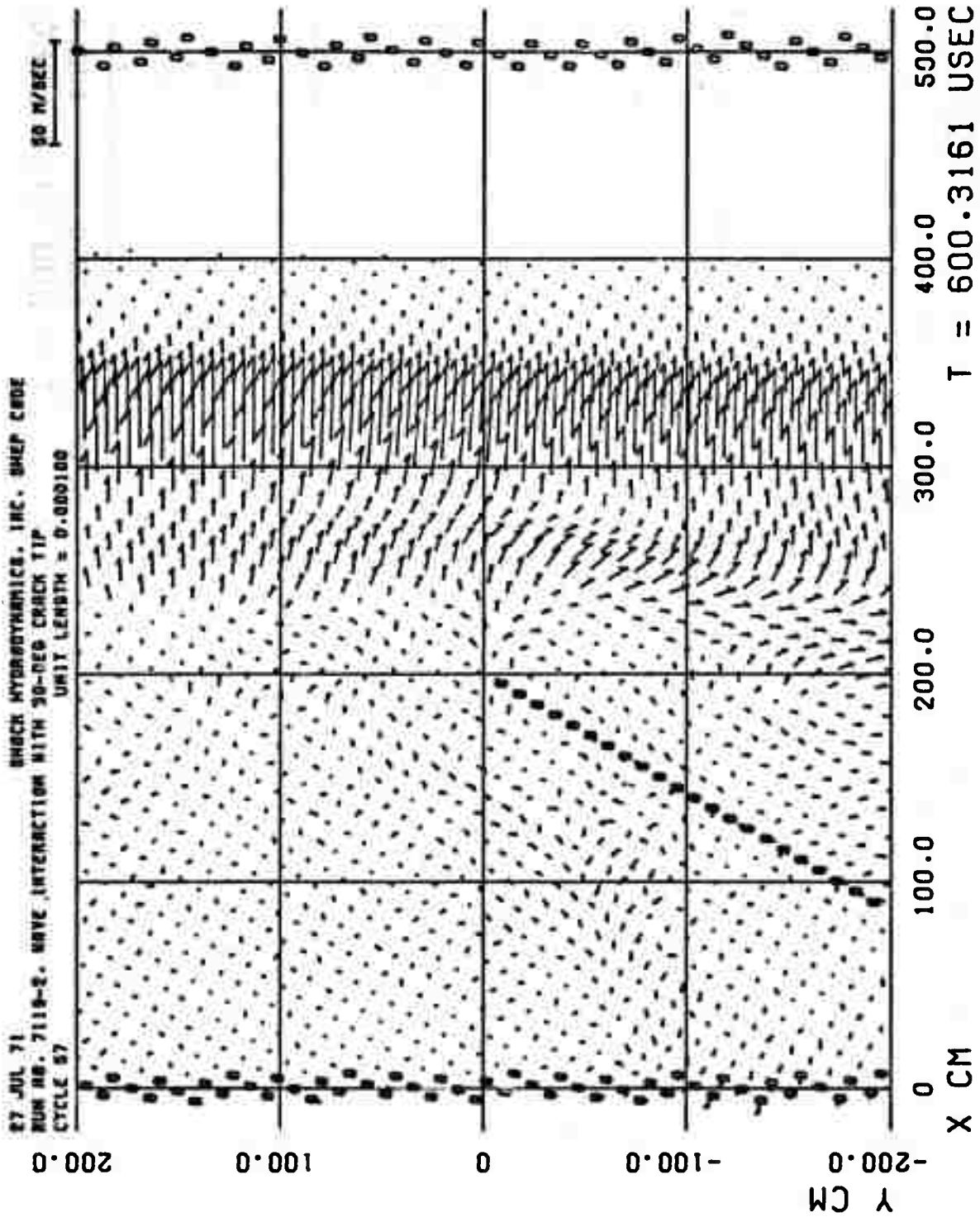


Figure 4. Particle Velocity Field, Case 2.

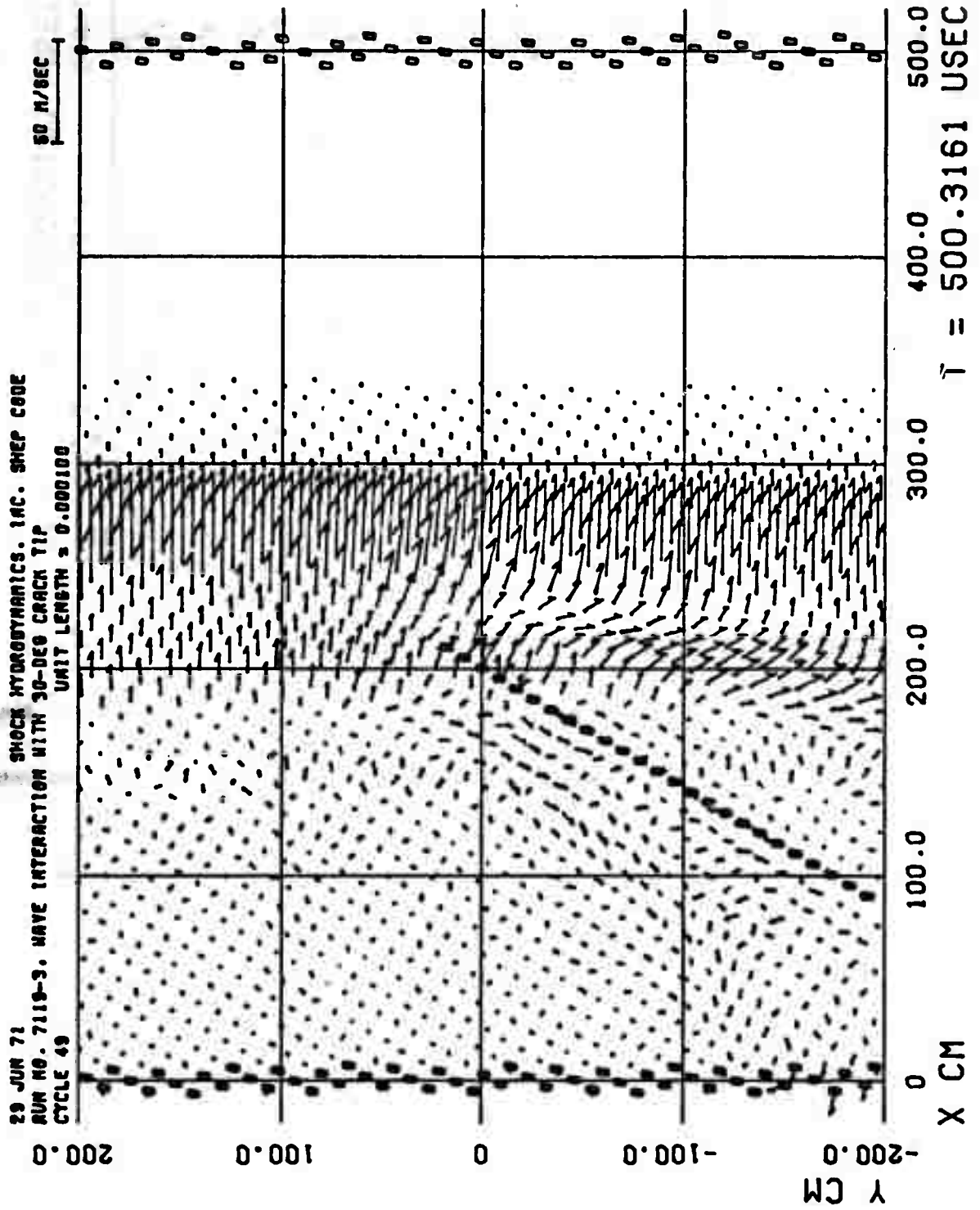


Figure 5. Particle Velocity Field, Case 3.

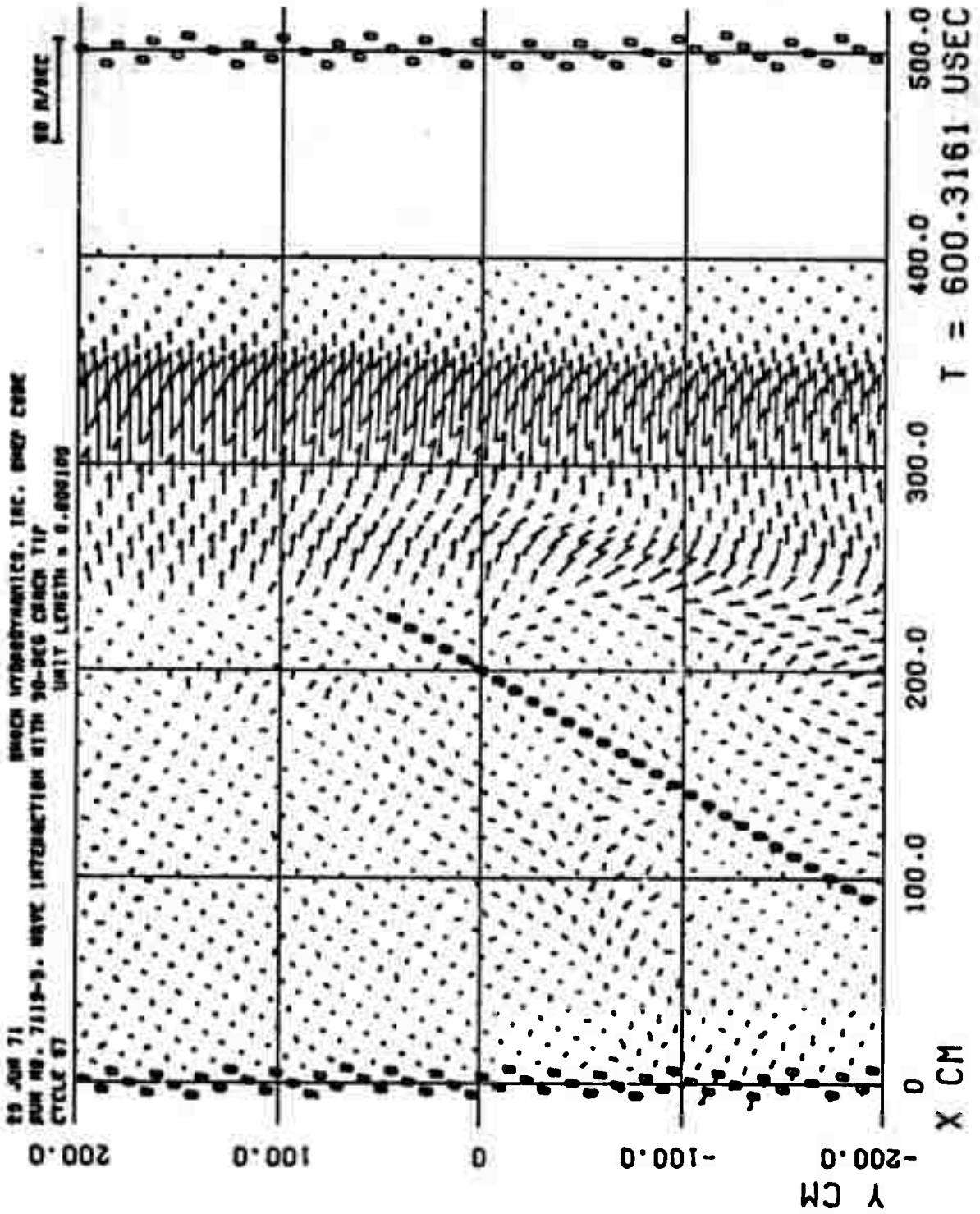


Figure 6. Particle Velocity Field, Case 3.

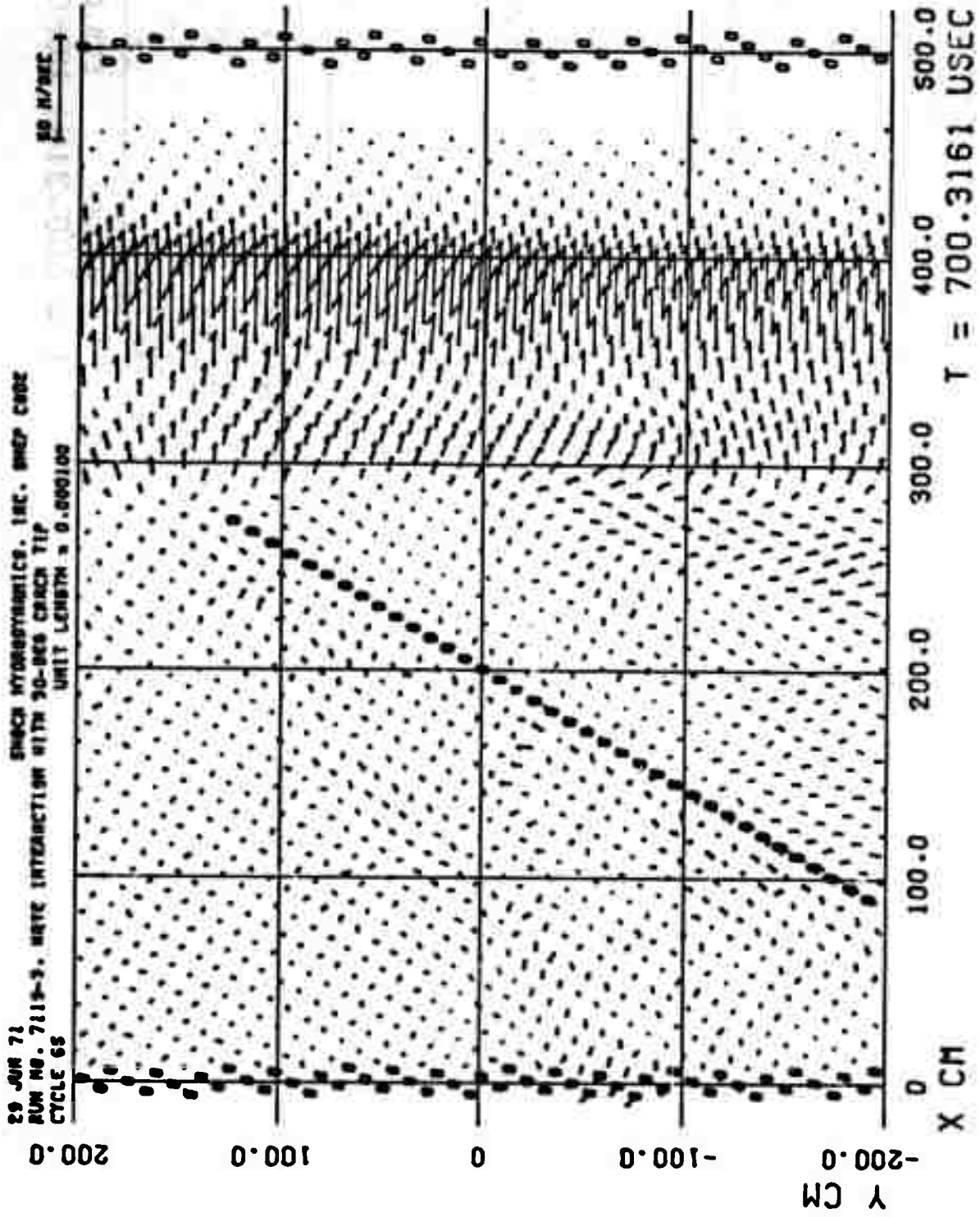


Figure 7. Particle Velocity Field, Case 3.

An example of the results of the Case 2 solution is shown in Figure 4, which depicts the particle velocity field occurring at a time of .6 msec. In this interaction, the wave system is divided approximately in half, the part above the crack tip appearing as a simple plane wave, and that below as a dilatational wave and trailing shear wave, as in the previous solution. Starting from the crack tip, a disturbance propagates into the plane wave region above and the "cracked" region below, altering both flow fields and creating an expanding region of transition between them.

In Case 3, where crack growth was allowed, the criterion used for decoupling of points beyond the crack tip was that each of the cells surrounding a lattice point must have failed, i.e., at some time reached a state on the granite failure surface. This was a conservative criterion, since the failure surface generally represents states where virtually complete fracture occurs. Use of more sensitive criteria can be employed, and development of a dynamic Griffith criterion was subsequently undertaken, as described below. The crack growth occurring in this solution is indicated in Figures 5, 6, and 7, which are plots of the particle velocity field for times of .5, .6, and .7 msec. The extent of the crack in each plot is indicated by the circled lattice points.

2.3.2 Dynamic Griffith Criterion

In connection with efforts made under the program to enable the study of propagation of cracks under stress wave loading, the incorporation of equations into the SHEP code which govern the rate of propagation of a brittle crack surface in an elastic material was undertaken. These equations are known as the Griffith criterion and they provide a relation between power input to the body and the rate of uptake of this power by strain energy, kinetic energy, and new surface energy. The concept of surface energy is the feature that was introduced by Griffith in the early 1900's, and it requires the determination of an additional material parameter, namely the surface energy per unit area. An algorithm appropriate for the SHEP code

was programmed and tested on a model problem. The results indicated that the effective crack propagation was slower than predicted theoretically. It is expected that improved results would be obtained with an alternate form of the fictive viscosity.

2.3.3 Analytical Comparison Problems

To verify the SHEP code solutions and the formulation changes made, comparisons of numerical results with analytical solutions of model problems were made.

As part of this effort, the capability was added to the code for the treatment of anti-plane shear, or out-of-plane displacements, with the restriction that the motions are independent of the z-coordinate, so as to retain the two-dimensional character of the code. This was done primarily since the only elasto-dynamic solutions currently available for an accelerating crack are those for the case of anti-plane shear, although it also represents a useful tool in numerical analysis which has heretofore been unavailable.

A model problem of simple, shear motion of a slab was first solved with the modified code. The results of the code solution showed excellent agreement with the analytical solution for this case. A full, two-dimensional problem involving the interaction of an anti-plane shear wave with a stationary crack was then set up and run. Excellent agreement with the analytical solution was also achieved for this case.

3. NUMERICAL SOLUTIONS OF IN-PLANE PROBLEMS

As noted above, numerical solutions of three problems involving the interaction of stress waves with cracks were performed. The specifications of these problems were given in Section 2.3.1.

3.1 COMPUTATIONAL METHOD

3.1.1 Physical Model

The computer program used in this study was the two-dimensional SHEP code, which solves the equations of motions for elastic-plastic bodies by means of a finite-difference Lagrangian-cell technique. SHEP has been under intensive use and development for the past six years and has been previously documented¹ and distributed to interested parties. The mathematical formulation is basically the same as that described by Wilkins². To delineate the boundary between elastic and plastic deformations, various yield criteria may be used, such as von Mises, Mohr-Coulomb, or arbitrary functions. Within the chosen yield surface, the deformations are considered to be elastic, i.e., when

$$\sqrt{3} J_2' < Y \quad (1)$$

where J_2' is the second invariant of the deviatoric stress tensor and Y is the yield strength. Excursions on the yield surface can be made in accordance with either the Prandtl-Reuss or plastic potential flow rules.

To model a crack surface, SHEP contains provisions for inserting surfaces of discontinuity, which consist of grid lines having a dual set of lattice points. These surfaces are discussed in the following section.

3.1.2 Surfaces of Discontinuity

In a normal Lagrangian computational grid, material elements on either side of an interface at any point are coupled to each other for the entire problem; they are, i.e., locked or welded together along the line segment connecting any two lattice points along the interface. At any interface, which may represent a crack within a material or the boundary between two different materials, there are, however, in general, special boundary conditions which apply, and, in addition, there is the possibility of forces

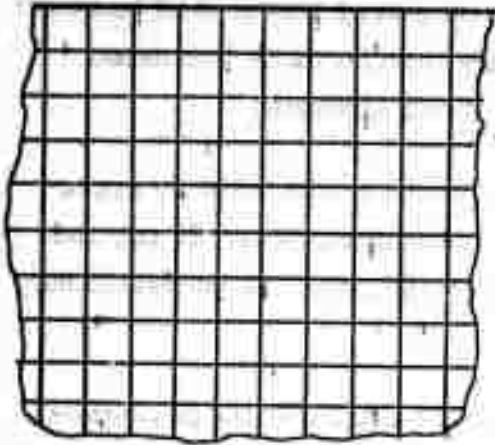
which may be set up that tend to cause the materials to slip past each other or to separate. A gas flowing past a metal surface is an example of such a case. The onset of material fracture during a problem also gives rise to the requirement for treating the decoupling or uncoupling of elements which are, in this case, within an originally competent material. For application to problems in fracture mechanics, such as in this program, the latter requirement is particularly important.

A formulation of sliding interfaces for Lagrangian codes, as reported by Wilkins², provided a capability for the numerical treatment of problems involving sliding of two materials along an interface. This formulation served as the basis for development of the surface of discontinuity capability currently available in the SHEP code.

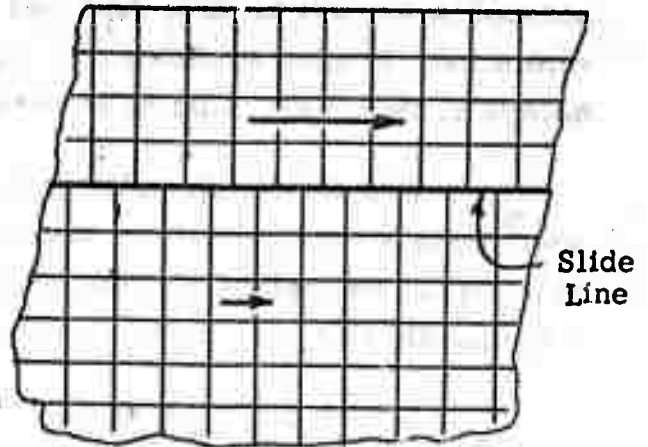
The basic features of the surface of discontinuity formulation are illustrated in Figure 8. The grid line corresponding to the surface of discontinuity is known in common parlance as a slide line. At the start of a problem, the lattice points along the slide line may be individually designated as decoupled points, corresponding to their lying on an interface, or as coupled points, in which case their behavior is the same as in an ordinary mesh. For decoupled points, special sets of governing equations are used to individually determine the motion of the point pairs, to reflect the fact that there is an interface, such that, e.g., shear stress cannot be supported. If forces are present which tend to cause slippage, the decoupled points will thus disengage and move separately along the slide line.

Additionally, the development of tensile stresses normal to an interface will tend to cause material separation and formation of voids. Provisions have been made in the code to treat this phenomenon, also.

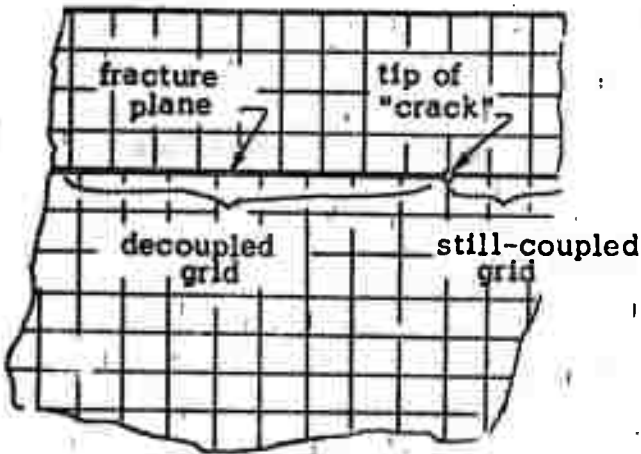
The void opening test is made by computing the stress normal to the interface at a decoupled slide point and comparing this value with a selected critical value of stress required for uncoupling. If the computed stress is greater than the critical value (in tension), then that point is designated as a free surface point. The newly formed free point is then moved in accordance with the regular equations of motion for a point on a free surface.



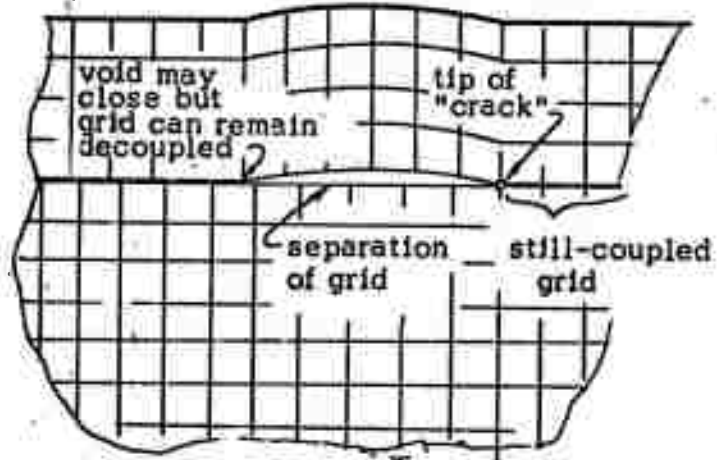
a. Normal Coupled Lagrangian Grid



b. Decoupled Grid With Relative Motion (Slippage) Along Material Interface, Fracture Surface, or Plane of Weakness



c. "Crack Propagation" With Subsequent Slippage Along Fracture Surface



d. "Crack Propagation" With Subsequent Separation and Rejoining Along Fracture Surface

Figure 8. Schematic Illustrations of the Treatment of Slippage, Fracture, Void Opening, and Void Closing Along Surfaces of Discontinuity in the SHEP Code.

For the problems performed in this study, the critical value for uncoupling was set to zero, such that any tensile stress would tend to cause separation. In other applications, e.g., for the interfaces in laminated materials, this value could be set equal to the bond strength.

Void closure may also occur and is treated in the code by appropriate tests to determine if the materials have come in contact. If so, the equations of the surface of discontinuity are restored, and the materials may subsequently slip or re-open, as before.

Lattice points along the slide line which are initially designated as coupled points may dynamically decouple, individually, during the course of a problem, if a selected criterion is met. Various decoupling, or fracture, criteria may be used. Once the lattice points are decoupled, the equations of the surface of discontinuity are invoked. A mechanism is thus provided which can be used to model crack propagation within a material.

Additional information on the code operations and the mathematical basis of sliding interfaces has been previously reported.²⁻⁴

3.2 MATERIAL PROPERTIES

The rock medium in these problems was granite. The properties selected for the granite were:

Density:	$\rho_0 = 2.69 \text{ gm/cm}^3$
Dilatational Velocity:	$v_{d0} = .579 \text{ cm}/\mu\text{sec}$
Shear Velocity:	$v_{s0} = .330 \text{ cm}/\mu\text{sec}$

These values imply the following other properties:

Bulk Modulus:	$K_0 = .512 \text{ Mb}$
Shear Modulus:	$G_0 = .293 \text{ Mb}$
Poisson's Ratio:	$\nu_0 = .26$

The subscript o in the above indicates that these are normal, pre-shocked values. These values were selected from previous studies involving granite media.^{5,6}

The equation of state of granite, suitable for the low-pressure regime applicable in these problems, was formulated as follows.

$$P = A\mu + B\mu^2 \delta + Gpe \quad P < .04 \text{ Mb} \quad (2)$$

where

$$\delta = 1 \text{ for } \mu > 0$$

$$\delta = 0 \text{ for } \mu \leq 0$$

The symbols are defined as

e = specific internal energy

P = pressure

$\eta = \rho/\rho_o =$ relative density

$\mu = \eta - 1 =$ compression

$\rho =$ density

The values of the coefficients are:

$$A = .512 \text{ Mb}$$

$$B = 1.49 \text{ Mb}$$

$$G = 2.1$$

No hydrostatic tension was permitted, i.e., $P_{\min} = 0$.

A Mohr-Coulomb type yield model was used, i.e.,

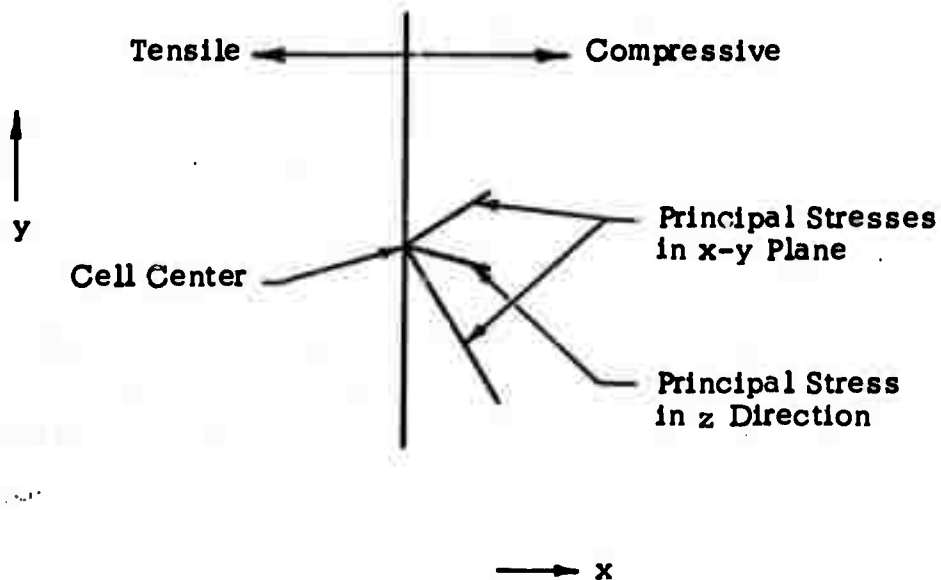
$$Y = .0003 + (1 - e^{-P/.0003})(.00094 + 1.33 P) \quad (3)$$

where Y is the yield strength, in megabars. The maximum value permitted for Y was 10 kilobars.

3.3 CASE 1 - INTERACTION OF STRESS WAVE WITH SINGLE, SEMI-INFINITE CRACK

The computational grid set up for the code solution of Case 1 is shown in Figure 9. This grid contains 2690 cells, with the basic cell size set at 10 cm x 10 cm. Beyond a central region of interest the cell dimensions geometrically increase in order to conserve the total cell count and computational time. Representative results of the code solution, as depicted by particle velocity fields and/or principal stress fields for times of .3, .5, and .92 msec, are shown in Figures 10 to 12 and in Figures 2 and 3 in the Summary, Section 2.3.1. For clarity in reading these plots, the field of view was limited to the central region of interest.

For the stress field plots, the principal components of the stress tensor for each cell are shown, as follows: The magnitude of the two principal stresses in the x-y plane are plotted in their corresponding principal directions. The third principal stress (in the z direction) is plotted along the line bisecting the other two principal directions. Vectors pointing to the right are compressive, to the left, tensile. An example of how a stress tensor is plotted is sketched below:



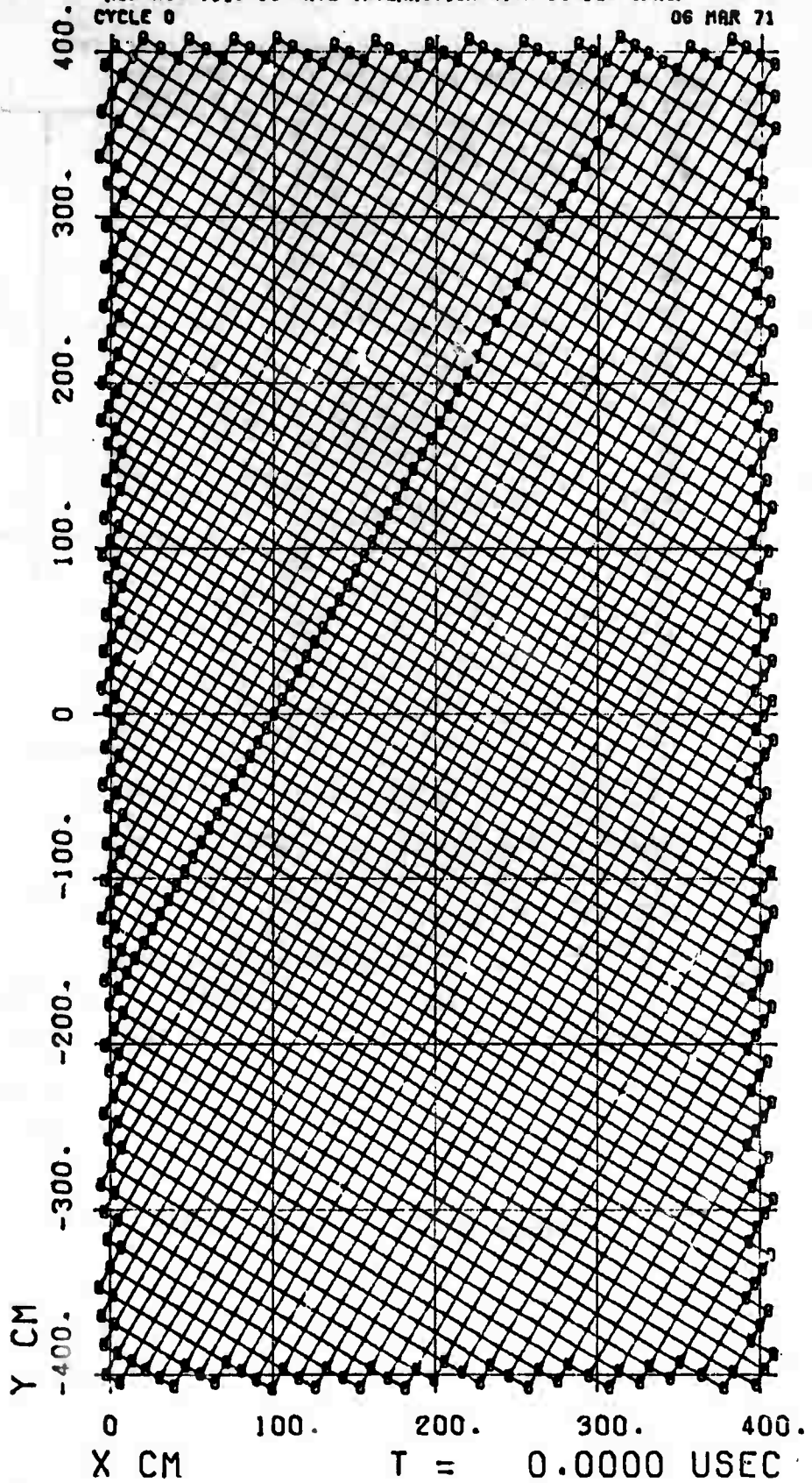


Figure 9. Initial Configuration of the Lagrangian Computational Grid, Case 1

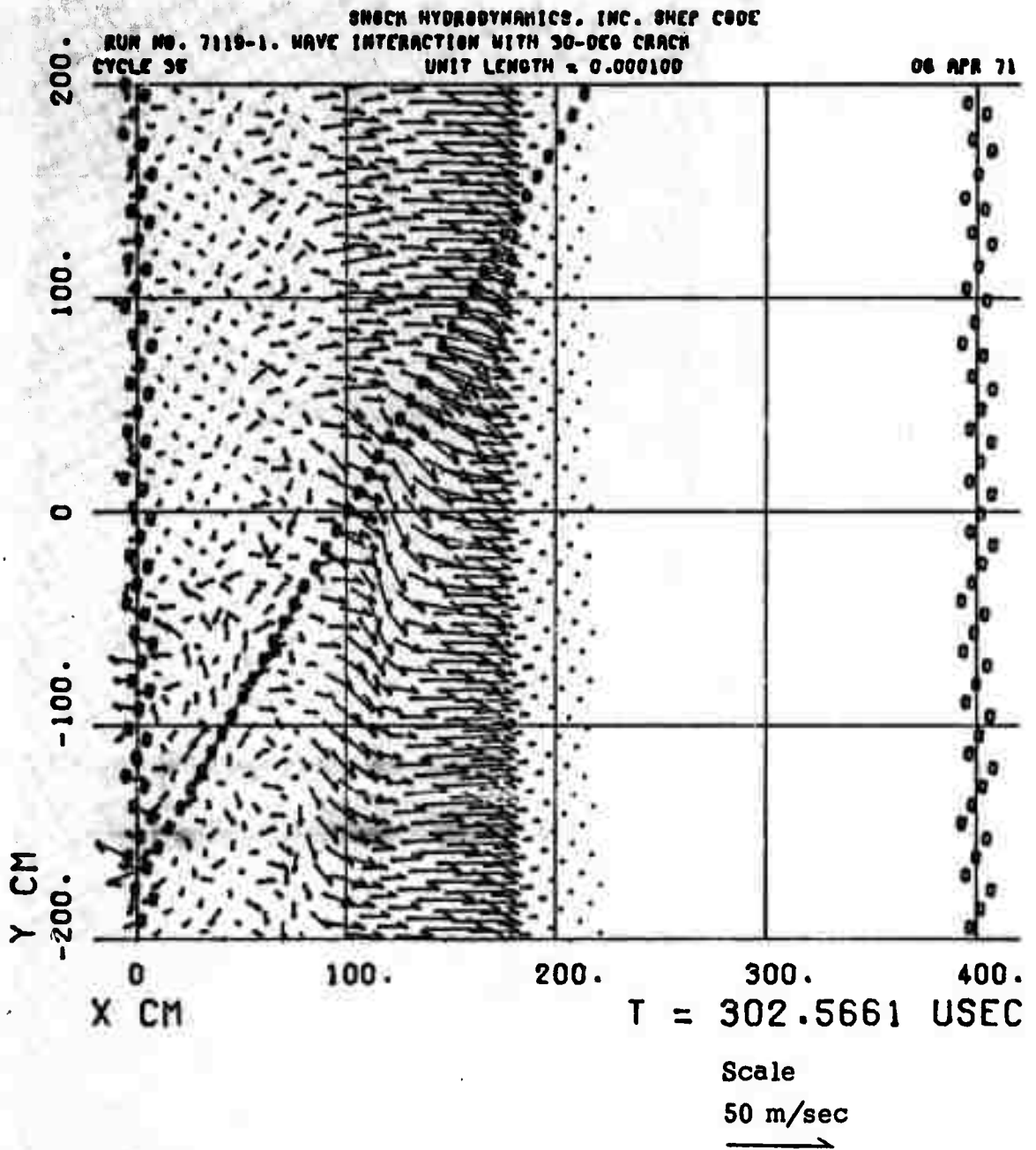


Figure 10. Particle Velocity Field, Case 1

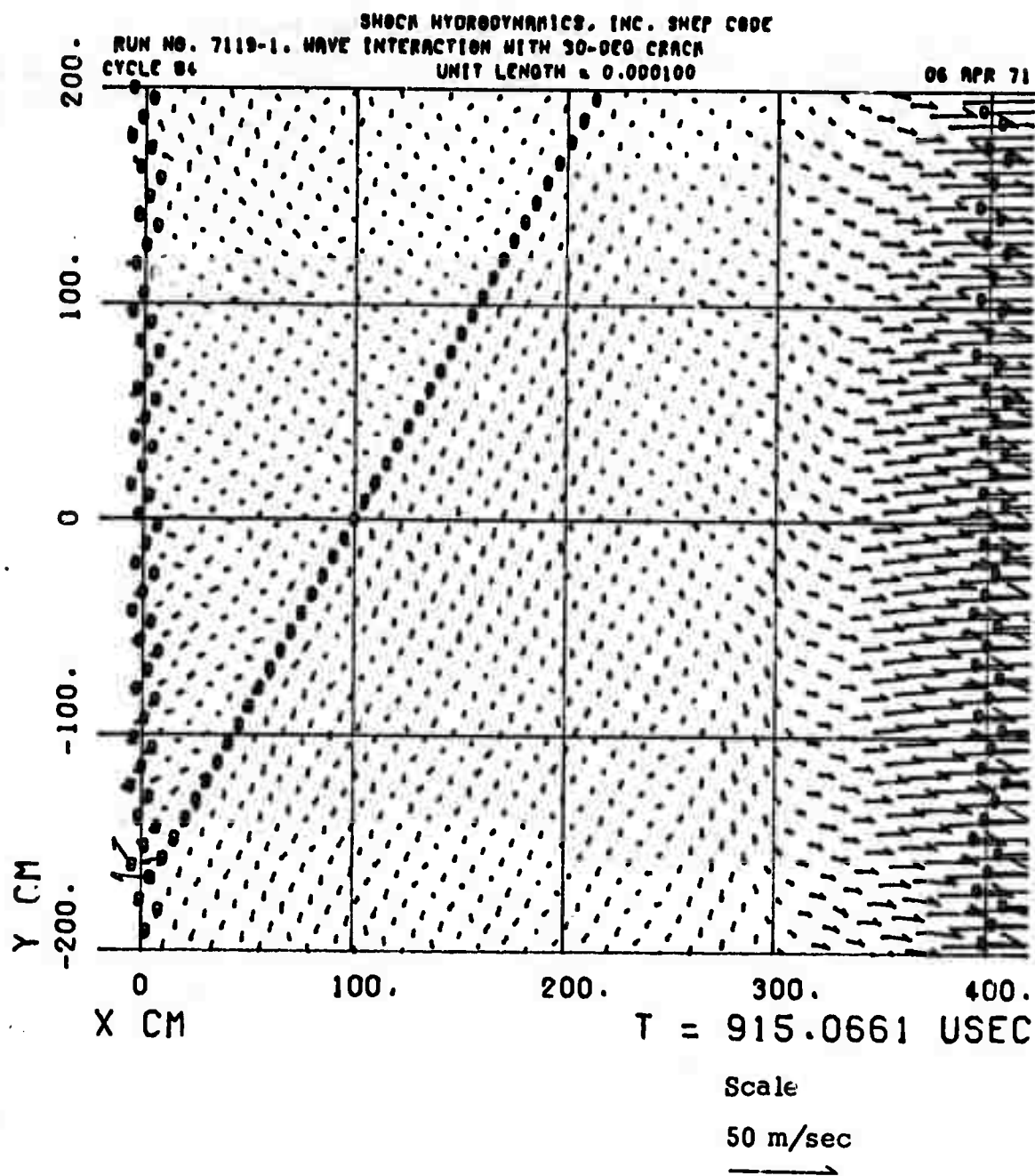


Figure 11. Particle Velocity Field, Case 1

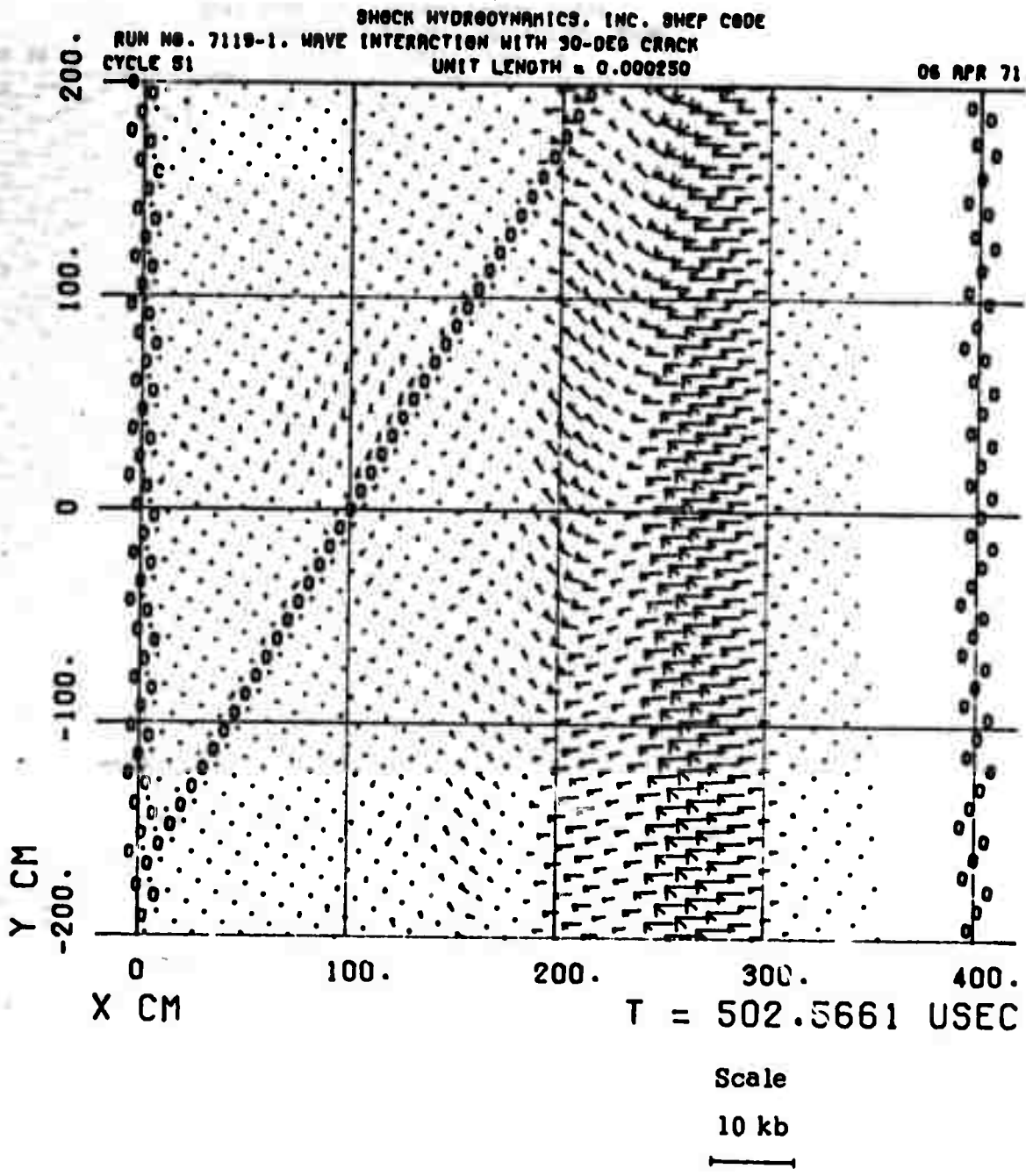


Figure 12. Principal Stress Field, Case 1

The edits of the velocity vector field plot the direction and magnitude of the velocity of each lattice point in the computing grid. The vector lengths for both the principal stress and velocity fields are scaled to the unit length indicated above each plot; the units are Mb/cm and (cm/ μ sec)/cm, respectively. On the more recently produced plots, the scale is also graphically depicted in the upper right hand corner.

As the stress wave interacts with the crack, the material on the right side of the crack is driven by the stress component normal to the crack, since shear stresses cannot be supported. As shown in Figure 10, the velocity vectors along the crack at the shock front are thus directed normal to the crack, turned downward 30° . Also, as shown in Figure 2, note that the principal stress tensors in the material along the right side of the crack are rotated into a direction transverse to the crack surface, again reflecting the fact that the crack surface can not bear shear stress. As the incident wave runs along the crack, a dilatational wave and trailing shear wave are formed which propagate across the block. The transmitted shock front remains approximately planar and oriented at 90° to the x axis. In the shear region behind the shock, a distinctly downward velocity flow is evident. This action induces material slippage along the crack, the material on the right side of the crack moving downward and to the left, along the crack, relative to the material on the left side. In addition, there was a slight separation, or opening-up, of the materials on either side of the crack, which were initially in contact.

Time histories of the material displacement at the points indicated in Figure 13 were recorded during the code solution. The slippage of material initially at the point $x = 100$ cm, $y = 0$ cm, as given by the distance between points on opposite sides of the crack (points B and C in Figure 13), is shown in Figure 14. The extents of the downward (y-direction) displacements of these points are shown in the time histories given in Figure 15. The downward displacements of other points in the field, at $x = 55, 158, 203,$ and 253 cm (points A, D, E, and F) along the central horizontal plane ($y = 0$), are shown in Figure 16. The forward (x-direction) displacements of

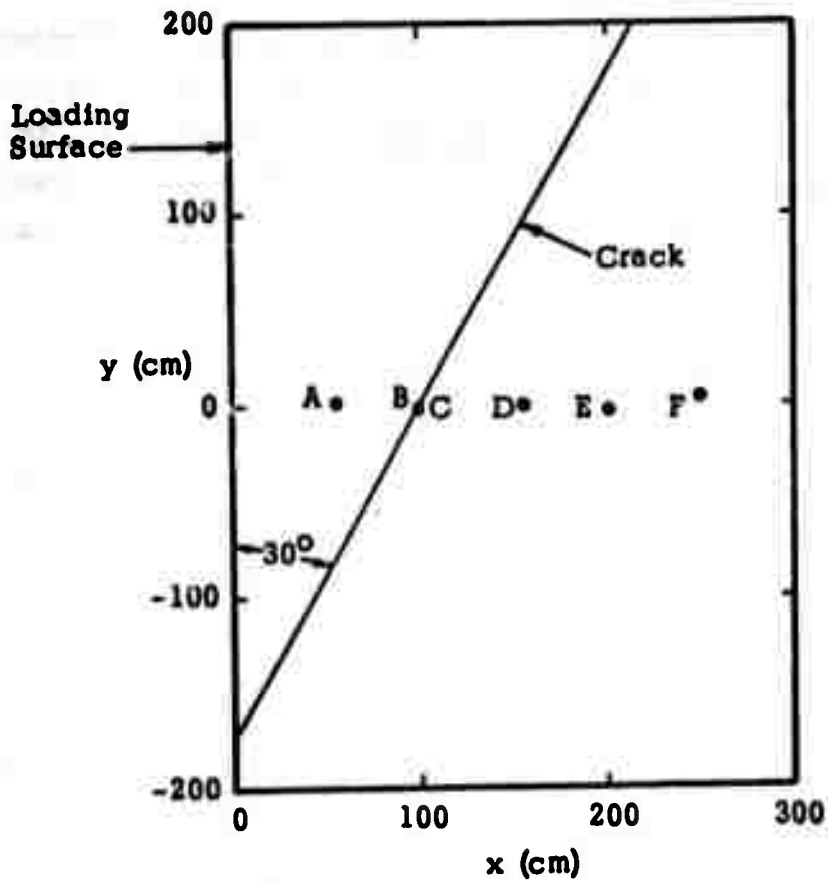


Figure 13. Location of Time History Data Stations

RUN NO. 7119-1. WAVE INTERACTION WITH 30-DEG CRACK

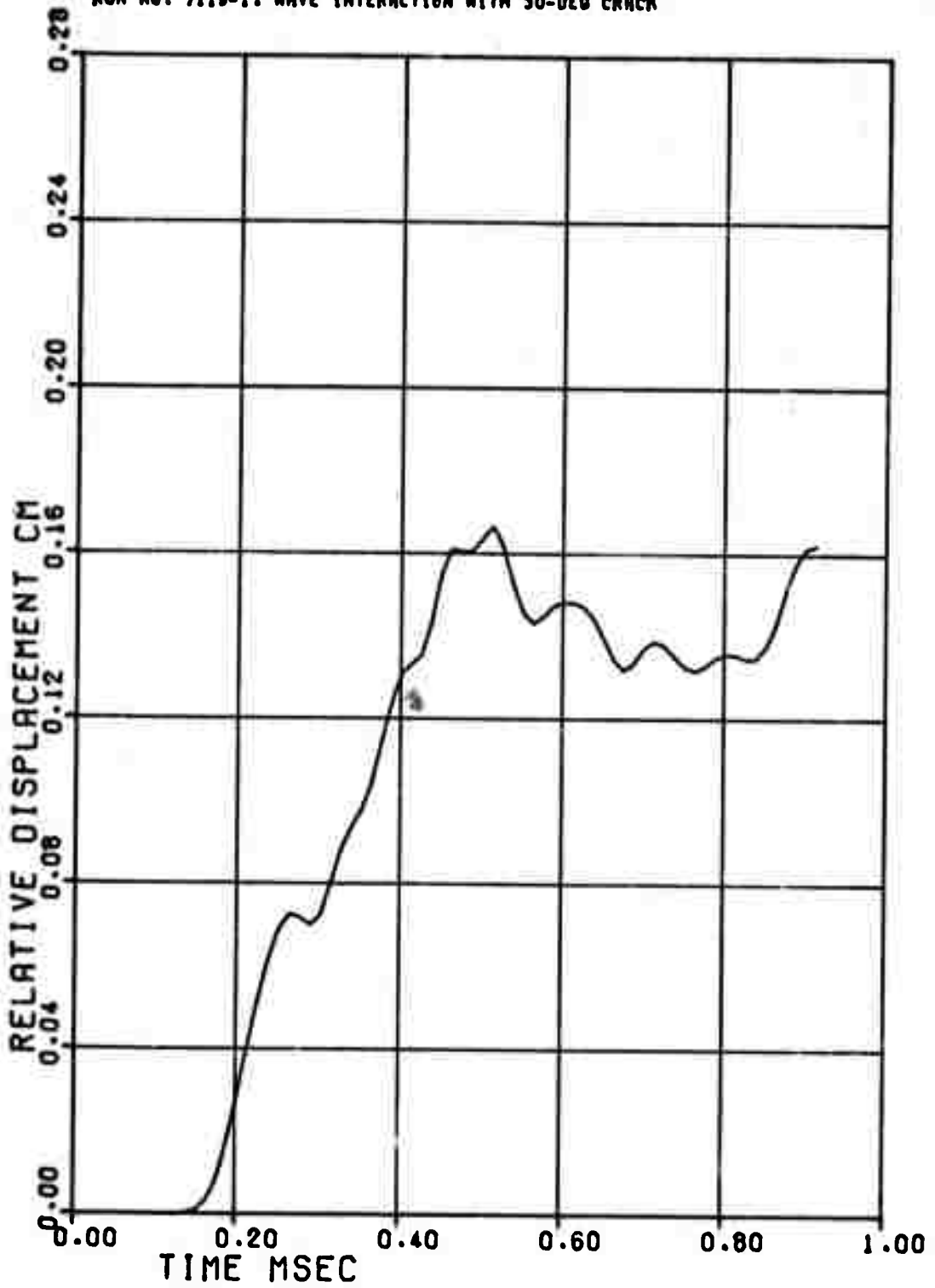


Figure 14. Material Slippage Along Crack at $x = 100$ cm, $y = 0$, Case 1

RUN NO. 7110-1. WAVE INTERACTION WITH 30-DEG CRACK

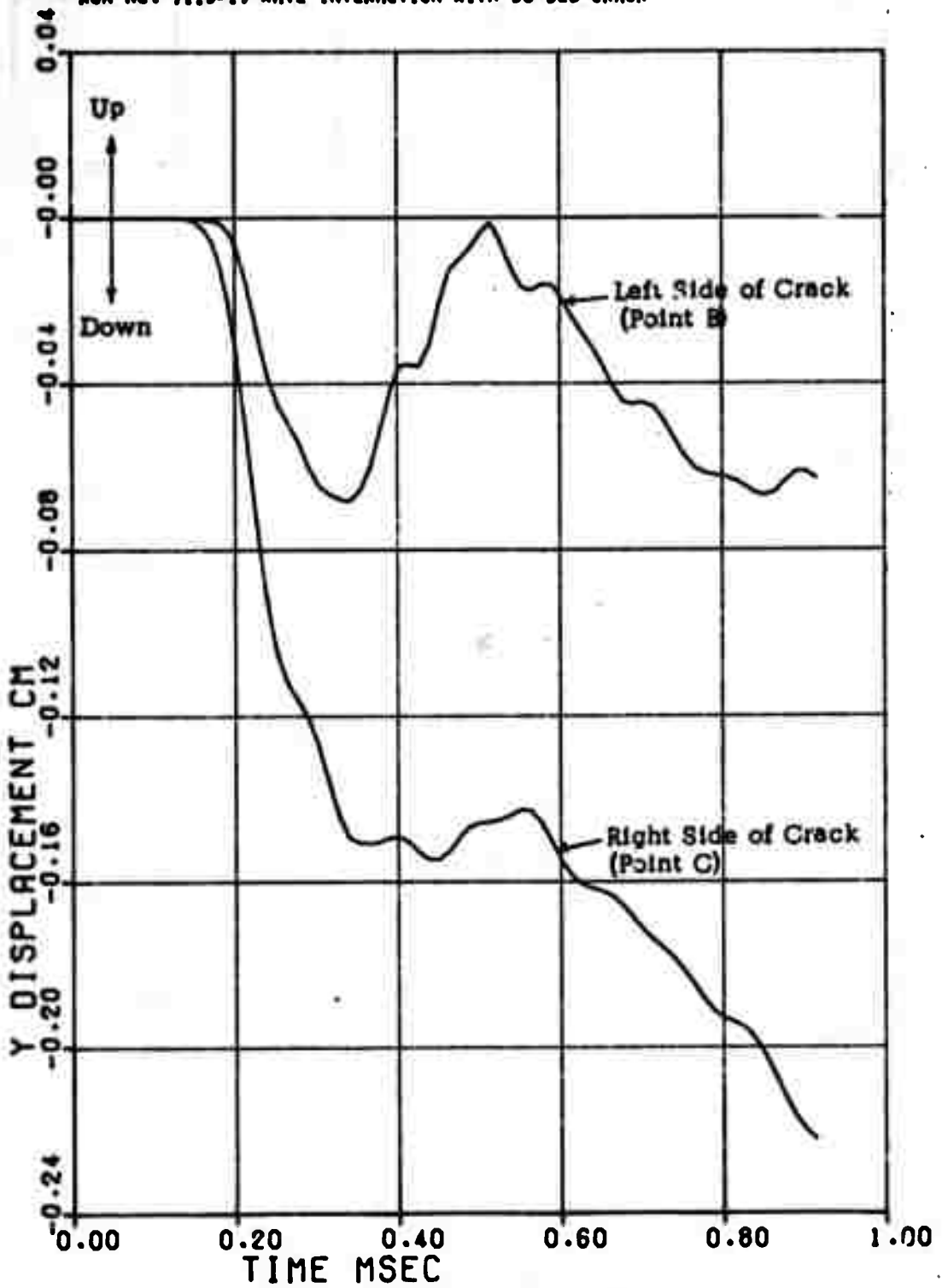


Figure 15. Vertical Displacement of Material Along Crack at $x = 100$ cm, $y = 0$, Case 1.

RUN NO. 7119-1. WAVE INTERACTION WITH 30-DEG CRACK

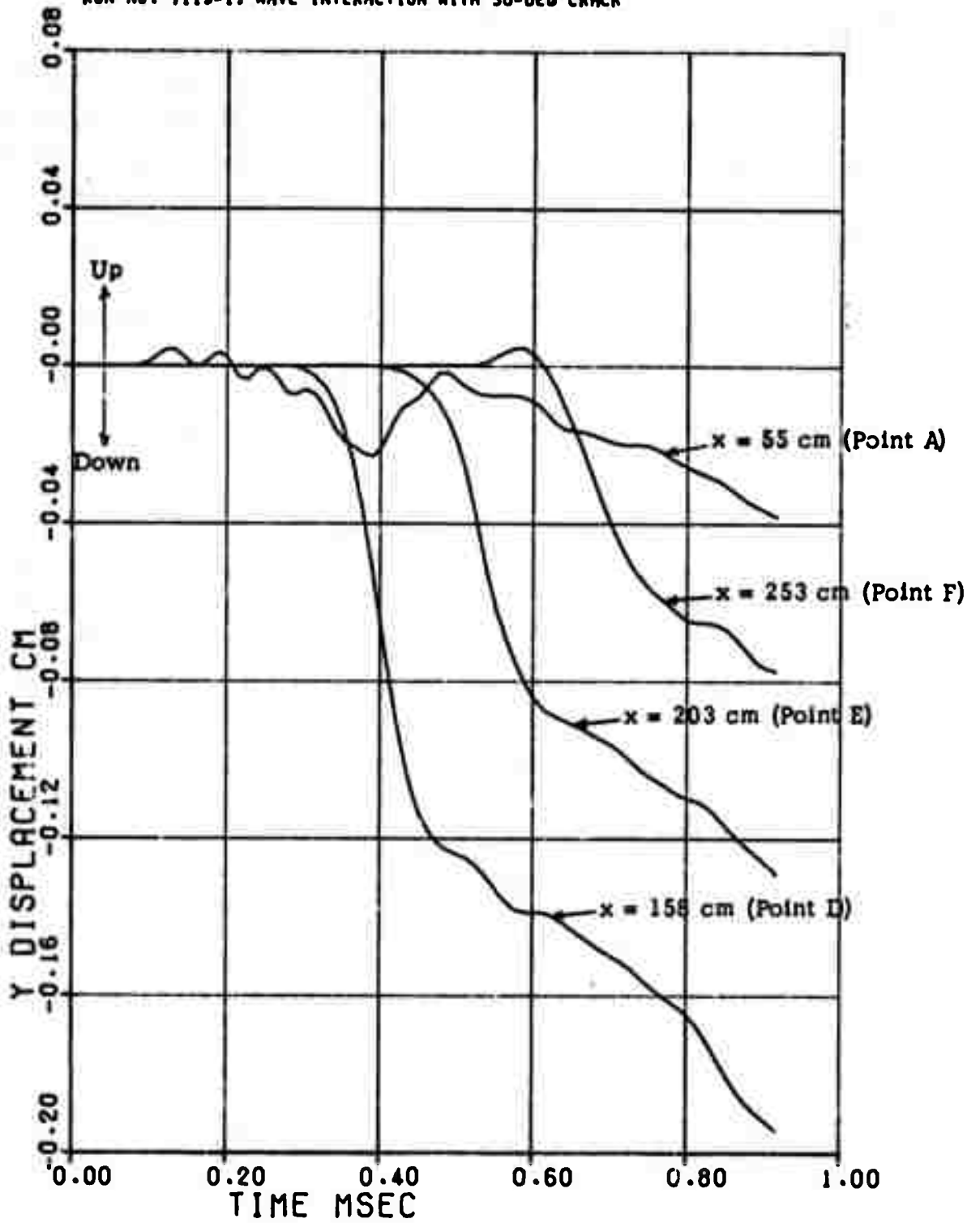


Figure 16. Vertical Displacement at Four Stations Along the $y = 0$ Plane, Case 1.

these points during this time were all ~ 0.25 cm. The perturbation of flow, as measured by the downward thrust of material, is seen to diminish as the distance from the crack increases.

Stress (σ_x) - time profiles at points A, D, E, and F are shown in Figure 17. The peak stress in the transmitted wave (points D, E, and F) is seen to be reduced by about 25% from that in the incident wave. The aforementioned two-wave structure in the transmitted wave and the reflected wave at point A are also displayed in these plots.

3.4 CASE 2 - INTERACTION OF STRESS WAVE WITH SINGLE, FINITE-LENGTH CRACK

The initial configuration of the Lagrangian grid set up for this problem is shown in Figure 18. The crack extends from the loading surface (lower left) to the crack tip at $x = 200$ cm, $y = 0$.

Representative results of the SHEP code solution of this problem, as depicted by the particle velocity fields for times of .3, .4, .5, .6, and 1 msec, are shown in Figures 19 to 22 and in Figure 4 in the Summary, Section 2.3.1. Associated principal stress fields for times of .4, .5, and .7 msec are shown in Figures 23 to 25. For clarity in reading these plots, the field of view is limited to the central region of interest.

The response of the granite in this problem is, of necessity, similar to that in the semi-infinite crack problem, until the wave front reaches the crack tip. Subsequently, the wave system is divided approximately in half, the part above the crack tip appearing as a simple plane wave, and that below as a dilatational wave and trailing shear wave, as in the previous solution. Starting from the crack tip, a disturbance, or bow wave, propagates into the plane wave region above and the "cracked" region below, altering both flow fields and creating an expanding region of transition between them. The diversion of flow around the crack tip may be seen in Figures 19 and 20.

RUN NO. 7119-1. WAVE INTERACTION WITH 30-DEG CRACK

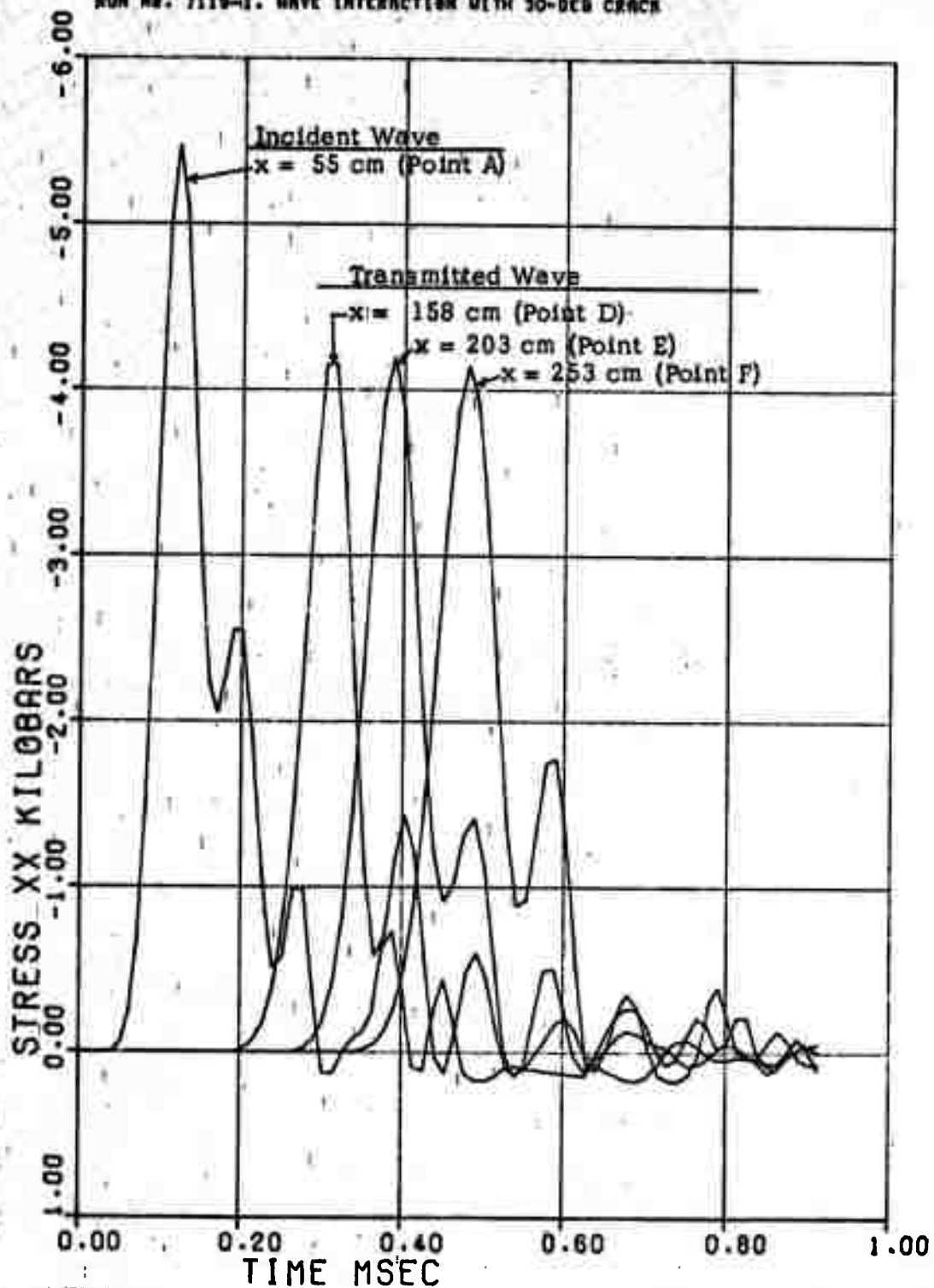


Figure 17. Stress (σ_x) Profiles at Four Stations Along the $y = 0$ Plane, Case 1.

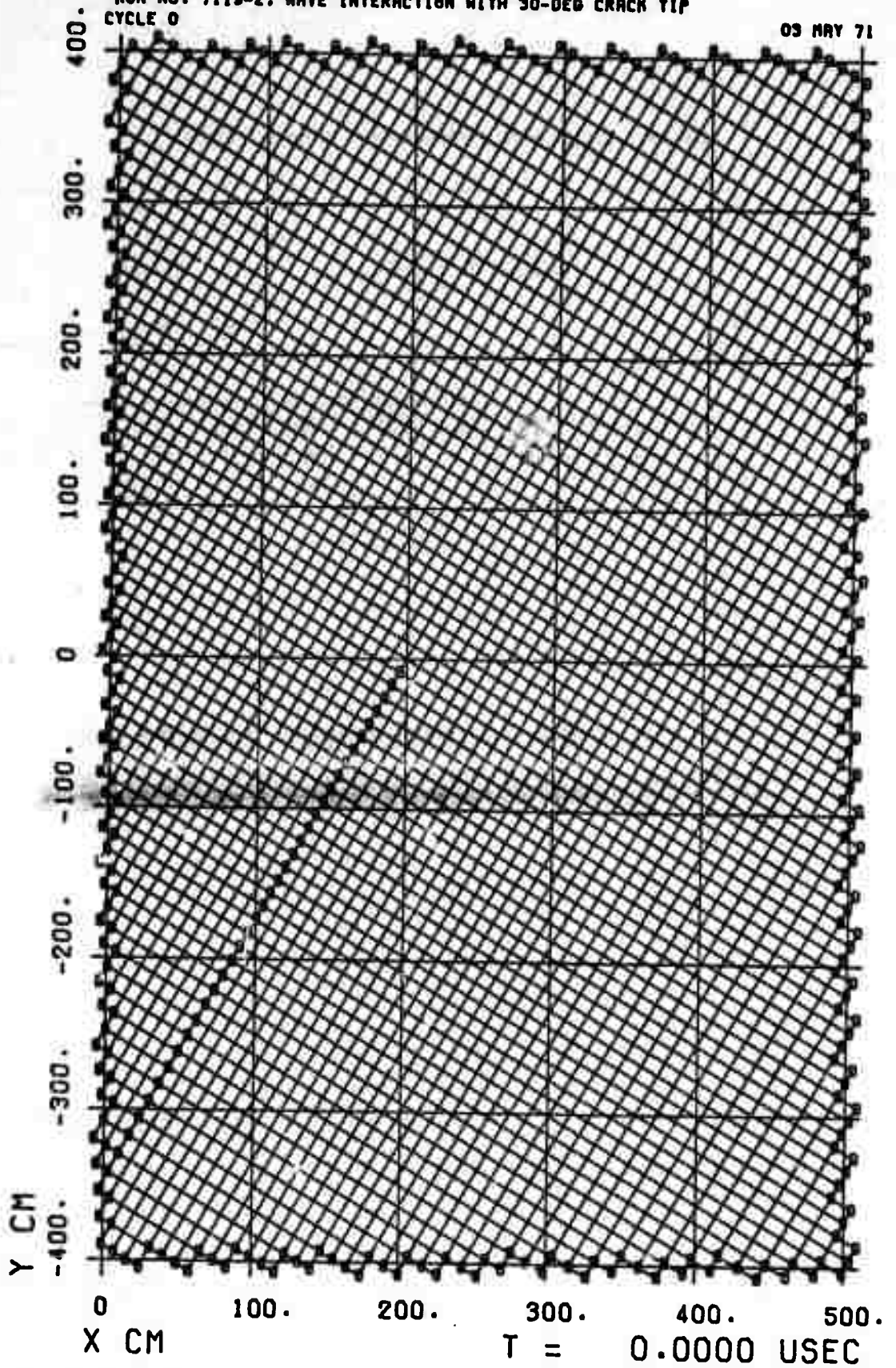


Figure 18. Initial Configuration of the Lagrangian Computational Grid, Case 2.

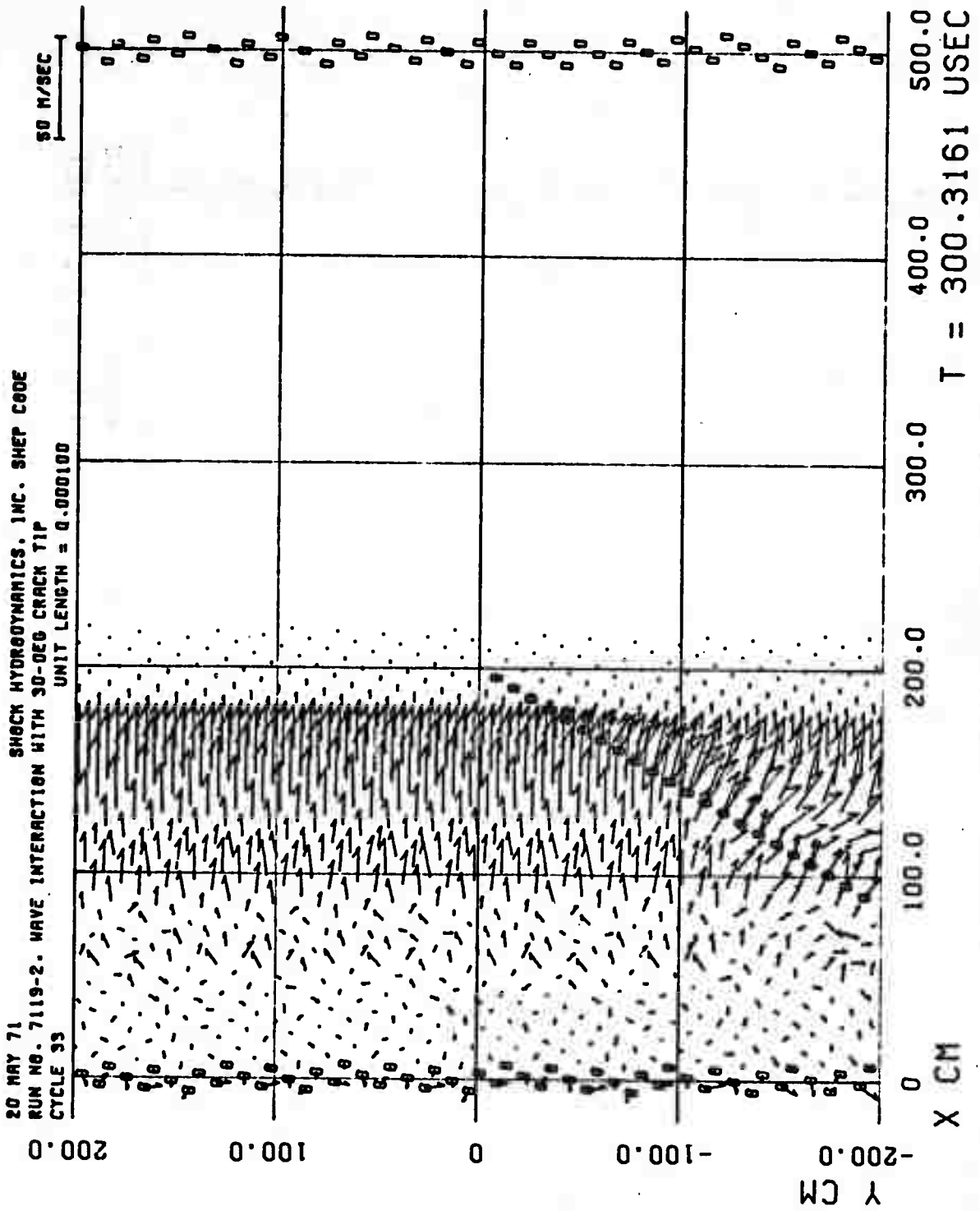


Figure 19. Particle Velocity Field, Case 2.

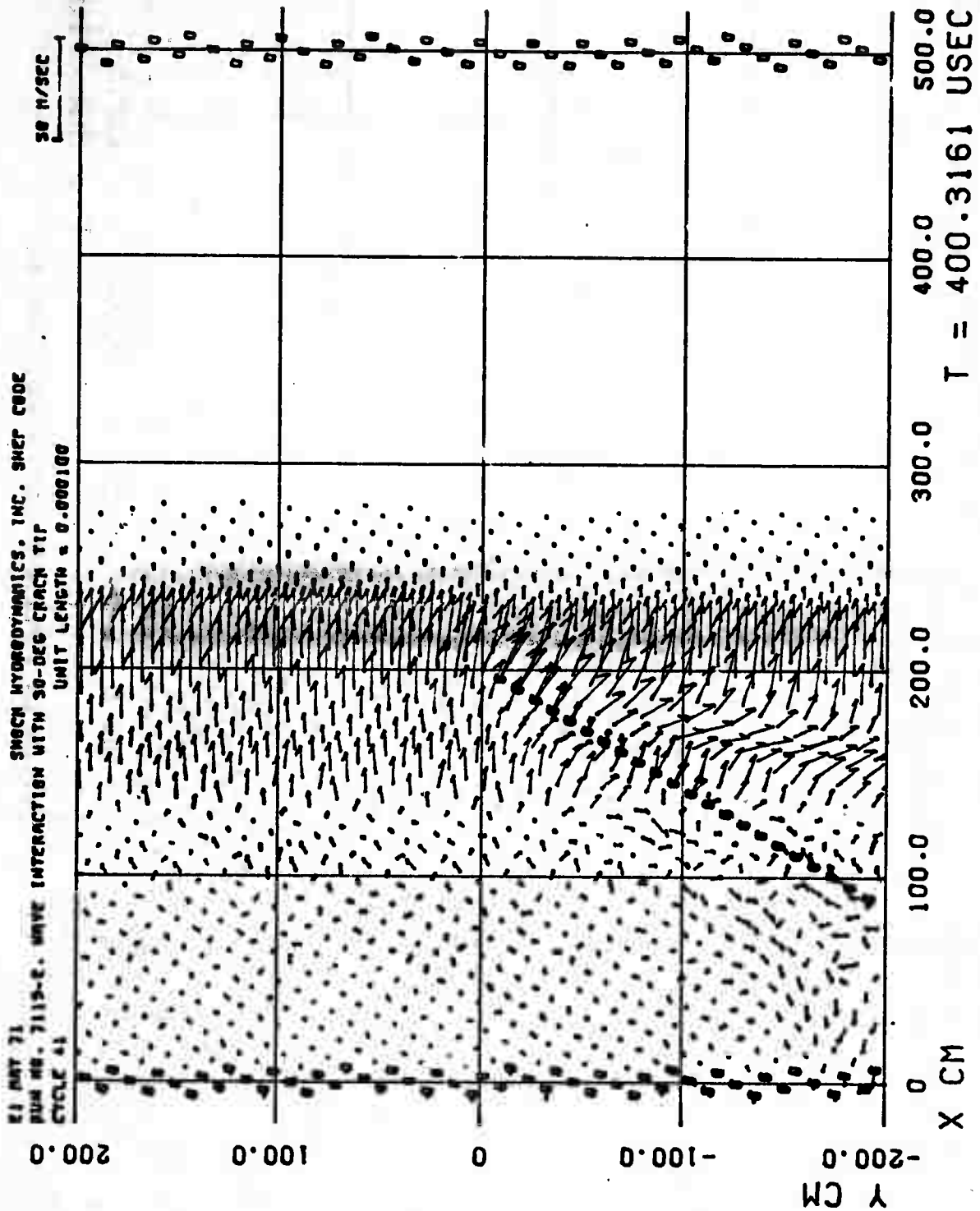


Figure 20. Particle Velocity Field, Case 2.

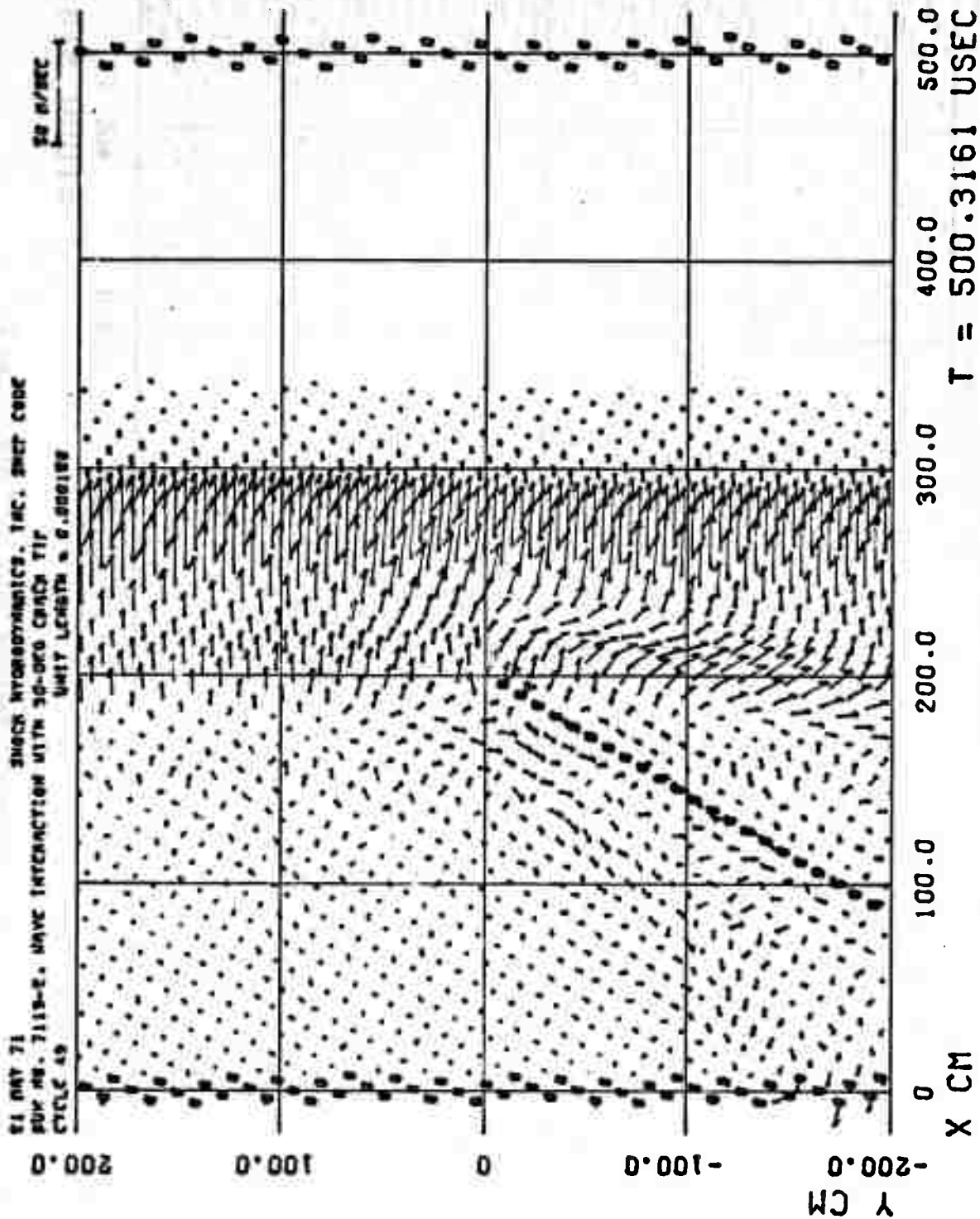


Figure 21. Particle Velocity Field, Case 2

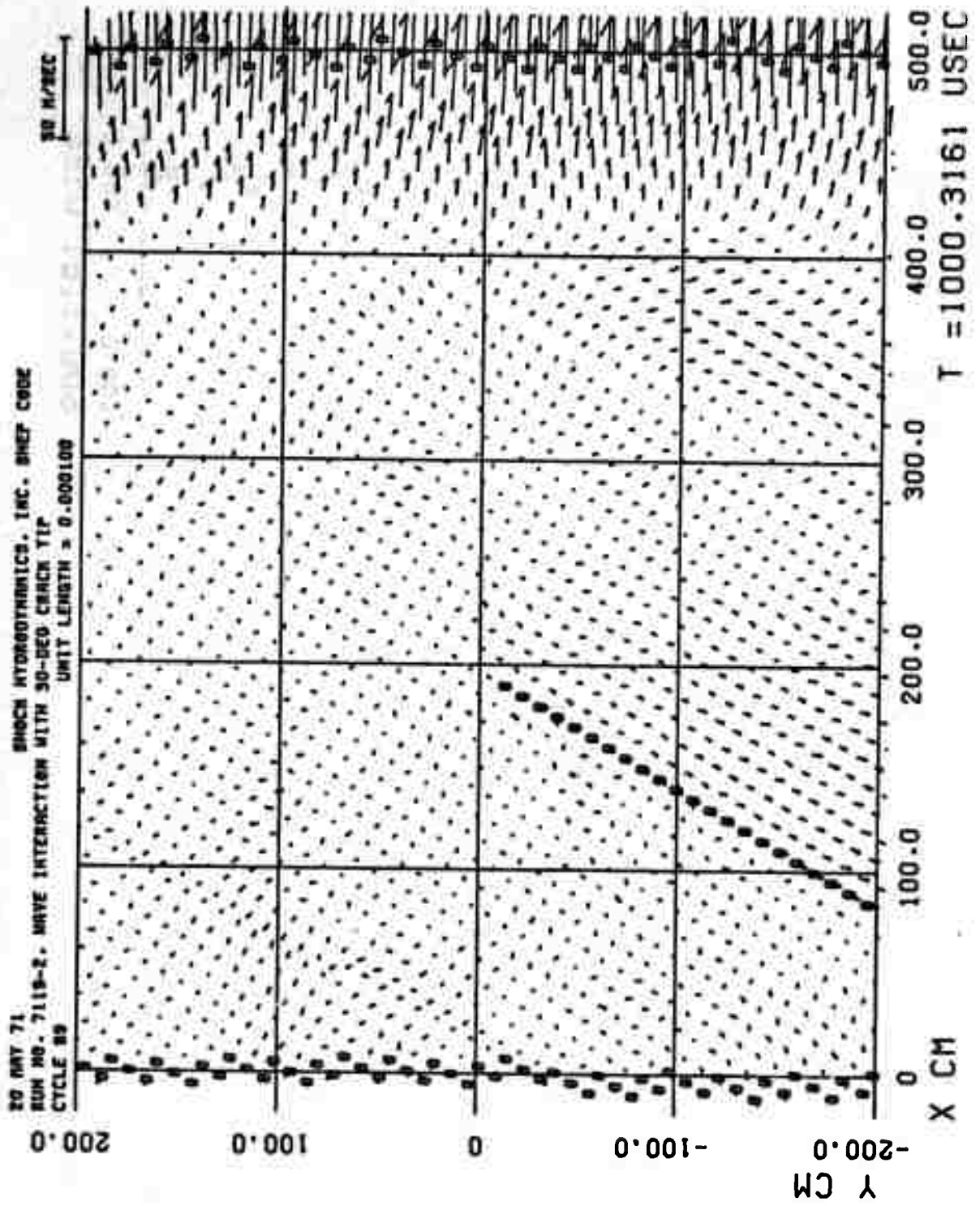


Figure 22. Particle Velocity Field, Case 2.

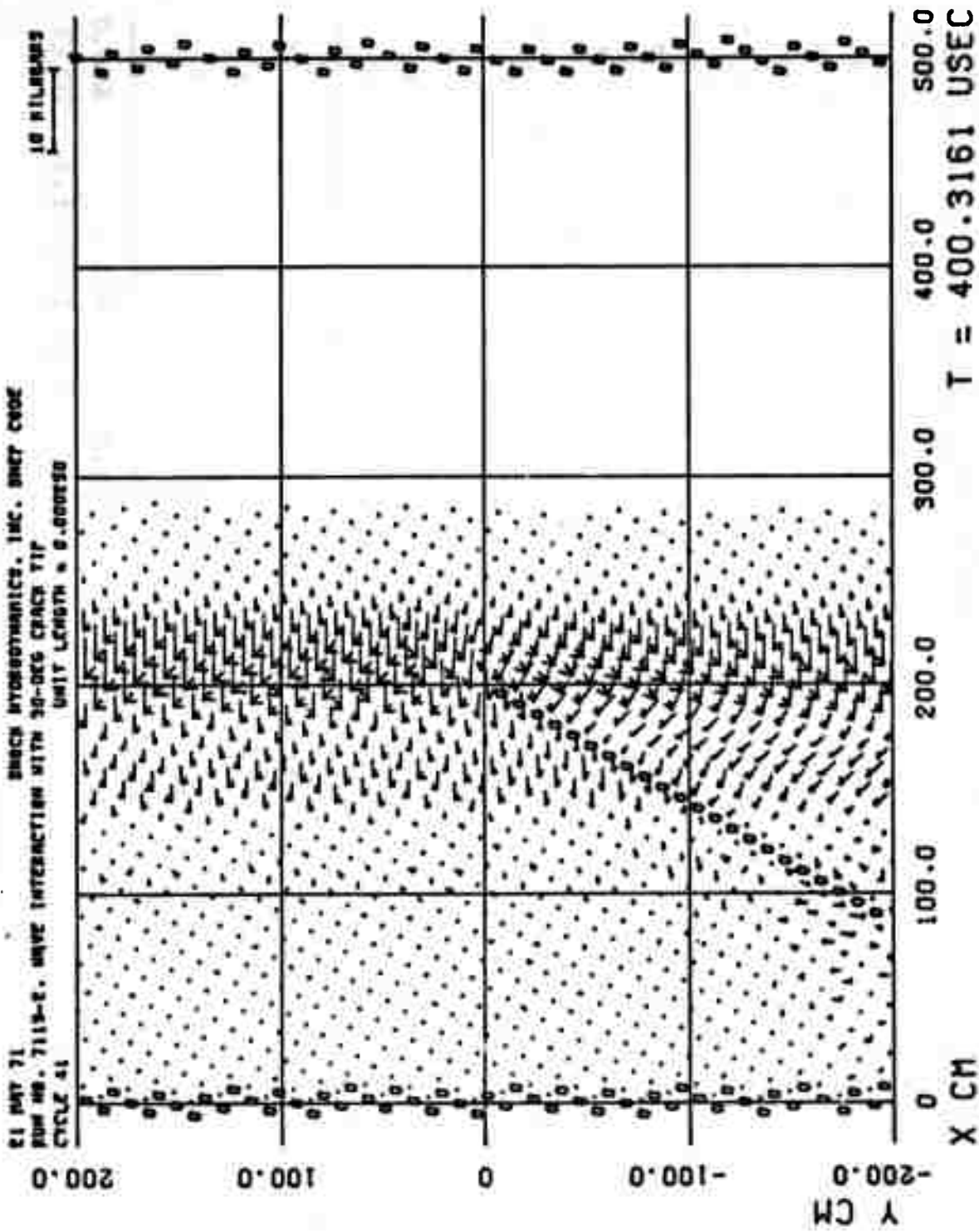


Figure 23. Principal Stress Field, Case 2.

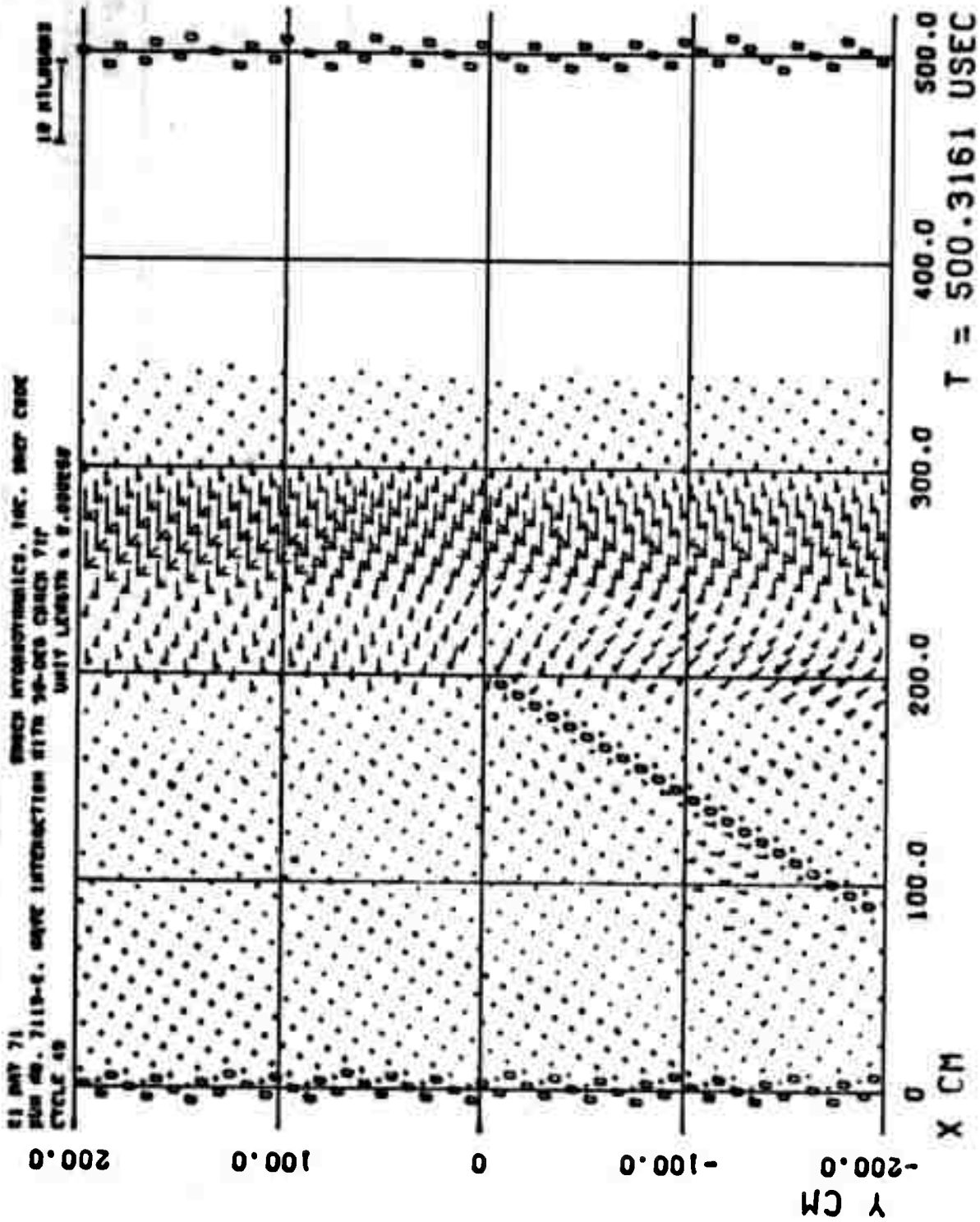


Figure 24. Principal Stress Field, Case 2.

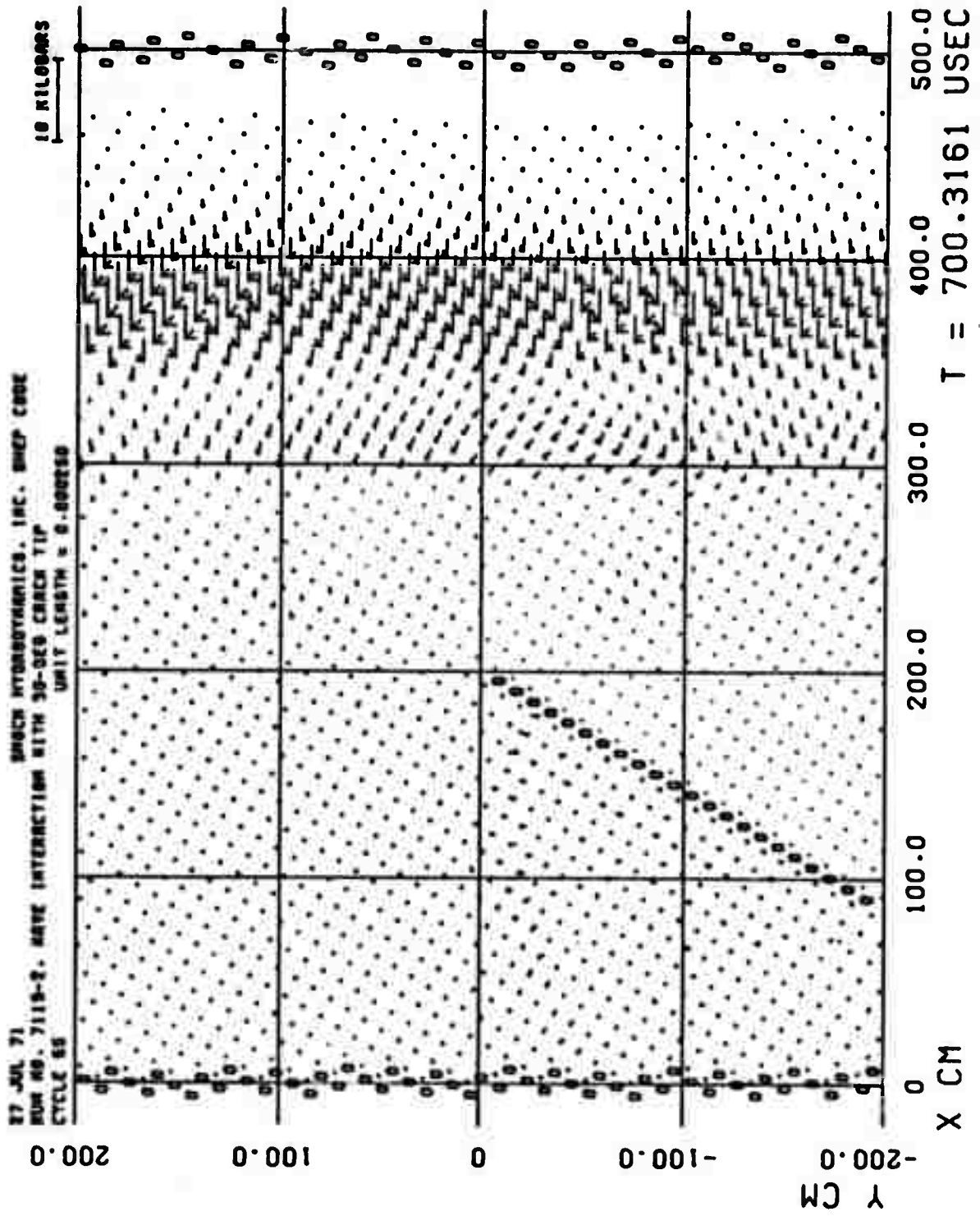


Figure 25. Principal Stress Field, Case 2.

Time histories of the material displacement at the locations indicated in Figure 26 were recorded during the code solution. The slippage of material at three points along the crack, as given by the distance between points on opposite sides of the crack, designated as (W,X), (R,S), and (M,N) in Figure 26, is shown in Figure 27. The material on the right side of the crack is moving downward and to the left, along the crack, relative to the material on the left side. The extents of the downward (y-direction) displacements of these points and the crack tip (point I) as a function of time are shown in Figure 28. The spatial trajectory of the point pair (W,X) on the crack surface during the time span of the solution is plotted in Figure 29. Time-histories of the vertical displacements of points above and below the crack tip along four vertical cuts ($x \approx \text{constant}$) through the target are shown in Figures 30 to 33. The downward shift of material persists at all these stations, but in smaller amounts as the distance from the crack increases.

Stress (σ_x) - time profiles at points H, I, J, and K, along the horizontal plane through the crack tip ($y \approx 0$), are shown in Figure 34. Note the increase in stress over that of the loading level near the crack tip. Stress profiles along the vertical plane through the crack tip ($x \approx 200$ cm) are shown in Figure 35. The points above the crack tip show a peak stress of 5 kb - corresponding to the loading or incident shock level, and those below the tip to about 4 kb - the transmitted stress level. Stress-time profiles along a vertical plane to the right of the crack tip, at $x \approx 300$ cm, are shown in Figure 36. Here the stress level is reduced at points above as well as below the crack tip. Time histories of the shear stress (σ_{xy}) at points along the vertical plane through the crack tip are shown in Figure 37.

3.5 CASE 3 - INTERACTION OF STRESS WAVE WITH SINGLE, FINITE-LENGTH CRACK, WITH CRACK GROWTH

For this case, the same problem as in Case 2 was solved, but with the provision in the code for permitting growth of the crack activated, as described previously.

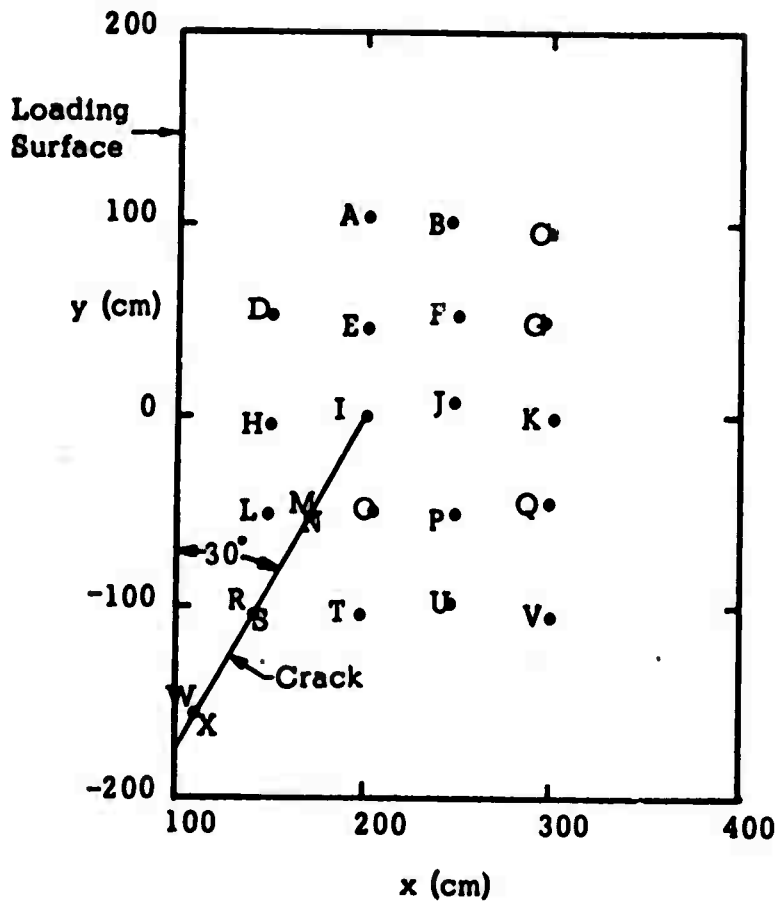


Figure 26. Locations of Time History Data Stations, Case 2.

RUN NO. 7119-2. WAVE INTERACTION WITH 30-DEG CRACK TIP

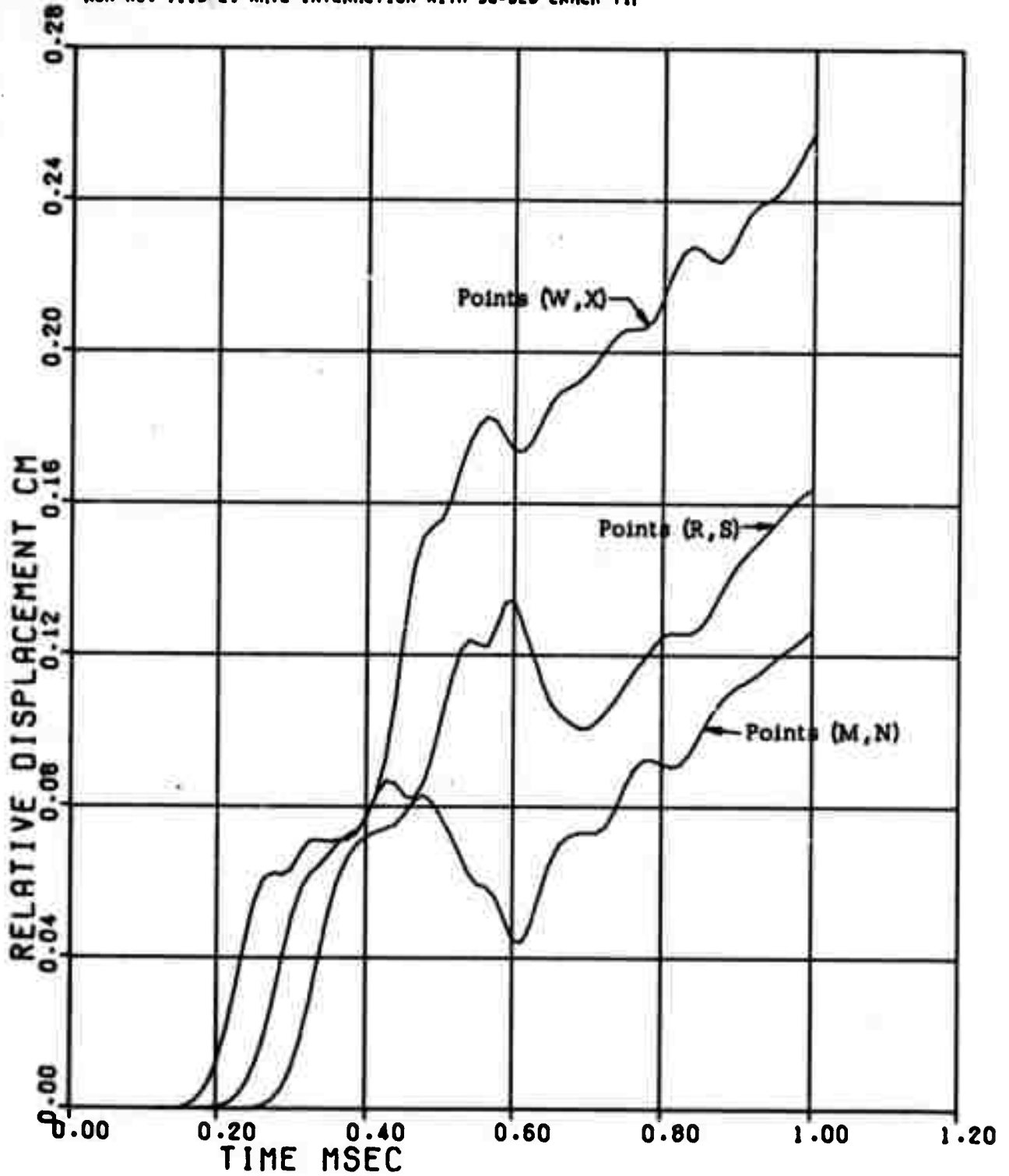


Figure 27. Material Slippage at Three Points Along the Crack, Case 2.

RUN NO. 7119-2. WAVE INTERACTION WITH 90-DEG CRACK TIP

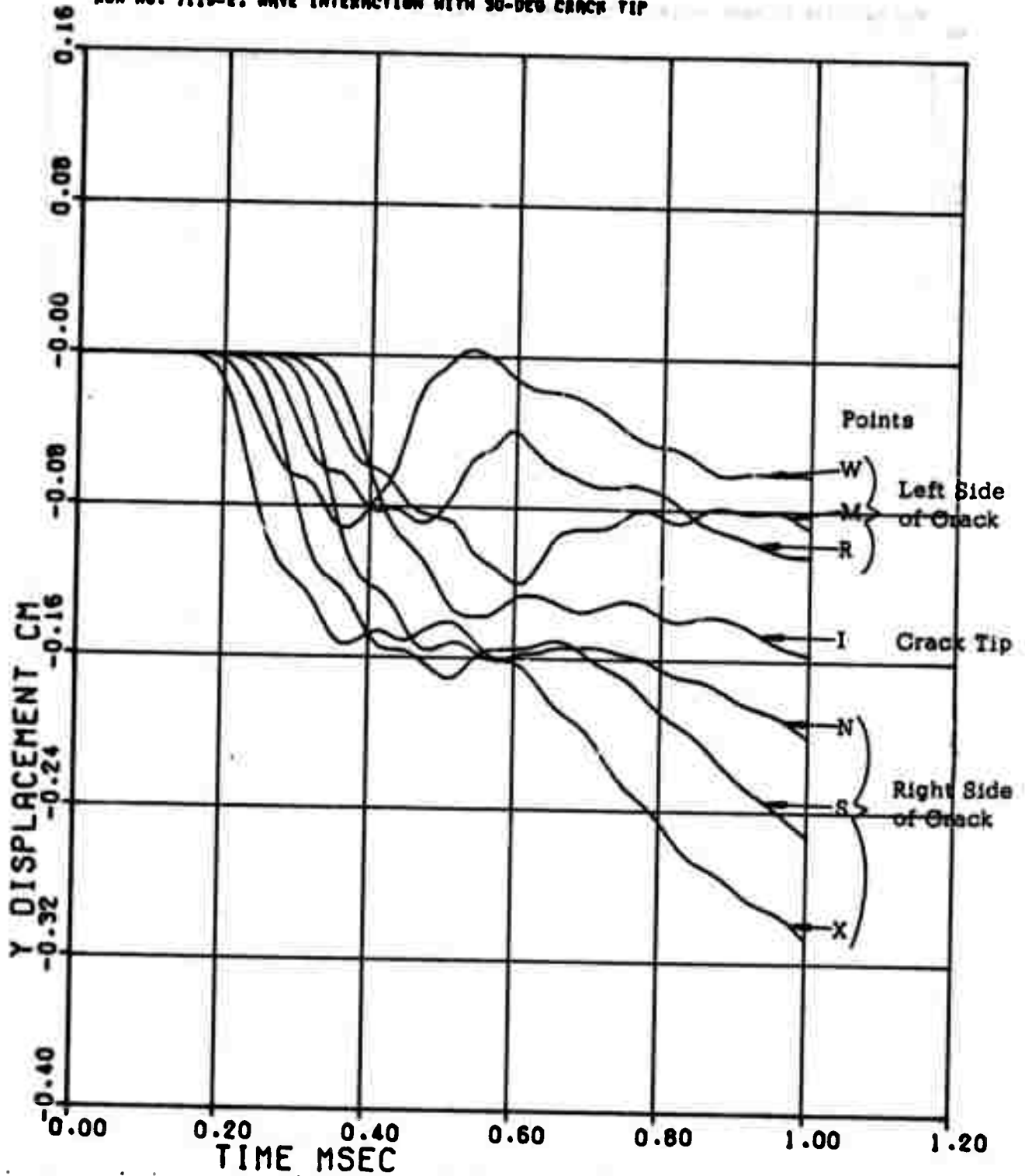


Figure 28. Vertical Displacement at Several Points Along the Crack, Case 2.

RUN NO. 7119-2. WAVE INTERACTION WITH 30-DEG CRACK TIP

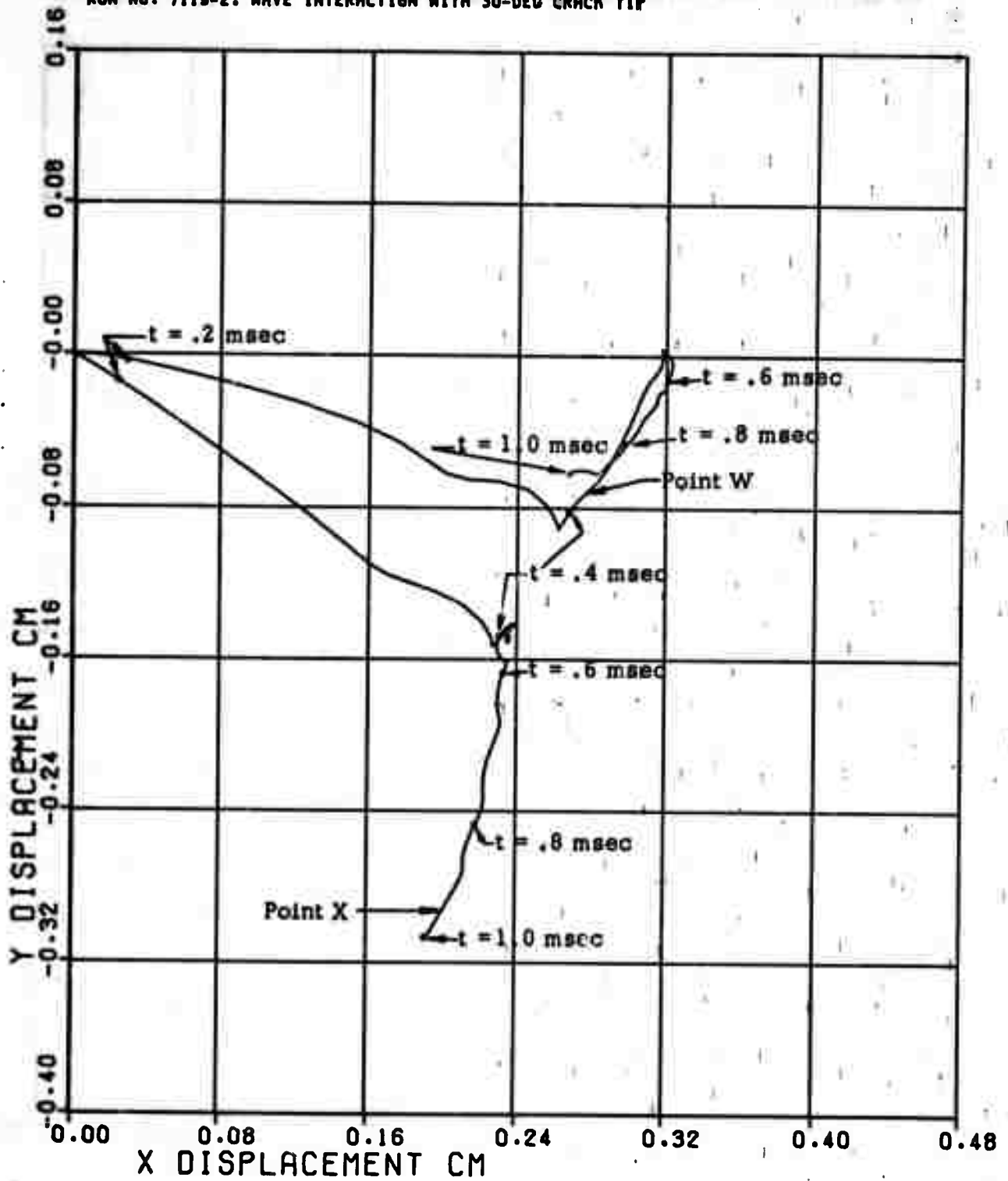


Figure 29. Spatial Trajectory of Two Initially Opposite Points on the Crack Surface, Case 2.

RUN NO. 7119-2. WAVE INTERACTION WITH 90-DEG CRACK TIP

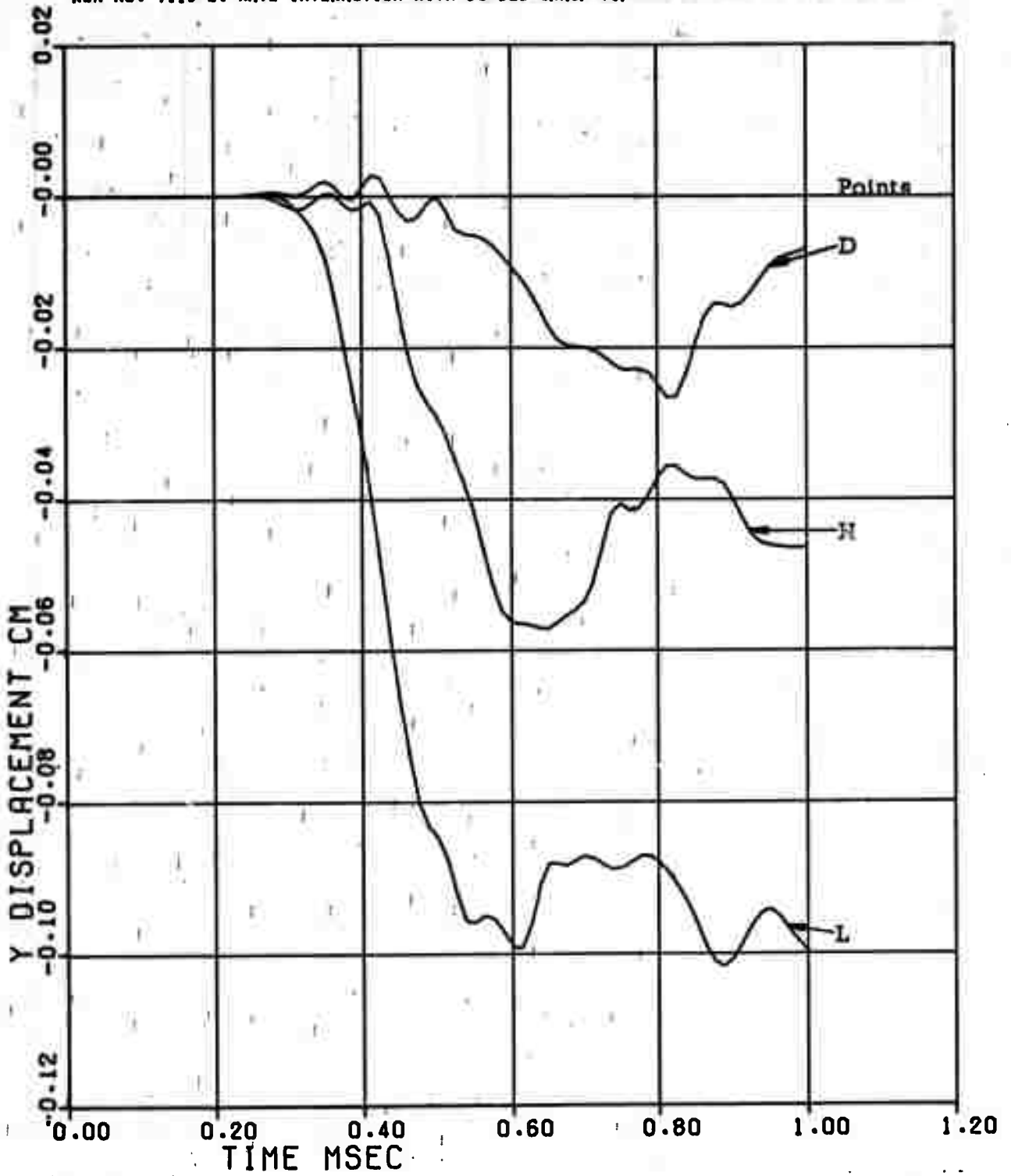


Figure 30. Vertical Displacement at Points Along the Vertical Plane at $x \approx 150$ cm, Case 2.

RUN NO. 7119-2. WAVE INTERACTION WITH 90-DEG CRACK TIP

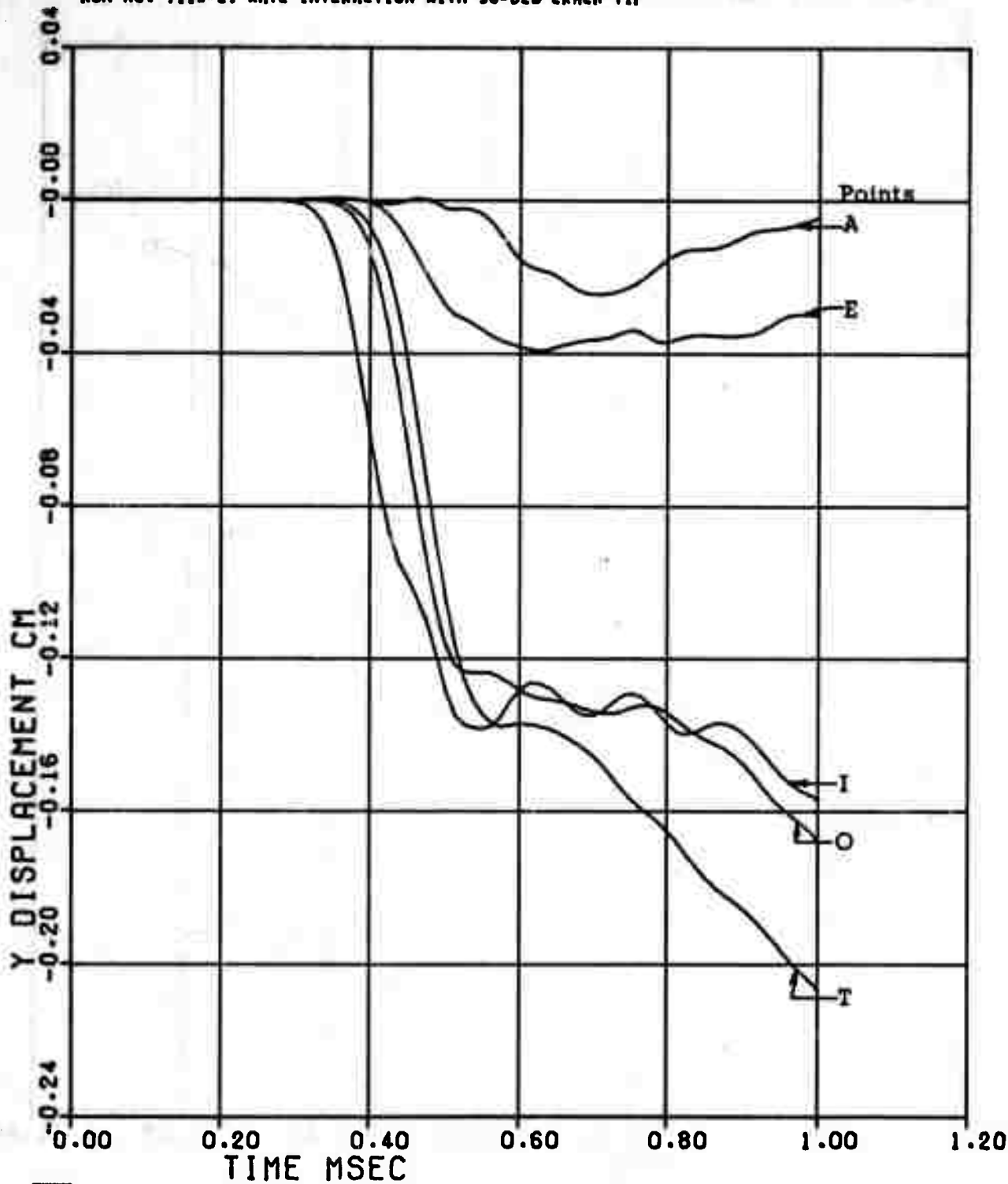


Figure 31. Vertical Displacement at Points Along the Vertical Plane at $x \approx 200$ cm, Case 2.

RUN NO. 7119-2. WAVE INTERACTION WITH 90-DEG CRACK TIP

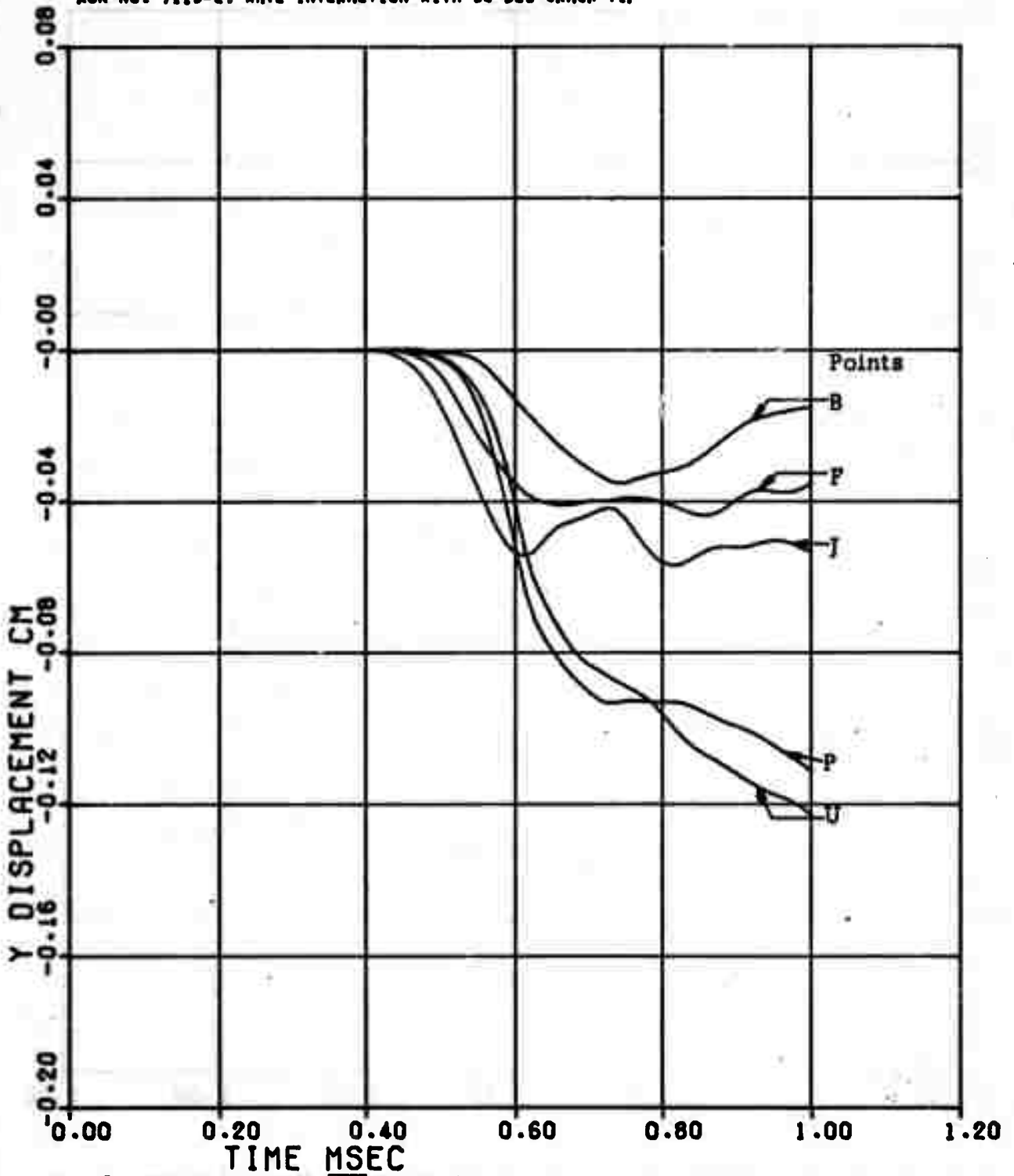


Figure 32. Vertical Displacement at Points Along the Vertical Plane, at $x \approx 250$ cm, Case 2.

RUN NO. 7119-2. WAVE INTERACTION WITH 30-DEG CRACK TIP

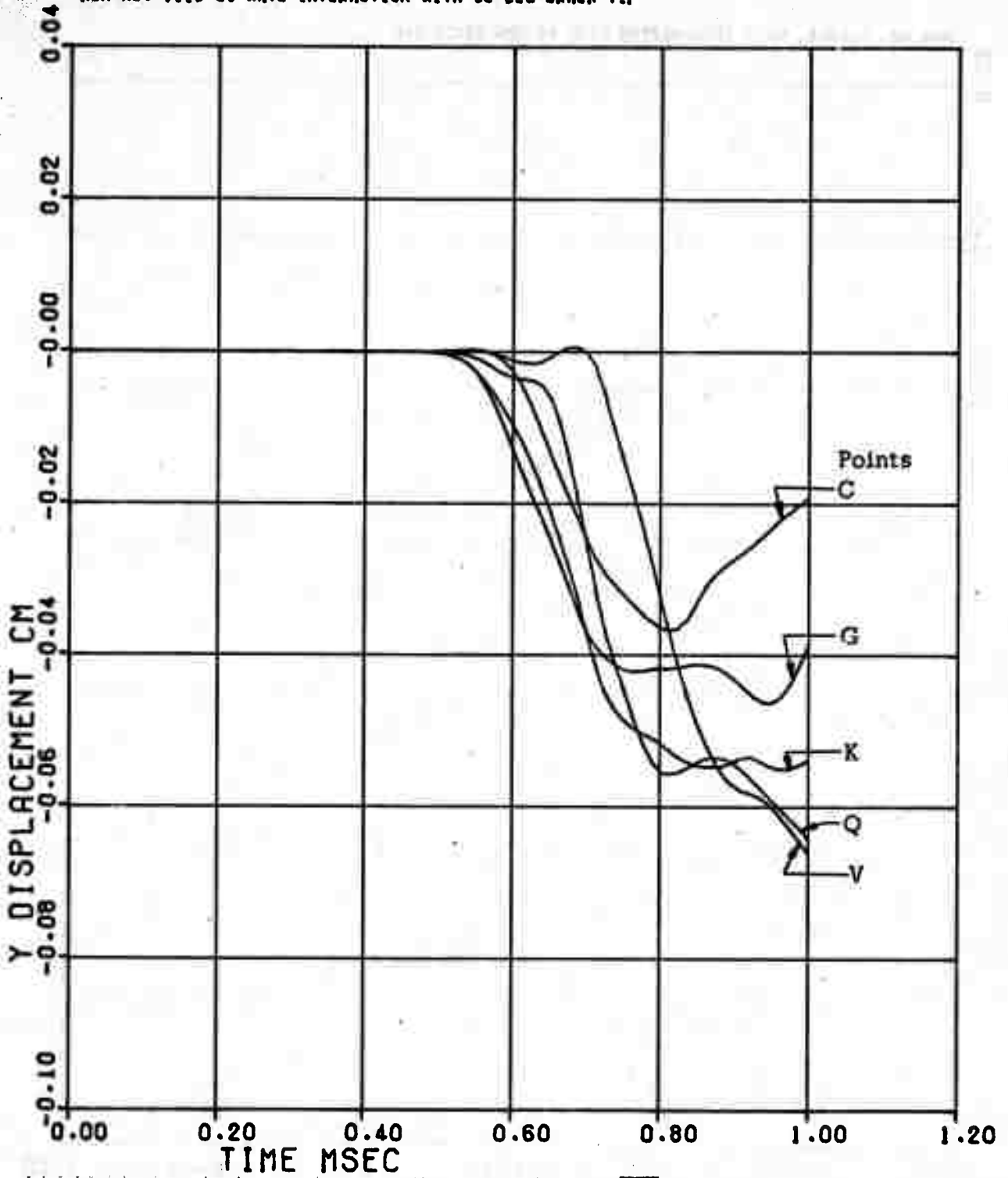


Figure 33. Vertical Displacement at Points Along the Vertical Plane at $x \approx 300$ cm, Case 2.

RUN NO. 7119-2. WAVE INTERACTION WITH 90-DEG CRACK TIP

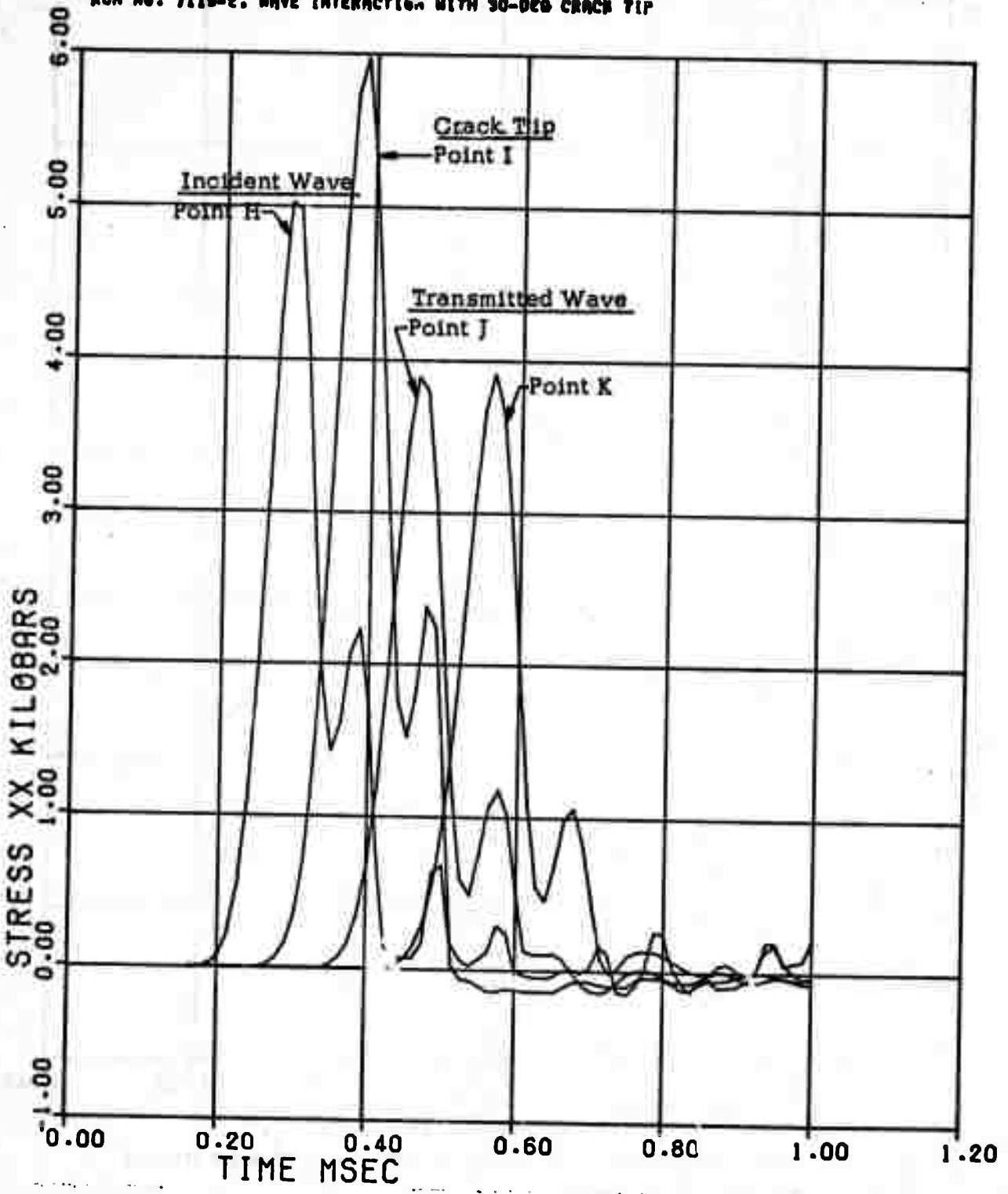


Figure 34. Stress (σ_x) Profiles at Points Along the Horizontal Plane at $y \approx 0$, Case 2.

RUN NO. 7119-2. WAVE INTERACTION WITH 90-DEG CRACK TIP

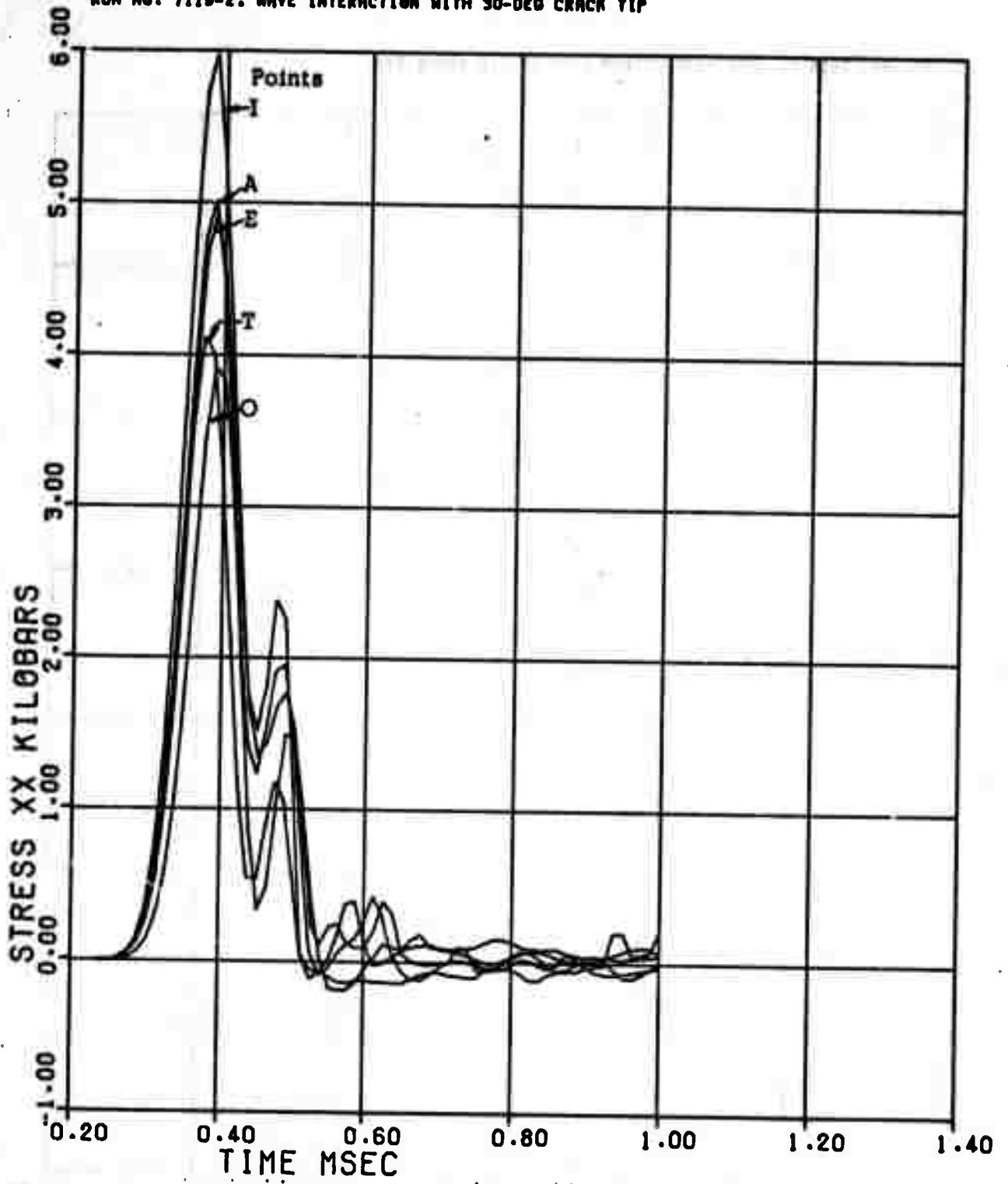


Figure 35. Stress (σ_x) Profiles at Points Along the Vertical Plane at $x \approx 200$ cm, Case 2.

RUN NO. 7119-2. WAVE INTERACTION WITH 90-DEG CRACK TIP

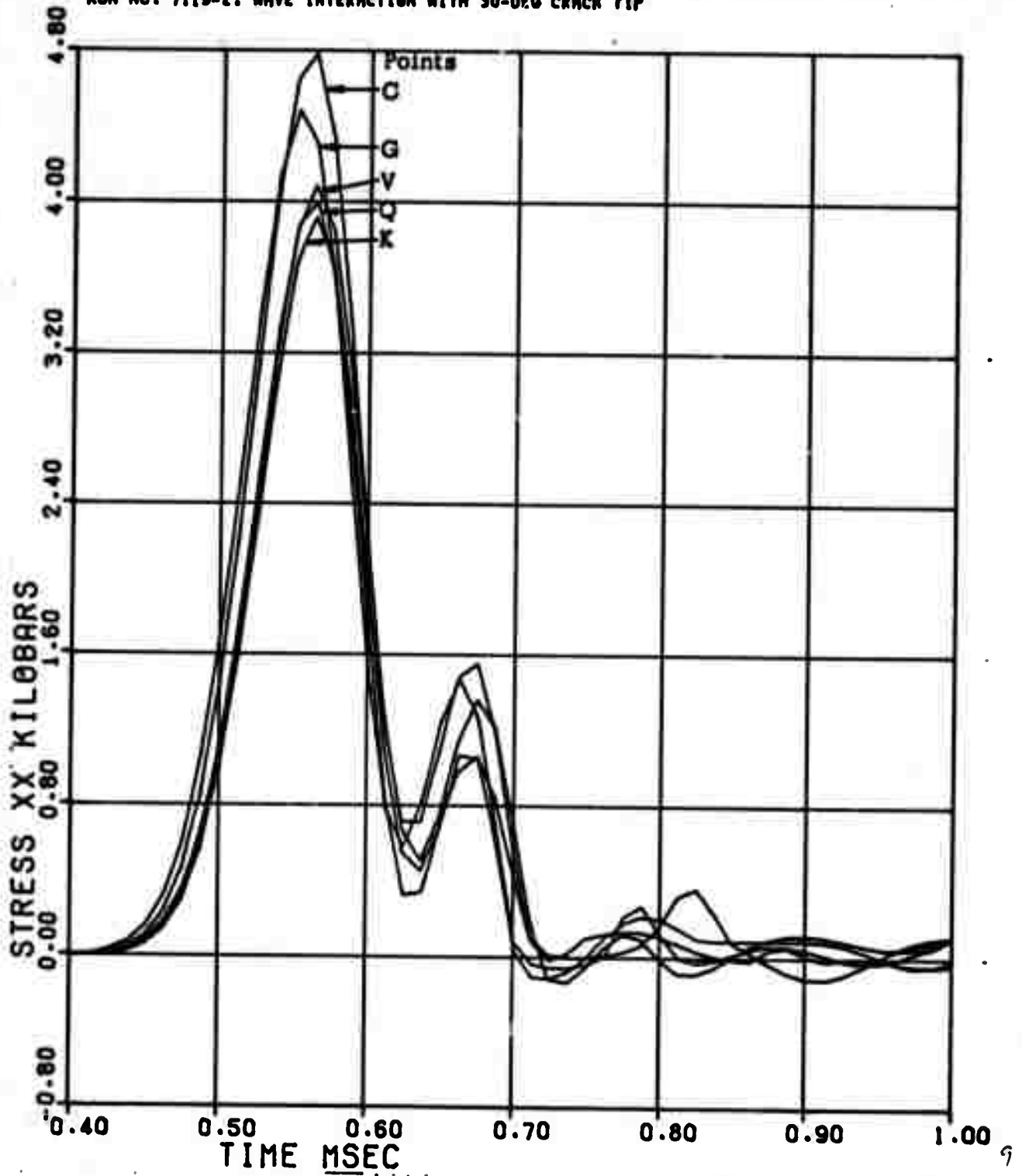


Figure 36. Stress (σ_x) Profiles at Points Along the Vertical Plane at $x \approx 300$ cm, Case 2.

RUN NO. 7119-2. WAVE INTERACTION WITH 90-DEG CRACK TIP

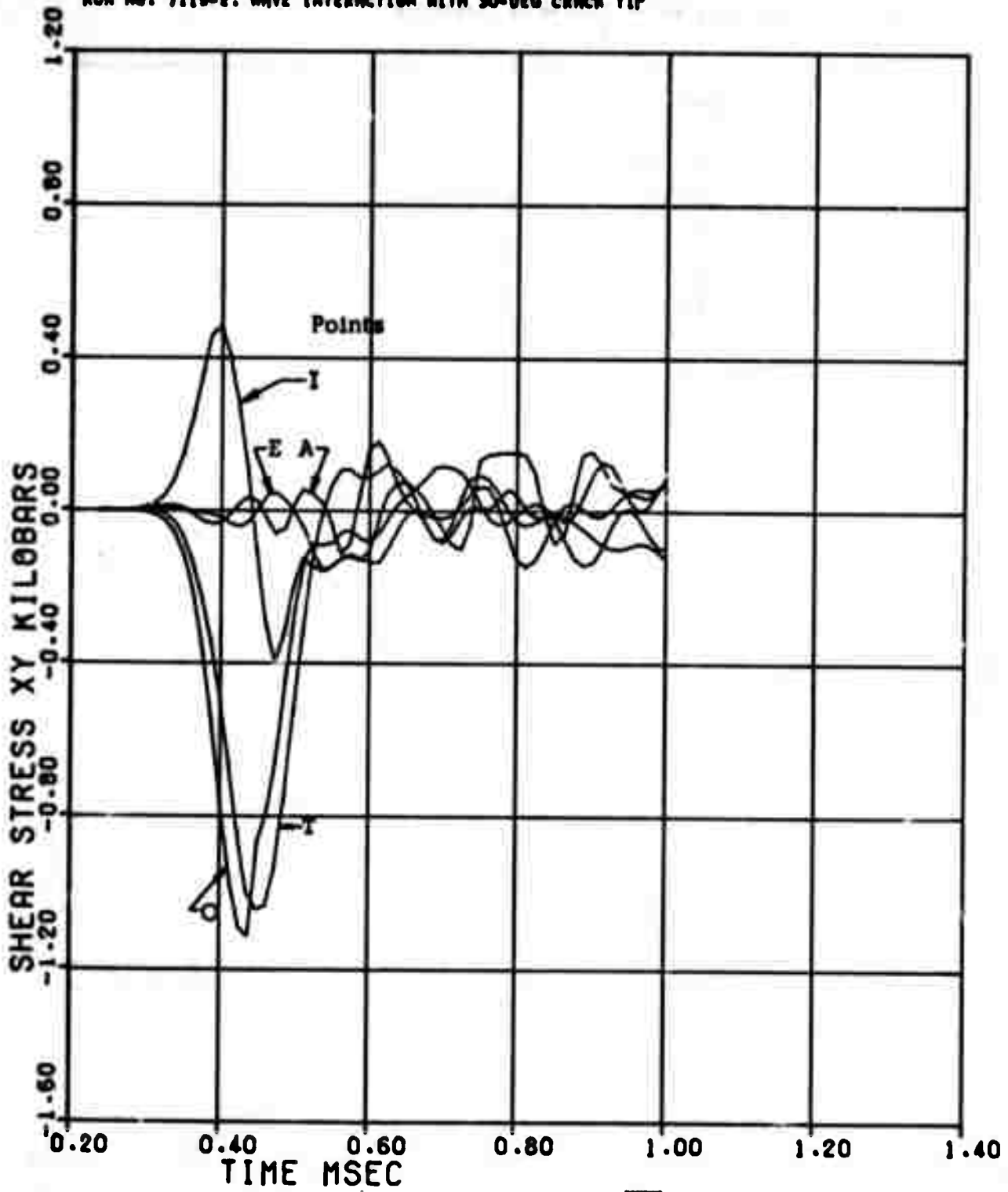


Figure 37. Shear Stress (Q_{xy}) Profiles at Points Along the Vertical Plane at $x \approx 200$ cm, Case 2.

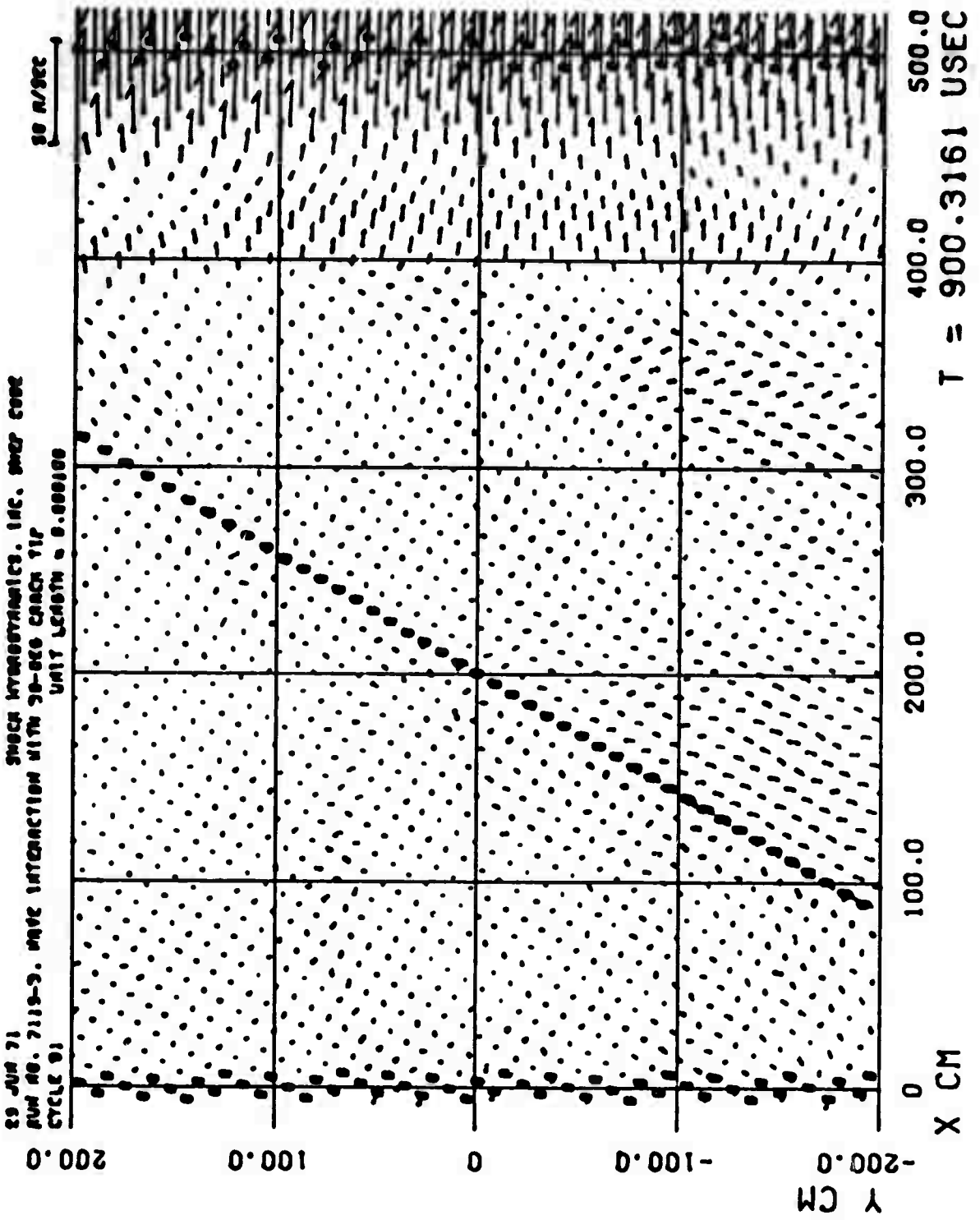


Figure 38a Particle Velocity Field, Case 3.

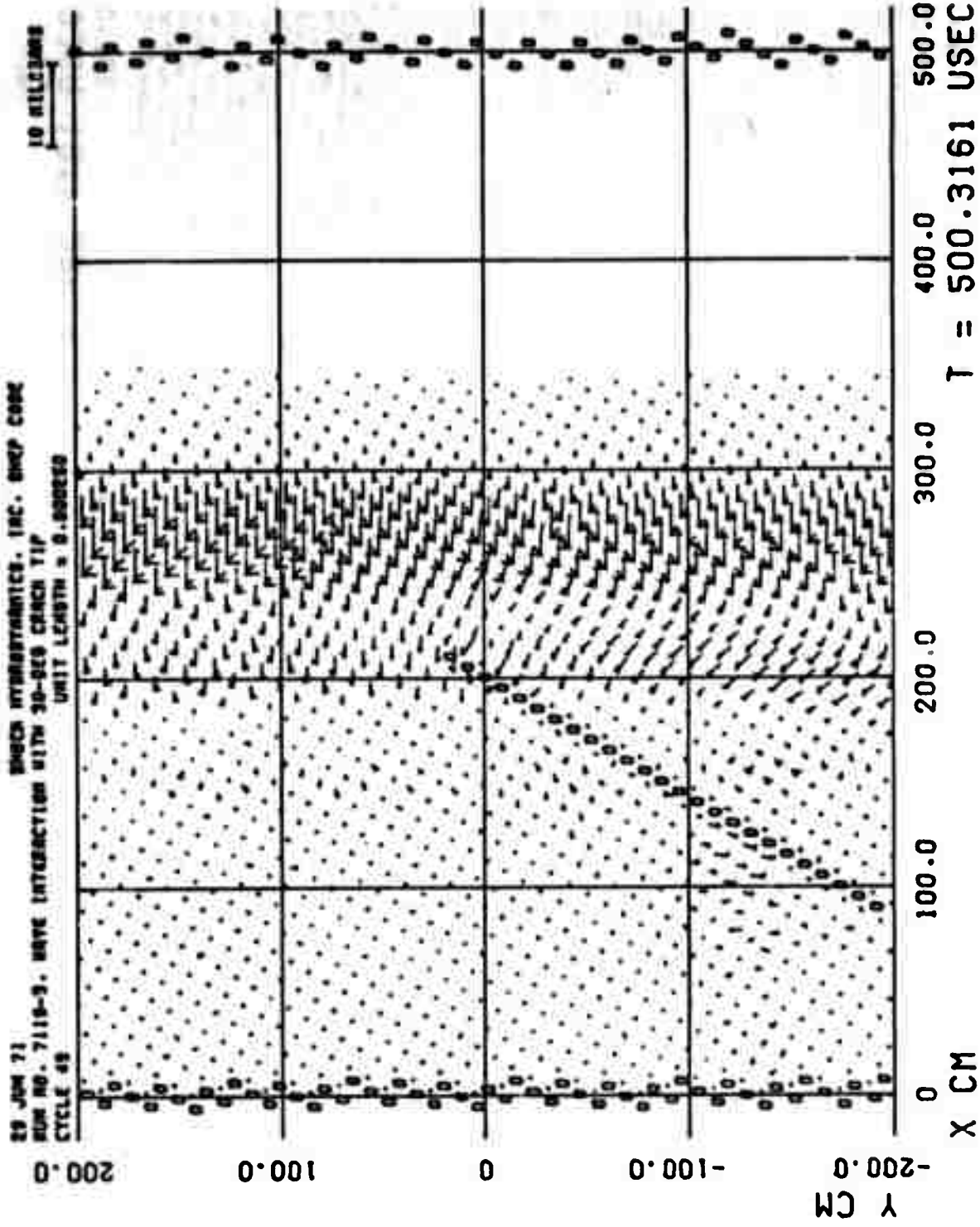


Figure 39. Principal Stress Field, Case 3.

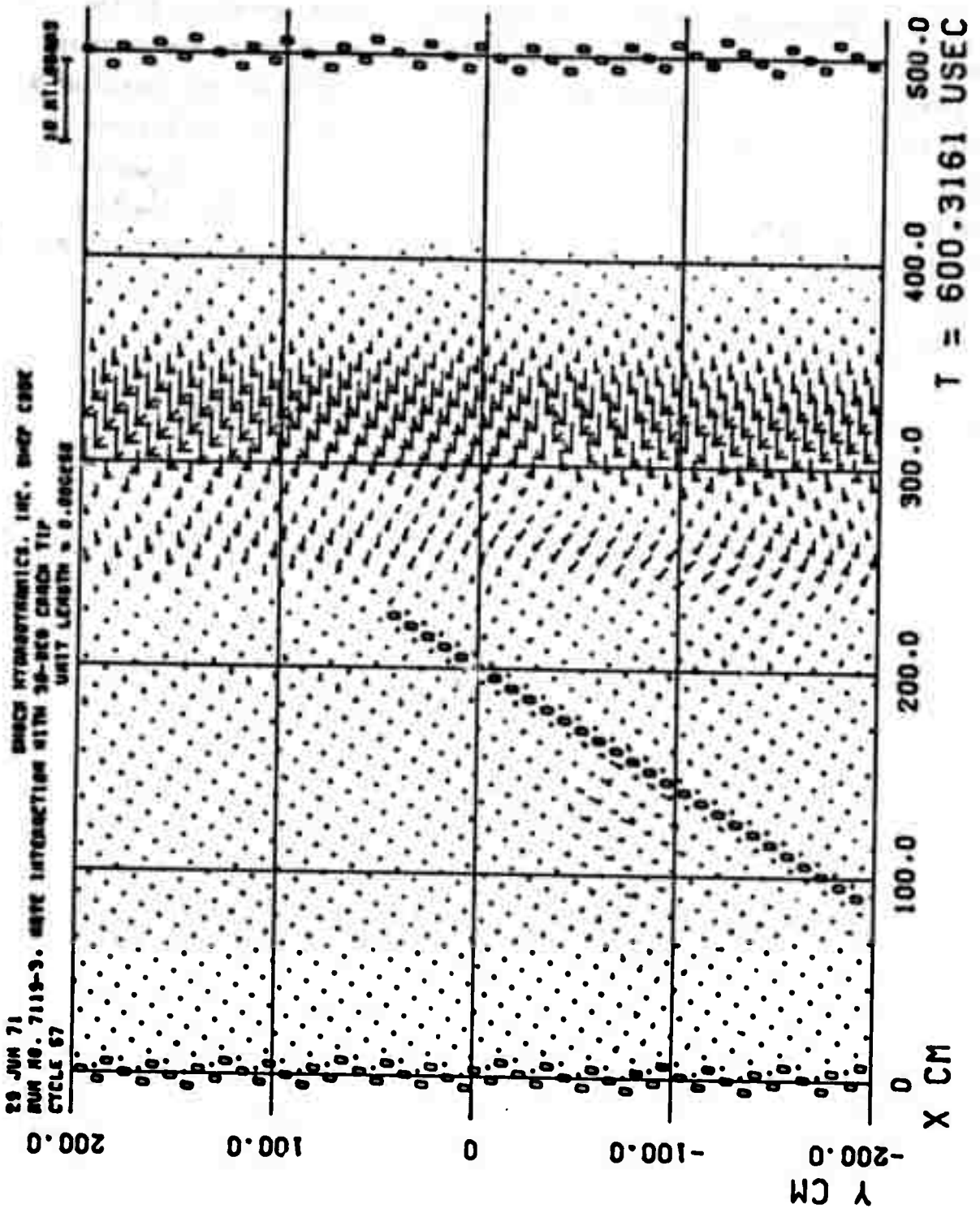


Figure 40. Principal Stress Field, Case 3.

Representative results of this code solution, as shown by the particle velocity fields for times of .5, .6, .7, and .9 msec, are given in Figures 5 to 7 in the Summary, Section 2.3.1, and in Figure 38. Associated principal stress fields for times of .5 and .6 msec are shown in Figures 39 and 40. Propagation of the crack does occur for this loading; the extent of the crack at any time is indicated by the circled lattice points. For this loading function, the fracture criterion used was met at relatively late times after the shock front has passed, so that the effect of crack growth on the transmitted wave is not large.

4. ANTIPLANE SHEAR LOADING OF A STATIONARY CRACK

4.1 FORMULATION

The antiplane shear loading of a crack results in equal and opposite out-of-plane displacements in the quarter planes adjacent to each of the two sides of the crack. When this type of shear loading is applied to a crack surface, no in-plane displacement components are generated. The one out-of-plane displacement component is then governed by D' Alembert's equation:

$$\square w \equiv w_{ss} - \Delta w = 0 \quad (4)$$

where

$$s = ct \quad (5)$$

$$c = \sqrt{\frac{G}{\rho}} \quad (6)$$

An immediate advantage thus accrues in dealing with an out-of-plane problem; namely the solution can be expressed in harmonic functions rather than biharmonic functions. In addition, the only elasto-dynamic solutions that are currently available for an accelerating crack are those of Kostrov⁷, Eshelby,⁸ and Achenbach⁹. Because of these advantages, it was decided to modify the SHEP code to include computations for the two out-of-plane shear stress components and the one out-of-plane displacement component,

all three of which depend only on the in-plane coordinates. The governing equations are as follows:

$$\frac{\partial \sigma_{xz}}{\partial x} + \frac{\partial \sigma_{yz}}{\partial y} + \frac{\sigma_{yz}}{y} |^* = \rho_0 \ddot{w} \quad (7)$$

$$\dot{\mathbf{E}} = -(P+q) \dot{\mathbf{V}} + \mathbf{V} [(\vec{\tau}_D + \vec{q}_D) : \nabla \vec{q}] \quad (8)$$

$$\dot{\vec{\tau}}_D = \frac{G}{2} (\nabla \vec{q} + \vec{q} \nabla) \quad (9)$$

$$\dot{\vec{q}}_D = \frac{\eta}{2} (\nabla \vec{q} + \vec{q} \nabla) \quad (10)$$

where

G is the shear modulus

and

η is the linear fictive viscosity, taken to be proportional to the mesh size.

The difference form of these equations follows the same format as used by the rest of SHEP. The form of the Jauman-Oldroyd derivative is given in the Appendix.

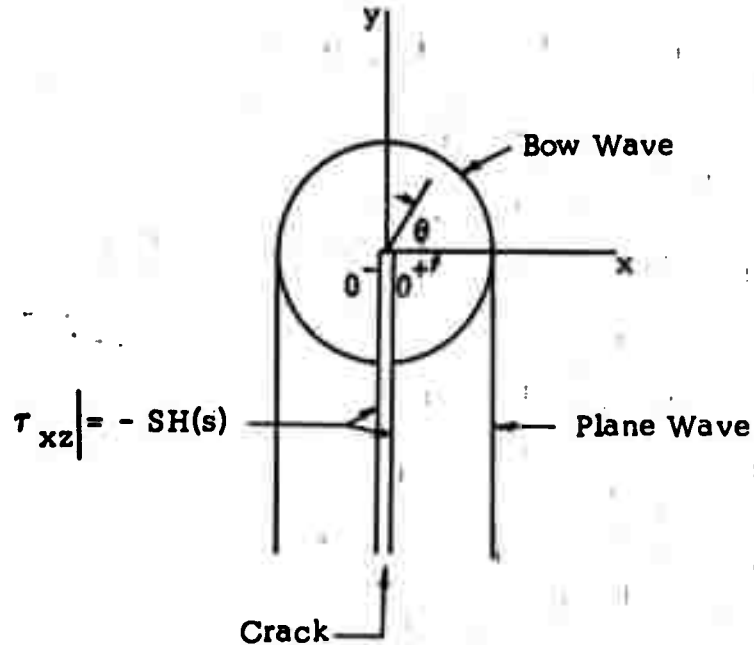
4.2 ANALYSIS

In order to check out the validity of the computer code, it is mandatory to compare the computational results with one or more analytical solutions. The most convenient solution available for this purpose is that which describes the propagation of an out-of-plane (antiplane) shear wave emanating from a uniformly loaded crack. In the following, the out-of-plane solution is presented and used to check out the corresponding code solution that was performed for this problem.

Consider an infinite elastic space perforated by a semi-infinite crack surface lying at $[x = 0, -\infty < y \leq 0]$. To the crack surfaces $x = 0^+$ and $x = 0^-$, we apply a step load in time uniformly distributed, namely

$$\tau_{xz} \Big|_{x=0} = -SH(s) \quad (11)$$

The loading situation and associated waves are shown in the following sketch:



The plane $[x = 0, 0 \leq y < \infty]$ is a plane of antisymmetry, on which the out-of-plane displacement w is zero. In the right half-space the displacement is positive, or out-of-the-paper, and vice versa.

This problem is a standard one in wave propagation theory and is readily solved by the Wiener-Hopf technique and the Cagniard method. It can also be treated by the method of characteristics and the theory of Abelian integrals. In either event, one arrives at the solution:

$$\frac{G}{S} w_{\pm}^B = \frac{1}{\pi} \left\{ \sqrt{2r(s-r)} \left(\cos \frac{\theta}{2} - \operatorname{sn} \frac{\theta}{2} \right) - (s + r \cos \theta) \arctan \sqrt{\frac{\frac{s}{r} - 1}{1 + \cos \theta}} \right. \\ \left. \pm (s - r \cos \theta) \arctan \sqrt{\frac{\frac{s}{r} - 1}{1 - \cos \theta}} \right\} \quad (12)$$

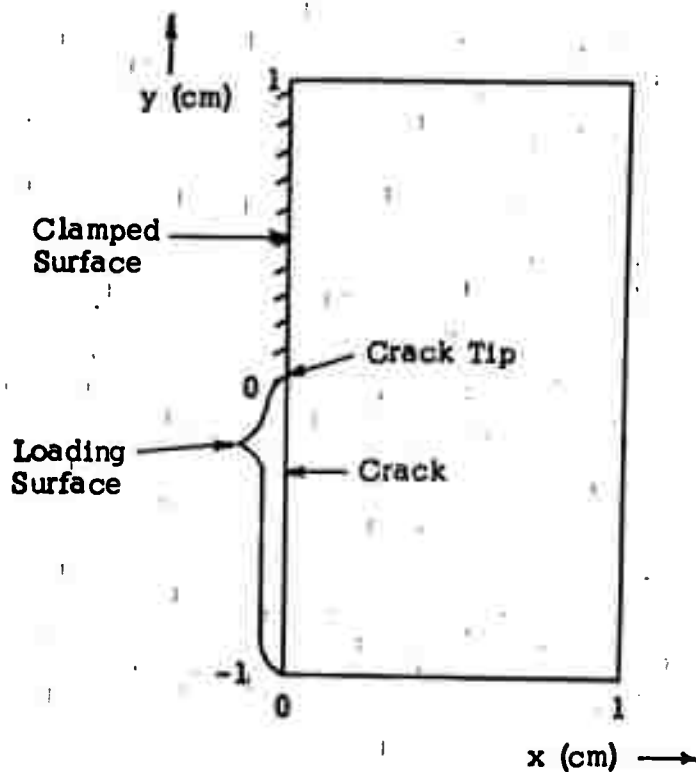
where \pm denotes θ positive or negative respectively, superscript B denotes the bow wave contribution, and r is the radial distance from the crack tip. The total solution is given by

$$\frac{\underline{\text{Total}}}{s} w_-^T = \frac{\underline{\text{Bow Wave}}}{s} w_-^B + \frac{\underline{\text{Plane Wave}}}{(s-x) H(s-x)} \quad (13)$$

$$\frac{s/G}{s} w_+^T = \frac{s/G}{s} w_+^B \quad (14)$$

4.3 NUMERICAL SOLUTION

A SHEP code run was set up for this problem using a grid containing 5000 cells of uniform size. The sample body was taken to be 1 cm in the x direction and ± 1 cm in the y direction, as shown in the following sketch:



Geometry for SHEP Code Run

Since the problem is antisymmetric, it is sufficient to compute the wave propagation in just one-half of the body and impose the boundary condition that the displacement is zero along the plane $x = 0$, $y \geq 0$, above the crack tip.

The material was characterized by a density = 2 gm/cm^3 and a shear modulus = 100 kb . The crack was loaded uniformly with a shear stress, τ_{xz} , of -1 kb .

With the analytic solution in hand, it is convenient to perform a number of checks on the computational solution. We have the following derived relations for the displacement or stress at three angles:

$$\frac{G}{S} \frac{w}{s} \Big|_{\theta = -\frac{\pi}{r}} = 1 + \frac{2}{\pi} \left\{ \sqrt{\frac{r}{s} \left(1 - \frac{r}{s}\right)} - \arctan \sqrt{\frac{s}{r} - 1} \right\} \quad (15)$$

$$\frac{\tau_{xz}}{S} \Big|_{\theta = +\frac{\pi}{2}} = \frac{2}{\pi} \left\{ \sqrt{\frac{s}{r} - 1} - \arctan \sqrt{\frac{s}{r} - 1} \right\} \quad (16)$$

$$\frac{\tau_{xz} + \tau_{yz}}{S} \Big|_{\theta = 0} = -\frac{1}{2} - \frac{1}{\pi} \arctan \sqrt{\frac{s}{r} - 1} \quad (17)$$

In addition, we have the relations:

$$P_B = \frac{S^2 c}{G} \frac{s}{2} \quad (18)$$

$$P_P = \frac{S^2 c}{G} (d_0 - s) \quad (19)$$

where P denotes the rate of work (power input) done on the body. In Eqns. (15 - 17) we note that the right-hand sides are all functions of $\left(\frac{s}{r}\right)$. This is so because there is no length-scale in the problem.

Figures 41, 42, and 43 show respectively plots of Eqn. (15), (16), and (17) versus $\frac{r}{s}$, the fractional distance to the wavefront, along with the corresponding results from the code solution. Excellent agreement is noted in all three cases.

The computer program also tabulates the total strain plus kinetic energy, the time rate of change of which is equal to the power input. At the time the bow wave has filled the sample body, the tabulated rate of energy change was 1.112×10^6 (ergs/cm)/ μ sec, in excellent agreement with the theoretical computed power input of 1.113×10^6 (ergs/cm)/ μ sec.

In Figure 44, we show the stress field at the time at which the bow wave has just about filled the sample body. At each field point is plotted a vector equal in magnitude to

$$M = \sqrt{\left(\frac{\tau_{xz}}{s}\right)^2 + \left(\frac{\tau_{yz}}{s}\right)^2} \quad (20)$$

and having a phase angle equal to

$$\varphi = \arctan \frac{\tau_{xz}}{\tau_{yz}} \quad (21)$$

Thus the field vectors are given by:

$$V = M e^{i\varphi} \quad (22)$$

One can clearly see the position of the plane and bow waves. In the plot, the front of the plane wave appears to have advanced a distance beyond the theoretical value of 1. This is due to the non-dissipative artificial viscosity terms used in the program which smoothly spread the wave across several cells at discontinuities, as seen, for example in the stress profile of Figure 43. In the bow wave, as the angle increases, the spreading is seen to narrow, since the amplitude of the wave front decreases to zero at

$$\theta = \frac{\pi}{2}.$$

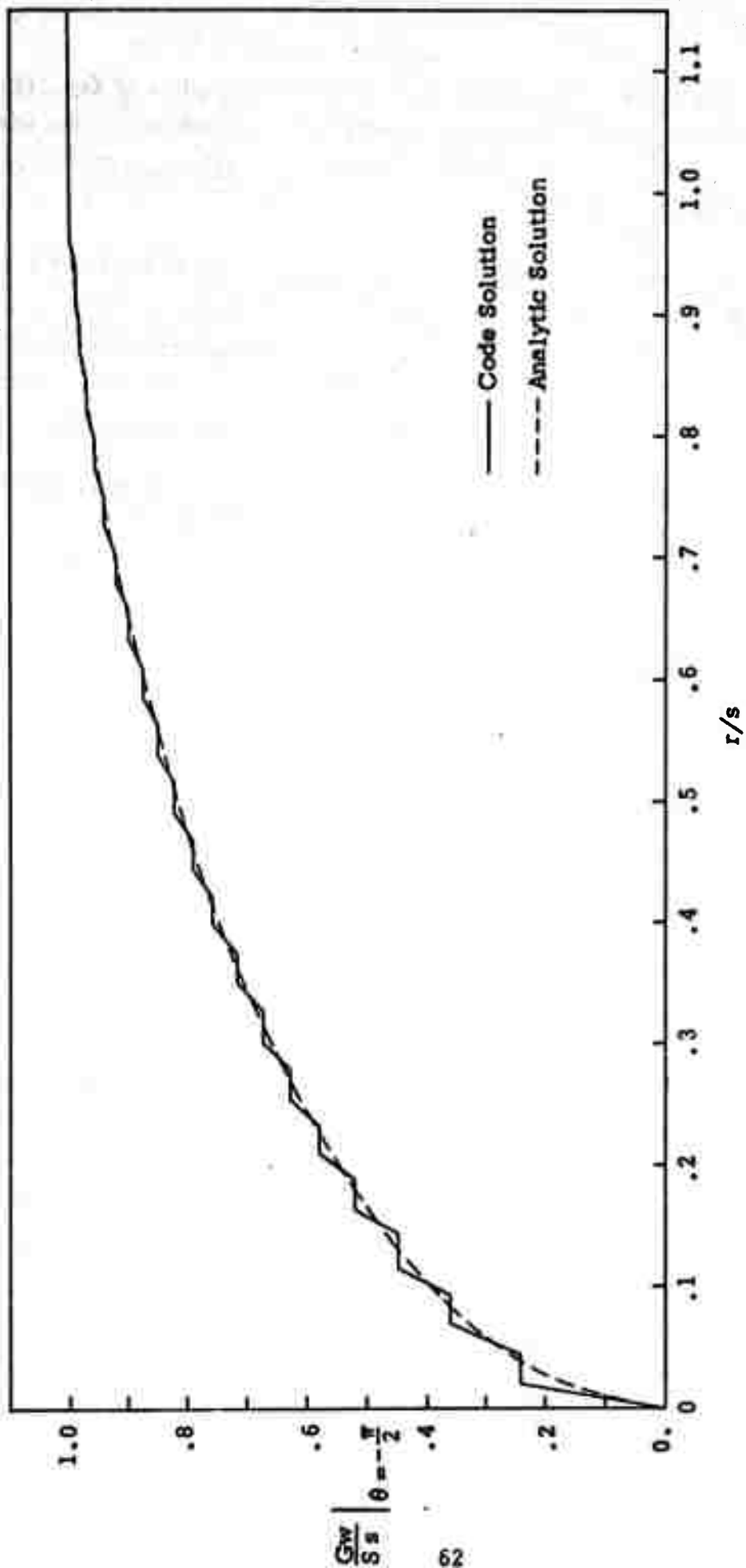


Figure 41. Crack-Opening Displacement Profile.

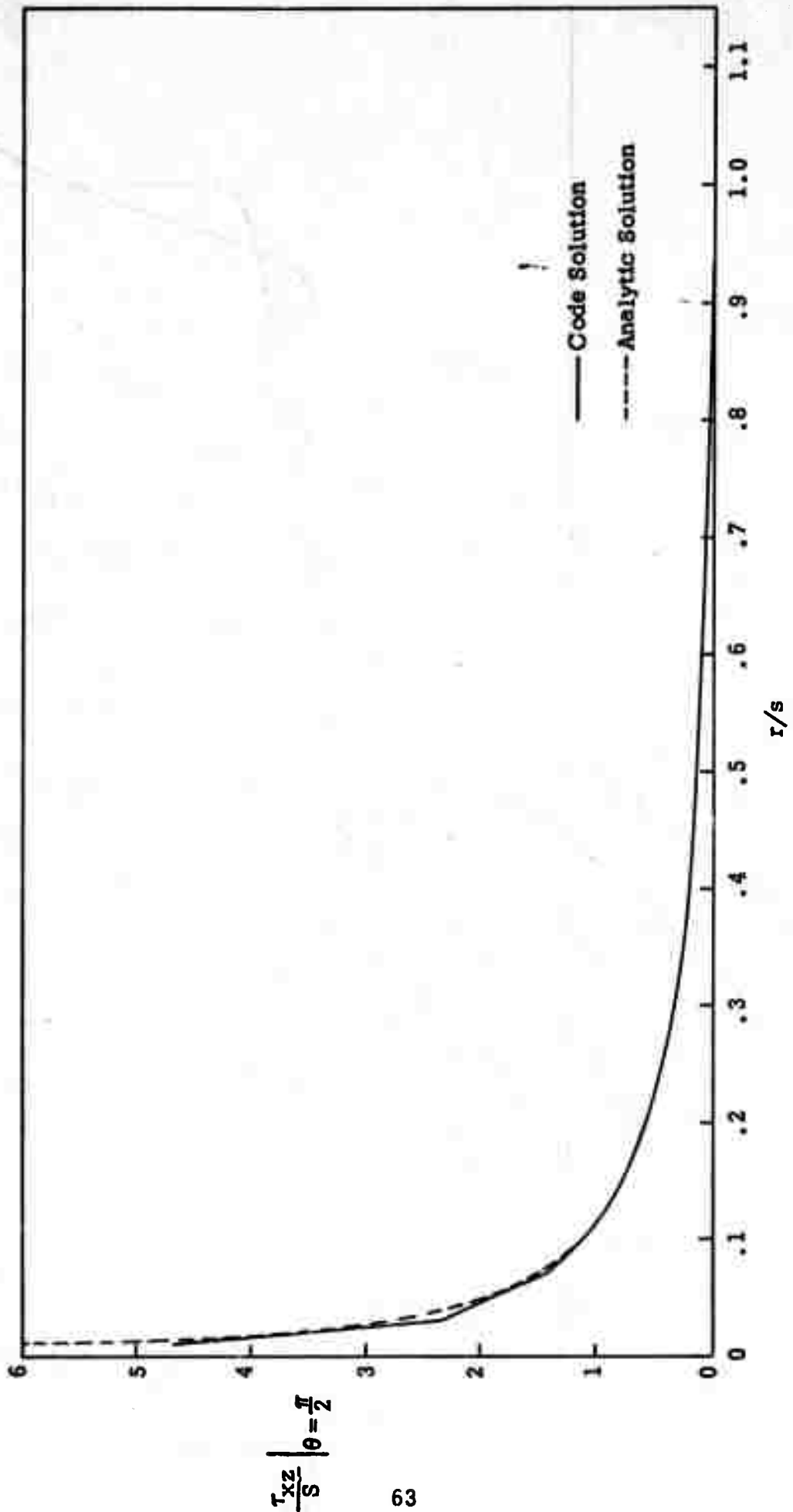


Figure 42. Shear Stress Profile Along Plane of Anti-symmetry ($\theta = \frac{\pi}{2}$).

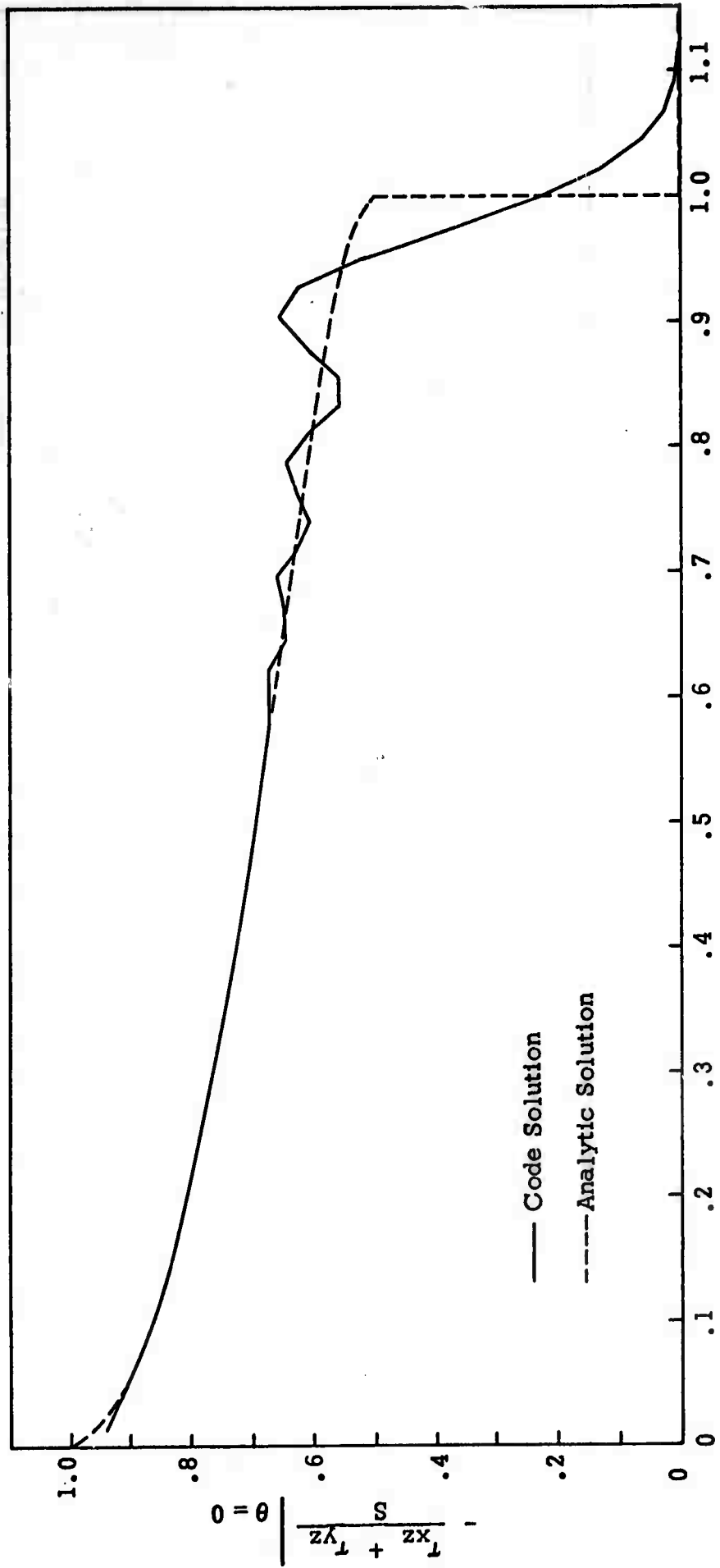


Figure 43. Shear Stress Profile Along Horizontal Plane ($\theta = 0$)

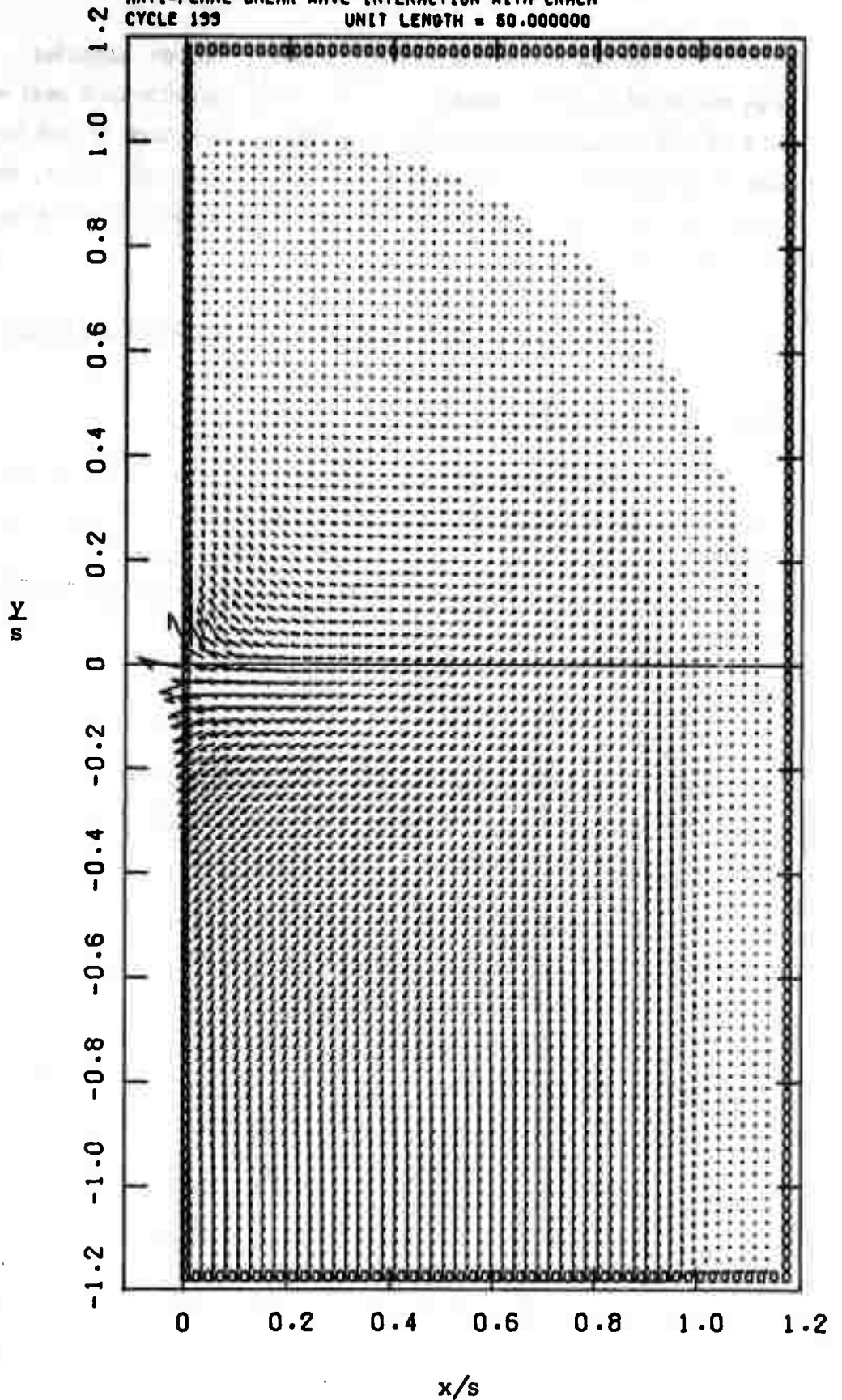


Figure 44. Shear Stress Field.

At the crack tip both τ_{xz} and τ_{yz} become singular. The computer run recorded highest values near the crack tip (one-half cell width away) of ~ 5 kb. The approach to infinity is limited therefore by the fineness of the mesh used in approximating the continuum by a grid. This, however, did not affect the good accuracy of the solution at points in the body away from the singularity.

5. ANTI-PLANE SHEAR LOADING OF AN ACCELERATING CRACK

5.1 ANALYSIS

In the case of a running crack, we have an infinite elastic space perforated by a semi-infinite propagation crack surface, lying at $[x = 0, -\infty < y \leq d(s)]$, where $d(s)$ is the distance the crack has propagated from the origin in time s . The driving force for the crack propagation is provided by an anti-plane shear stress

$$\tau_{xz} = -SH(s) \quad (23)$$

applied to both faces of the crack, and following the crack as it propagates. Ahead of the crack, on the plane $x = 0$, the displacement w is always zero.

The above problem may be attacked by first determining a Green's displacement function, which is the displacement arising from a unit force/unit thickness applied at a point on the $(x = 0)$ surface designated by y_0 , and at a time s_0 , for a duration Δs_0 . The solution to this problem is well known and has the form

$$w_G = \frac{F \Delta s_0}{\pi G} \frac{H [s - s_0 - \sqrt{(y - y_0)^2 + x^2}]}{\sqrt{(s - s_0)^2 - (y - y_0)^2 - x^2}} \quad (24)$$

The total displacement at any point (x, y) and at any time s is then given by:

$$w = \frac{8}{\pi G} \int ds_0 \left\{ \int \frac{dy_0}{\sqrt{(s-s_0)^2 - (y-y_0)^2}} + \int \frac{T_0/S dy_0}{\sqrt{(s-s_0)^2 - (y-y_0)^2 - x^2}} \right\} \quad (25)$$

where T_0 is the stress applied ahead of the crack and is to be determined by the condition that w is zero ahead of the crack on the surface $x = 0$.

The limits in Eqn. (25) are in part determined by the Heaviside function appearing in Eqn. (24), but are more simply described after carrying out an automorphic transformation⁹ to new variables.

$$\xi = \frac{s-y}{\sqrt{2}} \quad (26)$$

$$\eta = \frac{s+y}{\sqrt{2}} \quad (27)$$

These variables have the property that they allow the square root appearing in Eqn. (25) to be factored. One can then arrive at an Abel integral equation for (T_0/S) , under the condition that $w = 0$ ahead of the crack. After a little algebra, we arrive at the following results:

$$\frac{T}{S} = \frac{2}{\pi} \left[\arctan \sqrt{\frac{s-y+d(s-y+d)}{y-d(s-y+d)}} - \sqrt{\frac{s-y+d(s-y+d)}{y-d(s-y+d)}} \right] \quad (28)$$

$$\frac{GD}{S} = \frac{2}{\pi} \left\{ \arcsin \sqrt{\frac{d(s+y-d)-y}{s}} + \sqrt{[d(s+y-d)-y][s+y-d(s+y-d)]} \right\} \quad (29)$$

where

$$D = w \Big|_{x=0} \quad (30)$$

The function $d(s-y+d(s-y+d(s-y+\dots$ has the property that $d \rightarrow 0$ as $y \rightarrow s$ and the function $d(s+y-d(s+y-d(s+y-\dots$ has the

property that $d \rightarrow 0$ as $y \rightarrow -s$. We now apply the Griffith criterion (discussed below), perform a few operations with delta functions⁹, and arrive at the following result for the crack propagation function:

$$\frac{d}{s^*} = \left(\frac{s}{s^*} - 1 - \frac{\pi}{2} + 2 \arctan \frac{s^*}{s} \right) H(s - s^*) \quad (31)$$

where

$$s^* = \frac{\pi \Gamma G}{4 S^2} \quad (32)$$

and where Γ is the specific surface energy. From Eqn. (31) we conclude that

$$\frac{\dot{d}}{c} = \frac{1 - \left(\frac{s^*}{s}\right)^2}{1 + \left(\frac{s^*}{s}\right)^2} \quad (33)$$

so that the crack accelerates to sonic velocity. The start of crack propagation is delayed by a time s^* until the energy inside the bow wave has built up to a critical value. Figure 45 shows how d/s^* depends on s/s^* , a non-parameter plot.

5.2 THE GRIFFITH CRITERION

To improve the physical significance of the numerical solutions, the conclusion was reached that a more realistic, dynamic criterion for predicting and following the course of crack propagation in flawed, jointed, brittle media should be incorporated in the numerical method. A necessary step in making such a formulation change is to check the new code through comparisons with analytical results from a model problem, such as the one described in the previous section.

The modifications needed to follow crack propagation are three-fold. These are the logic associated with the crack geometry and crack propagation, the velocity threshold criterion, chosen here to be the Griffith

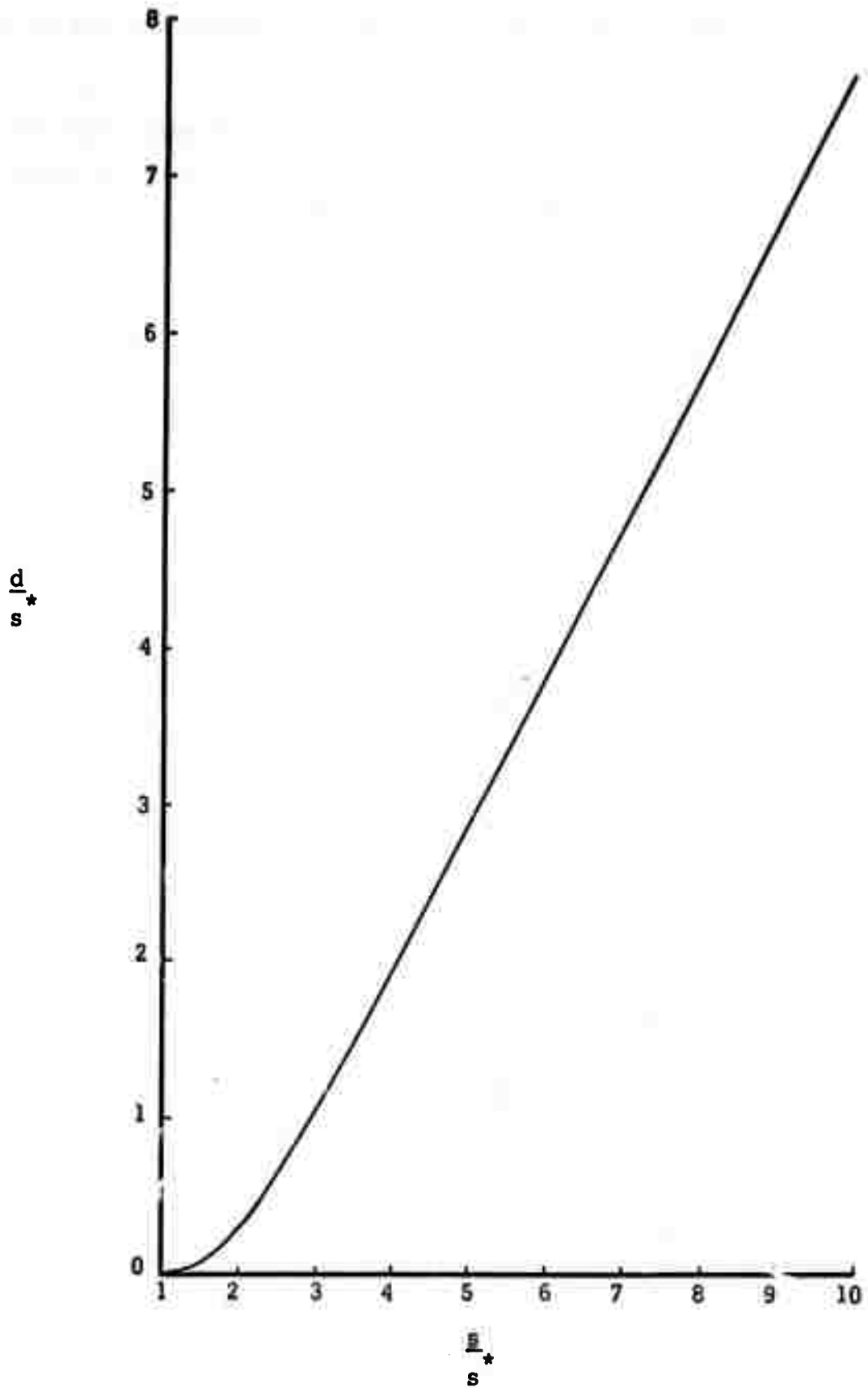


Figure 45. Antiplane Crack Propagation.

criterion, and the velocity orientation criterion, chosen to be the direction transverse to the maximum principal stress vector.

The Griffith criterion is a power balance. It states that the total work done on the body by surface traction goes into increase of strain energy, increase of kinetic energy, and increase of surface energy. This takes the form:

$$\int_0^t P(t') dt' = U_1 + U_2 + \Gamma (d - d_0) \quad (34)$$

where t' is a dummy time variable

$$P \equiv \oint t_j^i v^j da_i \text{ (the power input)} \quad (35)$$

$$U_1 = \int W dV \text{ (strain energy)} \quad (36)$$

$$U_2 = \int K dV \text{ (kinetic energy)} \quad (37)$$

$$W = -2G \gamma_2 + \frac{1}{2} (K + \frac{4}{3} G) \gamma^2 \text{ (strain energy density)} \quad (38)$$

$$\gamma = \epsilon_k^k \text{ (dilatation)} \quad (39)$$

$$\gamma_2 = \frac{1}{2} (\gamma^2 - \epsilon_k^i \epsilon_j^k) \text{ (second strain invariant)} \quad (40)$$

$$\epsilon_{jk} = \frac{1}{2} (u_{j;k} + u_{k;j}) \text{ (strain)} \quad (41)$$

$$v_i = \dot{u}_i \text{ (velocity)} \quad (42)$$

t_j^i is the stress tensor

u_i is the displacement vector

da_i is the tensor element of area

dV is the volume element

$$K = \frac{\rho_0}{2} v^k v_k \text{ (kinetic energy density)} \quad (43)$$

ρ_0 is mass density

U_1 and U_2 are zero at zero time

Γ is the specific surface energy

d is the instantaneous crack length (in 2D) or crack area (in 3D)

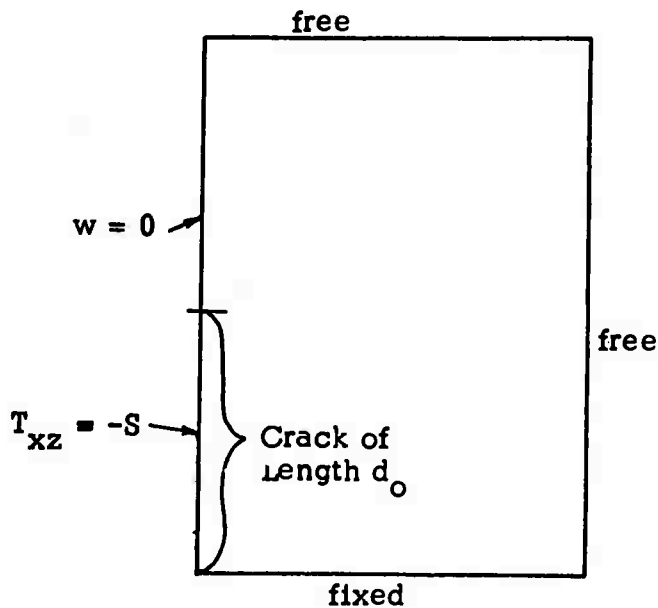
d_0 is the initial crack length

When the crack is not moving, $\dot{d} = 0$, in which case

$$\int_0^t P(t') dt' = U_1 + U_2 \quad (44)$$

The only basis for Eqn. (44) becoming an inequality arises when the boundary conditions involving the crack surface change with time. This statement requires elaboration.

Suppose we refer to the problem discussed in the previous section, namely, the one in which shear stress S is applied to part of the boundary of a rectangle, the remaining boundary being clamped. The stressed portion of the boundary is the crack, cf. figure below



For this case, when the crack is not allowed to run, Eqn. (44) is identically satisfied.

Imagine now, that after some time t_* , the crack starts to run, d_0 increases, and the stress S is allowed to follow the crack. In this case, the left hand side of Eqn. (44) becomes:

$$\int_0^{t_*} P(t') dt' \Big|_{d=d_0} + \int_{t_*}^{t_* + \Delta t} P(t') dt' \Big|_{d=d_0 + \Delta d} + \int_{t_* + \Delta t}^{t_* + 2\Delta t} P(t') dt' \Big|_{d=d_0 + 2\Delta d} + \dots \text{etc.}$$

Because of the crack motion, energy is absorbed by the creation of fresh surface and Eqn. (44) becomes an inequality.

In order to follow this motion, we proceed as follows: We allow the wave to propagate for some delay time (defined in Eqn. (32)) with the crack at its initial position. We then advance the crack a small distance Δd , which will be chosen to be a fraction of cell length. We then let the wave propagate for one increment of time Δt , and calculate the quantity:

$$\frac{\int_0^{t_*} P(t') dt' \Big|_{d=d_0} + \int_{t_*}^{t_* + \Delta t} P(t') dt' \Big|_{d=d_0 + \Delta d} - (U_1 + U_2)^{t + \Delta t}}{\Gamma} = \Delta d_{\text{calc}} \quad (45)$$

If this calculated Δd turns out to be equal to the chosen Δd , then the time increment Δt is recorded, and the crack is advanced another Δd . If the calculated Δd turns out to be less than Δd chosen, additional time increments are allowed to elapse until equality is achieved. Each time equality is achieved, the crack is advanced another Δd . A numerical plot of Δd vs time can thus be constructed and compared with the plot from the analytic solution shown previously (Figure 45).

In setting up the problem shown above, we have assumed that the load is applied directly to the crack surface. In the event a wave is allowed to impinge upon the crack by approach from infinity at any angle, the problem posed in this fashion can always be decomposed into a combination of a plane wave traveling in the absence of a crack, and the problem shown above, where the crack is loaded directly. Furthermore this problem can always be reduced from a full-space problem to a half-space problem by virtue of the antisymmetry of the shear loading. Similarly, in dealing with the in-plane problem, we can use symmetry to reduce the problem to that of a half-space. Thus the problem posed above is a very general model problem.

Initially, the code was checked for the case when the crack is not running (Eqn. (44)). To verify that the computation of the power integral on the left-hand side of Eqn. (44) matches within a few percent of the computation of the total energy, which is a standard output of the SHEP program, it was necessary to compare the computation of the velocity with the analytical solution given by:

$$\frac{G \dot{w}}{S c} = 1 - \frac{2}{\pi} \arctan \sqrt{\frac{s}{r} - 1} H(s-r) \quad (46)$$

At the point where the bow wave joins the plane wave, we have:

$$\frac{G \dot{w}}{S c} = 1 \quad (47)$$

Because of the discrete nature of the computational algorithm used to calculate \dot{w} in SHEP, the computed velocity is not constant in time, but rather fluctuates around unity, the vibration gradually damping to zero amplitude. Both the amplitude and logarithmic decrement of these vibrations can be controlled by varying the artificial viscosity and the time increment. We therefore performed a series of runs to determine appropriate values for the viscosity coefficient and time step.

Figure 46 shows a plot of normalized velocity at the wave front as a function of time measured in numbers of cells in the bow wave. It is observed that critical damping occurs somewhere between the values of the viscosity coefficients, $C_A = .25$ and $C_A = .75$. Variation of the time step had little or no effect upon the vibration in the range of Δt studied.

The meaning of Figure 46 is that the front of the wave is spread out over about 4 cells on either side of the front. As we shall see below, this uncertainty in \dot{w} implies an equivalent uncertainty in P , and, a fortiori, an exaggerated uncertainty in $[\int_0^t P(t') dt' - U_1 - U_2]$. Thus it will be extremely important to develop a better form for the fictive viscosity in order to narrow the spreading of the wave front. Such a form will be discussed below.

Holding in abeyance for the moment the question of improving the viscosity function, the Griffith criterion as displayed above was used to follow the propagation of the semi-infinite crack. The wave was allowed to propagate for 90 cycles with the crack unextended; then the crack was extended one cell, and the additional time needed for dynamic instability to arise was computed according to the algorithm provided above. In this way the crack was extended three times, and the results of the computation are shown in Figure 47. We note that the crack runs effectively slower than the theoretical sonic value. Further work remains to be done to refine the algorithm and the viscosity.

5.3 THE FICTIVE VISCOSITY

As soon as a continuum is replaced by a discrete grid, it becomes possible to replace a slowly changing function by a periodic one. For example, the simple function

$$y = 0 \tag{48}$$

can be replaced by

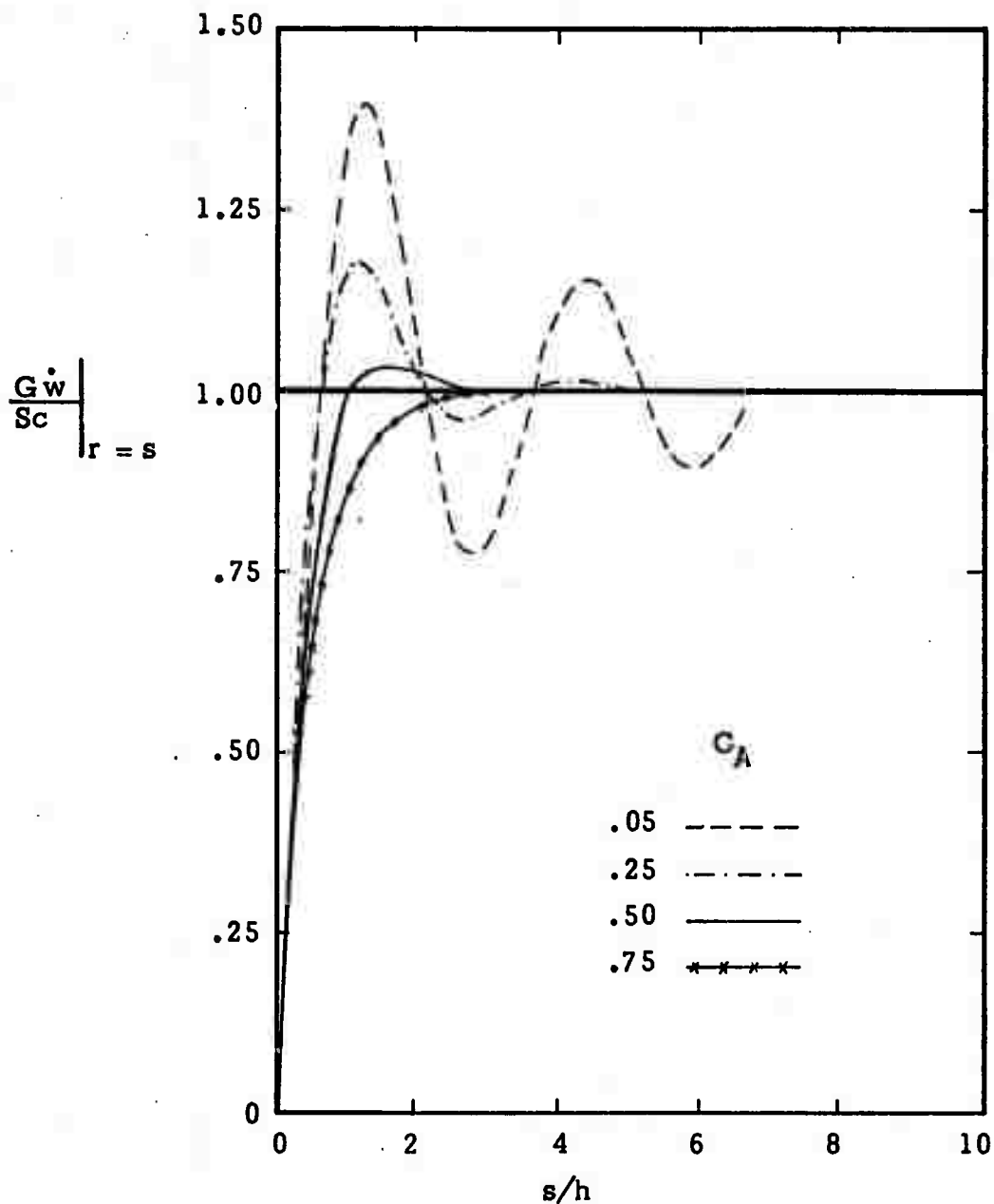


Figure 46. Velocity Time Histories for Various Artificial Viscosity Coefficients.

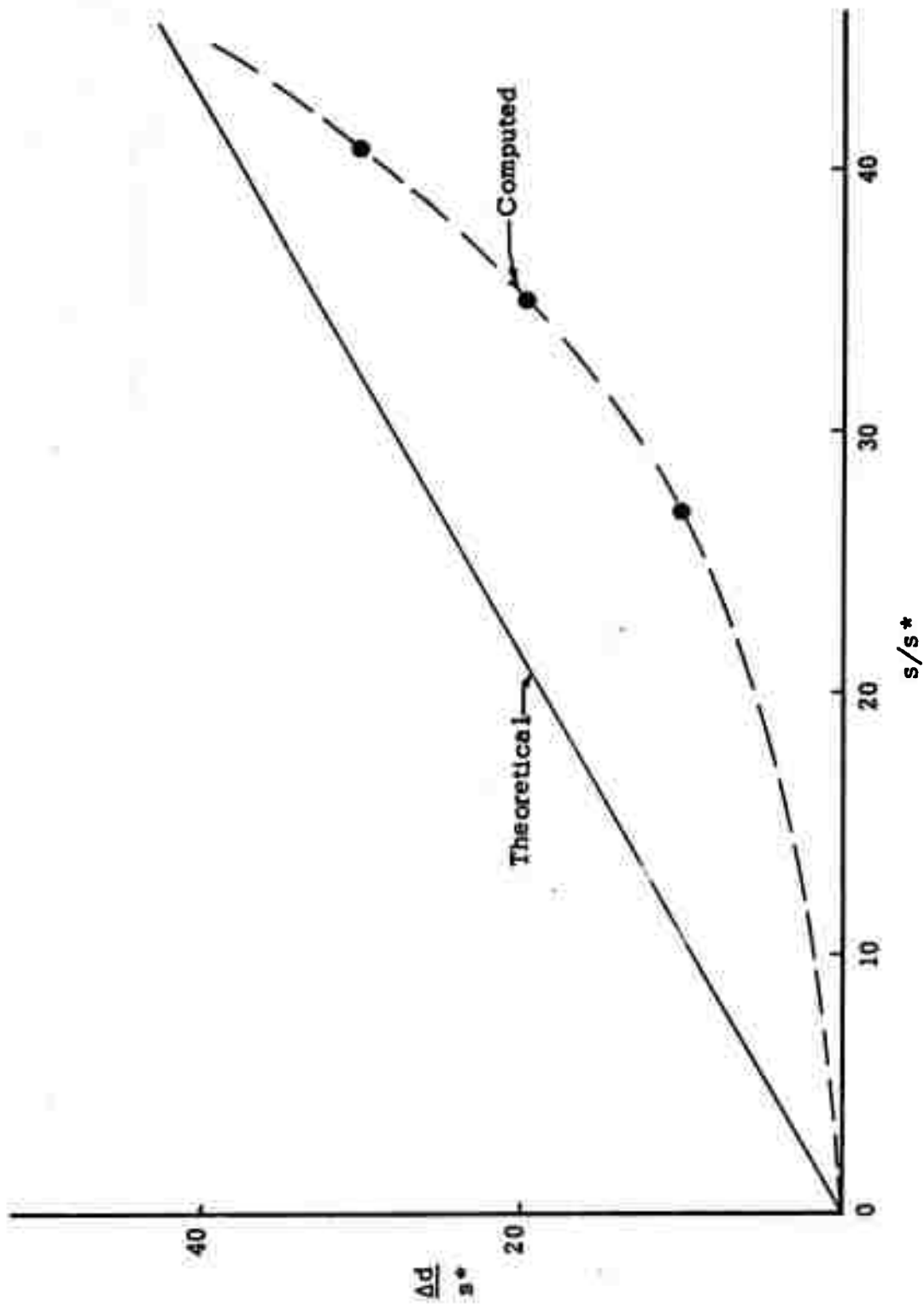


Figure 47. Crack Propagation History

$$y = A \sin n\pi \quad (49)$$

where

$$n = \frac{x}{\Delta x} \quad (50)$$

This is an extreme case but it demonstrates the point. What the difference equations actually offer depends on the outcome of a stability analysis. Such analyses have been carried out and they lead to the idea that a fictive viscosity must be incorporated in the constitutive law to produce damping and stability. The penalty that one pays is a spreading of a wave front.

Von Neumann and Richtmyer²⁰ suggested that a quadratic viscosity term be used to produce effective damping, and this has indeed been proved to be a useful tool. Other people have used a linear viscosity term with less striking results. The linear viscosity spreads the wave in an increasing manner. Thus it appears that the quadratic viscosity is an indispensable tool.

For the out-of-plane motion that we have been discussing, there is currently not available a quadratic viscosity formulation; thus a linear viscosity was used in the computation discussed above. It is possible however to suggest a cubic formulation, and the formulation which we propose below will be evaluated during work on a related program. The etymology is as follows.

The constitutive theory of fluid dynamics leads to the most general representation of one isotropic tensor (the stress tensor) in terms of another isotropic tensor (the strain rate tensor), namely:

$$\vec{\tau} = -p\vec{I} + \alpha_1 \vec{d} + \alpha_2 \vec{d} \cdot \vec{d} \quad (51)$$

where p is the hydrostatic pressure and α_1 and α_2 are scalar functions of the scalar invariants: $\{ I_d, II_d, III_d \}$

where

$$I_d = \text{Tr} \{ \bar{\dot{d}} \} = \nabla \cdot \bar{q} = \frac{\dot{V}}{V} = - \frac{\dot{\rho}}{\rho} \quad (52)$$

$$II_d = III_d \text{Tr} \{ \bar{\dot{d}}^{-1} \} \quad (53)$$

$$III_d = \text{Det} \{ \bar{\dot{d}} \} \quad (54)$$

The terms multiplied by (α_1, α_2) represent the dissipative contributions to the total stress. One way of incorporating quadratic dissipation is to take $[\alpha_2 = \text{constant}]$. This term however contributes only to the normal stresses, not to the shear stresses. The result produces what is known as a "normal stress" or Weissenberg effect. This effect is not useful for the flows that we deal with in fracture mechanics.

An alternative way of introducing nonlinear viscosity is to set $[\alpha_2 = 0]$ and take:

$$\alpha_1 = 2\nu_0 \rho (1 - \tau I_d) \quad (55)$$

where ν_0 is the kinematic viscosity
and τ is a relaxation time.

This form is very interesting for several reasons. First of all, the product $(\rho \nu_0)$ is the linear viscosity coefficient η_0 . Thus the effect of linear viscosity is included. Because of conservation of mass, Eqn. (55) may be rewritten as:

$$\alpha_1 = 2\nu_0 (\rho + \tau \dot{\rho}) \quad (56)$$

which evinces the typical form of viscous relaxation. Thirdly the quadratic term (τI_d) enters in the form according to which real materials behave; namely, the apparent viscosity decreases with increasing shear rate. Finally, if the linear term in Eqn. (55) is dropped, the expression above reduces exactly to the form suggested by Richtmeyer and Von Neumann. Thus Eqn. (56) displays a useful form for introducing quadratic viscosity into all components of the stress tensor.

In the event the flow is isochoric as it is in the case of anti-plane shear, one can not introduce a quadratic viscosity, because $I_d = 0$. One can however introduce a cubic viscosity by using the form:

$$\alpha_1 = 2 \nu_0 \rho (1 + \beta I_d) \quad (57)$$

In both forms suggested for α_1 , ν_0 can be taken proportional to the square of the mesh size. In the compressible form, involving quadratic viscosity, τ can be taken proportional to the time step, and in the isochoric form, involving cubic viscosity, β can be taken proportional to the square of the time step.

For the compressible or quadratic form, we have repeated the Von Neumann-Richtmeyer analysis. This analysis leads to the equation:

$$dx = \frac{-2 \tau du}{\sqrt{1 + (r+1) \frac{\tau}{\nu_0} u (u_p - u) - 1}} \quad (58)$$

It is easy to show that, as $u \rightarrow \{0, u_p\}$, $x \rightarrow \pm \infty$. This is in major contradiction to the Von Neumann analysis, where $x \rightarrow$ a finite length. What Von Neumann and Richtmeyer then did was to tack on to the shock front two straight-line constant velocity regions, with a concatenate discontinuity in curvature. Because the flow equations are second order, this solution does not satisfy the original differential equation and must be regarded as an approximate representation. The representation shown above does not suffer from this limitation, and can, by variation of τ and ν_0 , be made to approach the shock discontinuity as closely as desired. Figure 48 shows a plot of particle velocity profile for

$$\frac{\tau}{\nu_0} = 10^{-5}, 10^{-6}, \text{ and } 10^{-7}$$

and $\tau = 10^{-8}$ sec.

One observes that the shock thickness can be made to take on a broad range of values.

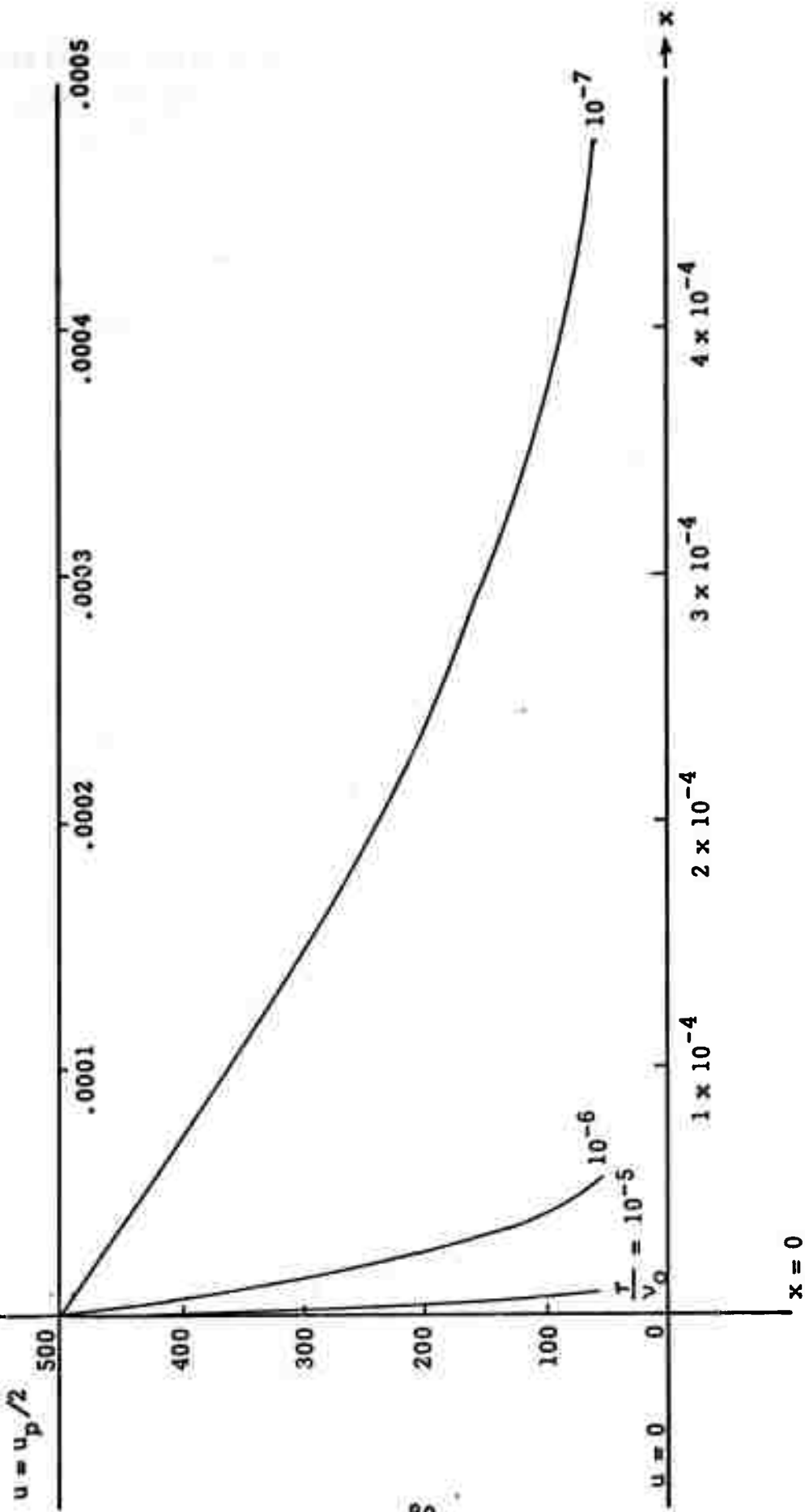


Figure 48. Particle Velocity Profile

REFERENCES

1. N. B. Brooks and R. L. Lansdale, SHAPE-II Code, Hardening Technology Studies-III, Space and Missile Systems Organization, SAMSO-TR-68-69 (1968).
2. M. L. Wilkins, Calculation of Elastic-Plastic Flow, Lawrence Radiation Laboratory, Livermore, UCRL-7322, Rev. 1 (1969).
3. M. H. Wagner, Analytical Studies of Penetration Mechanics, Shock Hydrodynamics, 3030-2020FR (1969).
4. M. H. Wagner, Analytical Studies of Projectile Design and Performance, Shock Hydrodynamics, 7584-06 (1971).
5. M. H. Wagner and N. A. Louie, HARD HAT/PILE DRIVER Ground Motion Calculations, Space and Missile Systems Organization, SAMSO-TR-69-47 (1969).
6. M. H. Wagner, Shock Conditioned Behavioral Model for Granite, Defense Nuclear Agency, DASA-2678 (1971).
7. B. V. Kostrov, "Unsteady Propagation of Longitudinal Shear Cracks," *Prikl. Mat. i. Mek.* 30, (English translation), 1241 (1966).
8. J. D. Eshelby, "The Elastic Field of a Crack Extending Non-Uniformly Under General Anti-Plane Loading," *J. Mech. Phys. Solids* 17, 177 (1969).
9. J. D. Achenbach, "Extension of a Crack by a Shear Wave," *ZAMP* 21, 887 (1970).
10. J. Von Neumann and R. D. Richtmyer, "A Method for the Numerical Calculation of Hydrodynamic Shocks," *J. Appl. Phys.* 21, 232 (1950).

APPENDIX

CORRECTION TO THE ROTATIONAL TERM IN THE STRESS CALCULATIONS

During the examination of the formulation of the code preparatory to making the modifications discussed in Sections 4 and 5 of the report, an error in the sign of the rotational correction term in the stress calculations, as originally proposed by Wilkins^{A1}, was discovered. In addition, from the standpoint of material objectivity^{A2}, the form of the rotational term is seen to be written in only an approximate form. These statements are documented below. The sign was corrected in our code and a check of the correction was made by running a model problem. The results confirmed the sign correction and, in addition, verified the accuracy of the SHEP code.

In SHEP, the constitutive equations are correctly* subsumed in the form^{A3}:

$$t_{ij} = s_{ij} - \delta_{ij} P \quad (A1)$$

$$\hat{s}_{ij} = 2G \left(\dot{e}_{ij} - \frac{1}{3} \dot{\theta} \delta_{ij} \right) \quad (A2)$$

$$\theta = \ln J \quad (A3)$$

$$J = \frac{dV}{dV_0} \quad (A4)$$

where

t_{ij} is the cartesian Cauchy stress tensor

s_{ij} is the stress deviator tensor

P is the pressure

J is the local volume ratio, equal to the square root of the third stretch invariant.

*The term "correctly" implies that Eqn. (A2) satisfies the principle of material objectivity.

G is the shear modulus

θ is the dilatation

\dot{e}_{ij} is the Cartesian strain rate tensor

V is the local instantaneous specific volume

and in (A4), $\frac{d}{dV_0}$ is the particle-differentiator.

From Eqn. (A3) and (A4), it follows that

$$J = \frac{\dot{V}}{V} \quad (A5)$$

Furthermore in Eqn. (A2), the dot over \dot{e}_{ij} denotes the material derivative while the hat over \hat{s}_{ij} denotes the Jaumann-Oldroyd derivative. The form of the latter is given by:

$$\hat{s}_{ik} = \dot{s}_{ik} - v_{i,j} t_{jk} + t_{ij} v_{j,k} \quad (A6)$$

where

$$v_{i,j} = \dot{e}_{ij} + \omega_{ij} \quad (A7)$$

or

$$\frac{v_{i,j} + v_{j,i}}{2} = \dot{e}_{ij} \quad (A8)$$

where

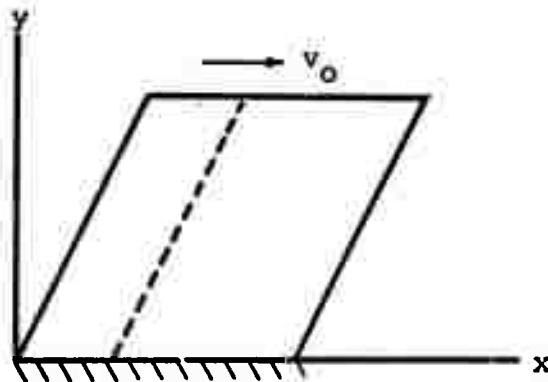
ω_{ij} is the spin tensor.

The last two terms on the right hand side of Eqn. (A6) correspond to Wilkins' δ_{ij} ; a simple calculation reveals that the entire form of Eqn. (B-14) on page 78 of Reference A1 is formally incorrect because of a sign error.

The sign error apparently arose in the following way: Wilkins introduces an angular velocity vector, which he denotes by $[\sin \dot{\omega}]$. The angular velocity vector is correctly taken as the curl of the velocity vector which, according to the usual right-handed correction, corresponds to a counter-

clockwise rotation. Wilkins then uses the rotation angle ω to transform the stress components to new rotated components. The transformation equations he adopts are taken from Timoshenko^{A3}. Presumably Wilkins changed the signs of the terms that are odd in ω , because Timoshenko shows a diagram in which the rotation is clockwise. What one must notice, however, is that Timoshenko's picture is based on a left-handed system of axes. Thus Timoshenko's equation should have been subsumed without the sign change.

To further check our logic, we ran the following simple problem. A slab is set into simple shear motion, cf:



Nonlinear (Poynting) effects are associated with the lengthening of the originally upright fibers. The correct rotation terms (with the right sign) predict a tensile stress in the lengthened fibers, in agreement with the analytical solution. The original program, with the incorrect sign, predicts compression. Keep in mind that these are second order stresses and thus the effect of this error on the overall computation becomes important only when the first order stresses are comparable to the shear modulus of the material. The reason is that the second-order stresses go as the square of the first-order stresses, e.g., in the shear problem:

$$\frac{\sigma_y}{G} \sim \left(\frac{\tau_{xy}}{G}\right)^2 \quad (\text{A9})$$

In the process of making these changes in SHEP, we checked out a model problem, namely the simple shear at constant velocities of an infinitely long slab (a 1-D problem). The results, in terms of the stress at the moving

surface and the stress at the fixed surface are plotted in Figures A1 and A2, respectively. The analytical solution is just a sum of Heaviside step functions. The agreement with the analytical solution is attested to by the fact that the computed jumps fall directly (within 1%) on the grid line (both coordinate axes are non-dimensionalized). The general solution looks like

$$-\frac{\tau_{xy}}{M_0 G} = \sum_{n=0}^{\infty} [H(s - y - 2nh) + H(s + y - 2h - 2nh)] \quad (A10)$$

where

$$M_0 \text{ (the Mach number)} = \frac{v_0}{c}$$

$$s = ct$$

$$c = \sqrt{\frac{G}{\rho}}$$

and h is the height of the slab.

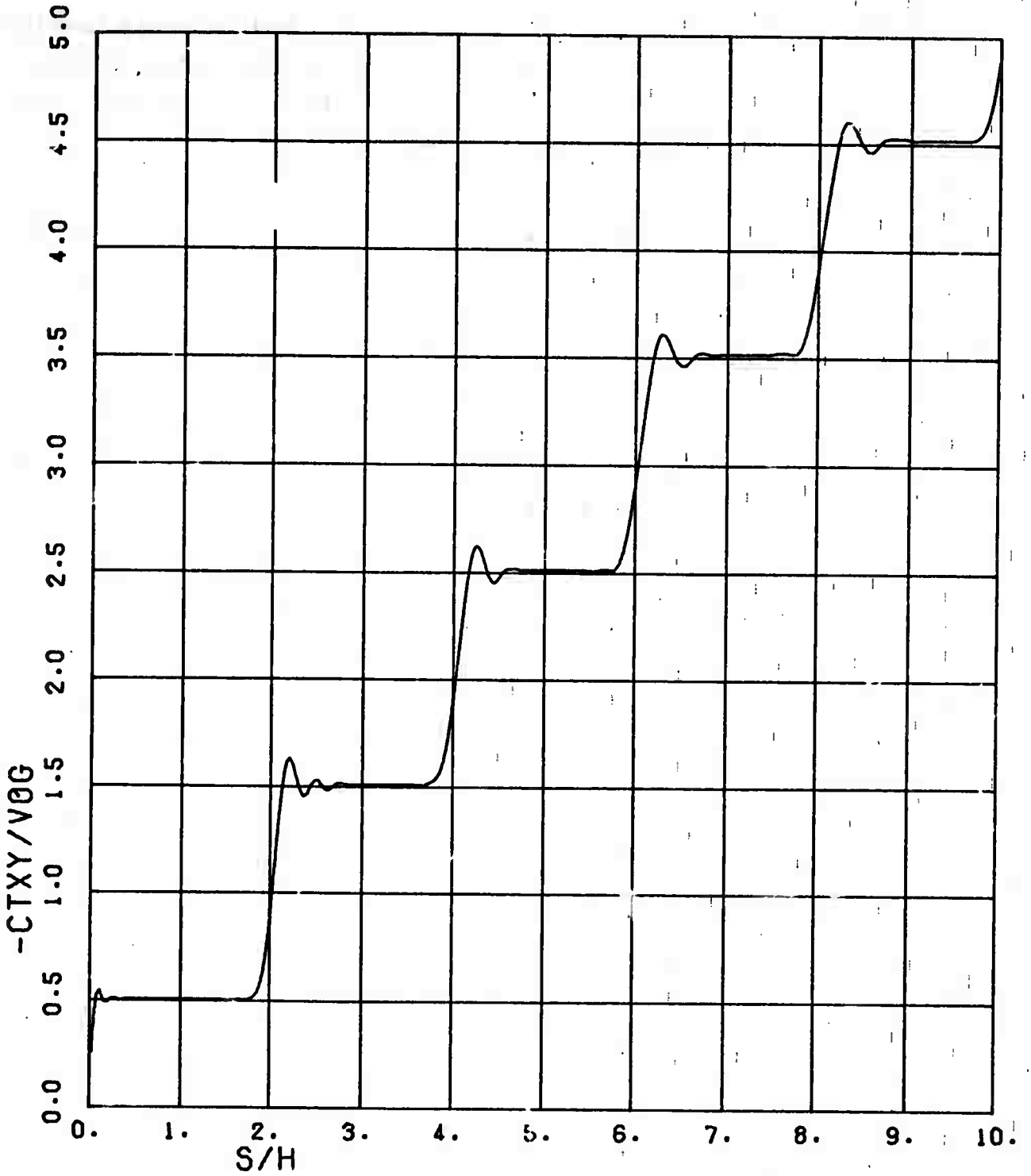


Figure A1. Shear Stress at the Moving Surface

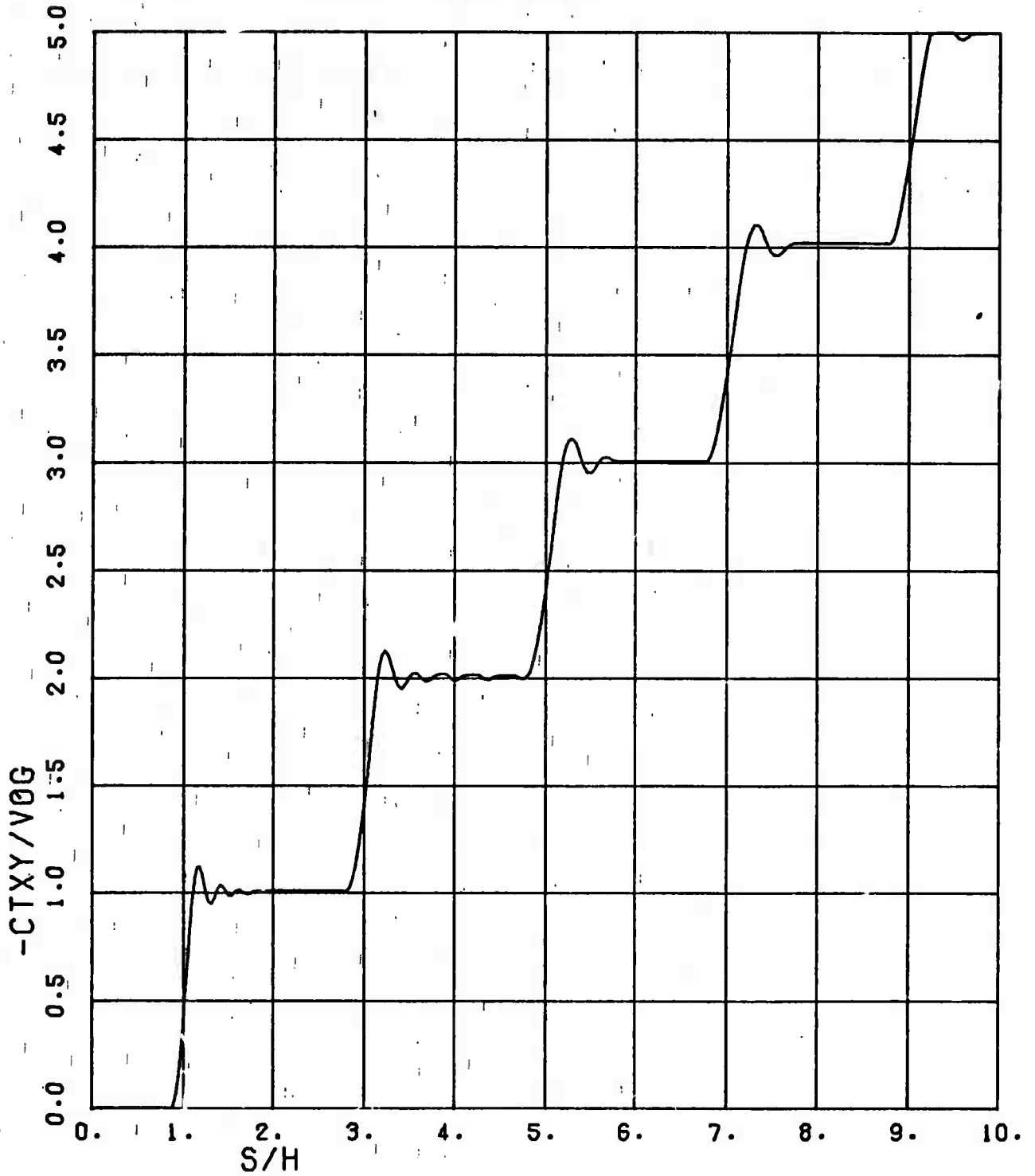


Figure A2. Shear Stress at the Clamped Surface

REFERENCES

- A1. M. L. Wilkins, Calculation of Elastic-Plastic Flow, Lawrence Radiation Laboratory, Livermore, UCRL-7322, Rev. I (1969).
- A2. A. C. Eringen, "Nonlinear Theory of Continuous Media," McGraw-Hill, New York (1962).
- A3. S. Timoshenko and J. N. Goodier, "Theory of Elasticity," McGraw-Hill, New York (1951).